UNIVERSITY OF CALIFORNIA, SAN DIEGO

# Dissecting Enhancer Functions in Signal Induced Transcription Programs

A dissertation submitted in partial satisfaction of the
requirements for the degree Doctor of Philosophy

in

Biology

by

Yiren Hu

Committee in charge:

Professor Michael Geoff Rosenfeld, Chair
Professor Christopher K. Glass
Professor Cornelis Murre
Professor Amy Pasquinelli
Professor Samuel Pfaff

2018

The Dissertation of Yiren Hu is approved, and it is acceptable in quality and form for publication on microfilm and electronically:

Chair

University of California, San Diego
2018

Table of Contents

List of Figures

Acknowledgements

Having Dr. Michael G. Rosenfeld as my mentor is the most valuable part of my experience at University of California, San Diego. His creative ideas, critical thinking and hardworking all set an extraordinary role model for me. I'm thankful for his encouragements that we should study the most interesting and challenging topics. I'm thankful for his high standards that we need to push research works to the most exciting level. I'm also thankful for his generous support each time when I experienced down times in graduate school. With his guidance, I'm honored to write this thesis.

I want to thank my committee members Professor Cornelis Murre, Professor Christopher K. Glass, Professor Sam Pfaff and Professor Amy Pasquinelli. They have given valuable inputs towards the thesis projects as well as genuine advices on my presentation skills.

I also want to thank all my collaborators and Rosenfeld lab members. Discussing science, learning from each other and doing research projects with them is a rewarding experience that I'll cherish forever.

During my years at graduate school, I've always been blessed with the friendship of many fantastic people. I'd like to devote my thanks to all my friends for the happiness and support they've given me all these years.

Lastly, special thanks devoted to my boyfriend Dr. Zhanglong Ji and my families. They've given me the courage to pursue my dreams without much hesitation or fear.

Chapter 1 is an adaptation of the material as it appears in Molecular Cell, 2015. The authors of this study are Wenbo Li, Yiren Hu, Soohwan Oh, Qi Ma, Daria Merkurjev, Xiaoyuan Song, Xiang Zhou, Zhijie Liu, Bogdan Tanasa, Xin He, Aaron Yun Chen, Kenny Ohgi, Jie Zhang, Wen Liu, and Michael G. Rosenfeld. The dissertation author was co-first author of the paper, contributing to this study through performing all the experiments and leading all the analysis related to condensin II, as well as intellectual input.

Chapter 2 is an adaptation of a manuscript that is being submitted for publication. The authors of this study are Weiwei Gao, Rongquan Xiao, Wenjuan Zhang, Yiren Hu, Yaohui He, Bingling Peng, Haifeng Shen, Wenjuan Li, Jiancheng Ding, Ying Li, Zhiying Liu, Michael G. Rosenfeld, and Wen Liu. The dissertation author was co-first author of the paper, contributing to this study through performance of experiments related to Gro-seq, Pol II ChIP-seq, Med12 ChIP-seq, as well as intellectual input.

Chapter 3 and 4 are currently being prepared for submission for publication. Yiren Hu, Yuliang Tan, Jia Shen, Wubin Ma, Feng Yang, Haifeng Shen, Kenny Ohgi, Jie Zhang and Michael G. Rosenfeld are participants of the project. The dissertation author was the primary investigator and author of this paper.

## Vita

2010 Bachelor of Science, Peking University, China

2018 Doctor of Philosophy, University of California, San Diego

## Publications

"The intra-S phase checkpoint targets Dna2 to prevent stalled replication forks from reversing" Cell 149 (6), 1221-1232.

"Condensin I and II complexes license full estrogen receptor α-dependent enhancer activation" Molecular cell 59 (Dunham et al.), 188-202

"Glucocorticoid Receptor: MegaTrans Switching Mediates the Repression of an ERα-Regulated Transcriptional Program" Molecular Cell 66 (3), 321-331. e6

Abstract of the Dissertation

Dissecting Enhancer Functions in Signal Induced Transcription Programs

by

Yiren Hu

Doctor of Philosophy in Biology

University of California, San Diego, 2018

Professor Michael Geoff Rosenfeld, Chair

This dissertation, by Yiren Hu, discusses how enhancer activity is regulated to drive rapid, coordinated transcriptional response to signals like estrogen and inflammatory stimuli. Enhancer elements play a central role in instructing precise spatiotemporal gene expression and are capable of activating target gene transcription from a long distance. How do enhancers achieve these functions? And how are enhancers regulated in response to multiple signals at the same time? To answer these questions, we took a high-throughput approach with the power of next-generation sequencing technologies to study the genome wide transcription landscape changes of human breast cancer cells as well as mouse immune cells in response to stimuli like estradiol and TNFα.

We tackled enhancer regulatory mechanisms from three aspects and found that: 1) chromatin structure regulators Condensin Complex I and II play essential roles in activating Estrogen Receptor α-bound enhancers by balancing transcription co-activators versus co-repressors homeostasis (see Chapter 1) 2) histone demethylase JMJD6 activates Estrogen Receptor α-bound enhancers and controls coding gene Pol II pausing release by modulating mediator complex protein MED12 chromatin loading (see Chapter 2) 3) Estrogen Receptor α and histone demethylase KDM2B form a two-layer restriction mechanism to repress NFκB enhancers and corresponding pro-inflammatory genes (see Chapter 3 and 4).

# Introduction

One of the most fascinating parts about metazoans development is to generate a great variety of cell and tissue types, which can respond to internal physiological signals and cope with outside environmental challenges, from one identical set of genetic information(Lam et al., 2014b). At the heart of this process, it is the enhancer elements that instruct precise spatiotemporal control of gene expression.

Ever since the first discovery of enhancer about 35 years ago (Banerji et al., 1981), we have gained a growing knowledge of enhancer molecular attributes. Through the combination of a series of *in vitro* reporter assays and molecular genetic studies, researchers first characterized enhancers as short DNA fragments a) able to activate target gene expression b) activity independent of genomic distance or orientation relative to the promoter of target gene c) DNase hypersensitivity, which marks an open chromatin structure d) the presence of transcription factor binding DNA motif e) enrichment of transcription co-activators binding and acetylated histones (Li et al., 2016). Later, with the power of genomic study tools like ChIP-seq, we have witnessed the emergence of identification of more than 400,000 enhancers in the human genome(Consortium, 2012), which share characteristics like DNase I hypersensitivity, high H3K4me1 compared with H3K4me3 levels, and active histone marks like H3K27Ac presence via ChIP-seq analysis. Interestingly, at this stage, a lot of signal induced transcription factors like Estrogen Receptor α (ERα) were found to bind to primarily enhancer elements instead of promoters (Carroll et al., 2005). Furthermore, with the advancement of global run-on sequencing (GRO-seq) technology, putative enhancers with epigenetic marks were found

to be pervasively transcribed with examples like ERα-bound active enhancers (Hah et al., 2011). And works from our lab and others have shown that these RNA transcripts from enhancer elements (eRNAs) are functionally important for controlling target gene transcription (Li et al., 2013a), which greatly reshape our understanding of enhancers from DNA-protein combinations to DNA-RNA-protein three dimension elements.

Knowing that enhancers have transcription products just like promoters do, we are interested to know how enhancers are being regulated as transcription units themselves. Are there special molecular machinery dedicated for enhancer activation? What's more, how do enhancers coordinate to respond to multiple signals applied to the same cell? Intrigued by these questions, during my graduate research, I studied the enhancer functions in regulated transcription programs from three aspects: Aspect I, in order to influence target genes at a long distance, do enhancer rely on special chromatin structure regulators like Condensin Complex proteins to function? (See Chapter 1) Aspect II, even at a single active Estrogen Receptor α (ERα)-bound enhancer there are tens of co-activators, epigenetic enzymes, mediators, and other transcription factors loading, how is the enhancer association of these activators being regulated? To investigate the dynamics of activators recruitment, we interrogated the relationship between histone demethylase JMJD6 and Mediator complex protein Med12 recruitment to ERα active enhancers as an example. Aspect III, in physiological situation, cells are facing regulations from multiple signaling pathways, how do enhancers navigate the gene expression program under this condition? Following this direction, we treated MCF-7 breast caner cells with estradiol

and TNFα to stimulate ERα and NFκB signaling pathways at the same time and studied the enhancer regulation program in Chapter 3 and 4.

# Chapter 1: Condensin I and II Complexes License Full Estrogen Receptor α-Dependent Enhancer Activation

## INTRODUCTION

Enhancers empower the genome with a precise control of temporally and spatially necessary gene expression patterns (Bulger and Groudine, 2011b; Plank and Dean, 2014b). The recent discovery of pervasive transcription of enhancer RNAs (eRNAs) revealed enhancers themselves as transcription units (Kim et al., 2010a). eRNA levels showed high correlation with the activity of enhancers, and both enhancer transcription and transcripts were found to contribute to enhancer function (Andersson et al., 2014a; Hah et al., 2013a; Hsieh et al., 2014a; Kaikkonen et al., 2013a; Lai et al., 2013a; Lam et al., 2013a; Li et al., 2013a; Melgar et al., 2011a; Melo et al., 2013a; Mousavi et al., 2013a; Schaukowitch et al., 2014; Wu et al., 2014a), adding an important new layer of understanding into the fundamental mechanisms underlying enhancer action (Lam et al., 2014a; Natoli and Andrau, 2012a). However, the molecular mechanisms control the appropriate transcriptional output of enhancers and subsequent activation of coding genes remains elusive.

Cohesin has recently been shown to positively regulate transcription by modulating enhancer function and enhancer-promoter looping (Kagey et al., 2010; Li et al., 2013a; Schmidt et al., 2010), raising the possibility that other architectural complexes important in mitosis/meiosis, particularly condensins, might be involved in enhancer

function and transcription regulation (A.J. et al., 2010). Condensins are highly conserved multi-subunit complexes containing structural maintenance of chromosome (SMC) proteins. Together with two other such SMC-containing complexes - cohesin and SMC5/SMC6 complexes, they contribute to formation, maintenance and dynamics of eukaryotic chromosome architecture (A.J. et al., 2010; Hirano, 2012; Jeppsson et al., 2014). In vertebrates, two related condensin I and II pentameric complexes, exhibiting similar topological structures (A.J. et al., 2010; Hirano, 2012), were found to play non-overlapping but critical roles for chromosome packing in mitosis (Green et al., 2012; Hirano, 2012; Ono et al., 2003) (**Figure 1A**). Compared to roles in mitosis, little is known about condensin functions in interphase. Condensin I was originally considered mainly cytoplasmic during interphase, whereas condensin II has been recognized to exhibit a nuclear localization, thought to concentrate on chromatin until prophase (Hirano, 2012; Ono et al., 2003). In particular, it remains largely unclear where condensin I and condensin II are localized in the interphase chromatin, how do they get recruited and exert their functions, if any, in gene transcription regulation.

In this study, we found that, surprisingly, multiple condensin I and condensin II subunits are rapidly, specifically and strongly recruited to ER-α-bound functionally active enhancers in response to estrogen in human breast cancer cells. The loading of interphase condensins to these active enhancers was likely achieved by direct interaction with ER-α via the DNA-binding domain (DBD) of the latter. Mechanistically, condensins were required for full ligand-activated eRNA transcription based on its interaction with an E3 ubiquitin ligase HECTD1, which modulates proper recruitment of transcriptional

coactivators and corepressors via ubiquitinating and dismissing a specific corepressor RIP140. This hierarchical control then licenses RNA polymerase II (Pol II) to activate enhancers, eRNA transcription and enhancer:promoter chromosomal interactions, together lead to upregulation of target coding genes. Our current data has thus identified an unexpected, enhancer-based important transcriptional function of condensin complexes in the interphase chromatin, which is likely to be required for at least some other classes of DNA binding transcription factors in diverse cell types.

## RESULTS

### Loading of interphase condensin I and II to ER-α binding sites in breast cancer cells

Given the critical role of cohesin in 17-β-estradiol ($E_2$)-regulated coding gene transcription program (Li et al., 2013a), we became curious about possible roles of condensins. Consistent with findings in other cell types (Heale et al., 2006; Ono et al., 2003), up to ~10-30% and ~50% of condensin I and condensin II subunits, respectively, proved to be chromatin-associated in MCF-7 breast cancer cells (**Figure 1B**). Following 3-4 days of culture in serum-deficient ”stripping” medium, MCF-7 cells were largely (~80-95%) blocked in the G0/G1 phase(Villalobos et al., 1995) (**Figure S1A**), in contrast to the status without stripping (~42% G0/G1, **Figure S3A**), providing an ideal opportunity to study potential interphase functions of condensins. ChIP-Seq with an antibody against the NCAPG subunit of condensin I identified 2,916 binding peaks genome-wide in cells cultured in the absence of $E_2$, strikingly increasing to 7,292 peaks 1hr after $E_2$ treatment (**Figure 1C** and **Figure S1C**). The majority of NCAPG binding

peaks were found in intergenic (55%) and intronic regions (36%), with only ~4.6% located on RefSeq gene promoters (**Figure S1B**). Remarkably, ~77% (5,623/7,292) of all NCAPG binding peaks overlapped with those of ER-α **(Figure 1C**); ESR1/ERE was the most enriched motif for all the NCAPG binding sites by HOMER motif analysis (Heinz et al., 2010a) (p=1E-906) (**Figure S1D)**. Analogous experiments for condensin II (*i.e.* NCAPH2), revealed similar enrichment to intergenic/intronic regions (**Figure 1C**), remarkable gain of peaks after $E_2$ treatment (3,636 to 10,192) (**Figure S1E**) and high overlap with ER-α binding (**Figure 1C** and **Figure S1F**). Specificity of the condensin antibodies was confirmed by the knockdown of the mRNAs encoding these two proteins by small interfering RNAs (siRNAs), resulting in dramatic reduction of their binding by ChIP-qPCR (**Figure S1G**). ChIP-Seq by a specific antibody against NCAPH, another subunit of condensin I (**Figure 1A**), despite being less robust, also yielded predominantly intergenic and intronic locations, consistent with NCAPG results (**Figure S1B**), overlapping ER-α binding sites (**Figure 1D,E** and **Figure S1H**). $E_2$ treatment caused a switch of the motif enriched on NCAPH-bound intergenic sites to ERE (**Figure S1I**). The results of the condensin ChIP-Seq experiments were yet further confirmed by using a second antibody against NCAPG (NCAPG (Y.K.), a generous gift from K. Yokomori (UCI)) (**Figure 1D,E**). A representative UCSC browser screenshot of condensins localizing to ER-α-bound $E_2$-regulated enhancer and promoter of *TFF1* locus is shown in **Figure 1E**, and results were confirmed by ChIP-qPCRs (**Figure S1G,J,K**).

**Condensins preferentially enrich to ER-α-bound eRNA+ active enhancers in the interphase nuclei**

Previous work from our lab (Li et al., 2013a) and others (Hah et al., 2013a) established that upon estrogen signalling, a sub-group of ER-α/H3K27Ac co-bound enhancers (n=1,248), exhibiting $E_2$-upregulated eRNA transcription, high intensity of ER-α binding and close proximity to estrogen target coding genes, constitute the major $E_2$-activated functional enhancers in MCF-7 cells, referred to as $E_2$-induced "active enhancers" or "eRNA+ enhancers" (**Figure S2A**). In addition to active enhancers (n=1,248), ER-α/H3K27Ac co-bound sites contained another group of 5,763 "enhancers", which we referred to as non-active/"primed" enhancers, displaying no significant eRNA induction, a lower ER-α binding intensity and lack of Pol II or p300 increase in response to $E_2$ (**Figure S2A** and **Figure 1F,G**); these "primed" enhancers also exhibited higher levels of H3K27me[3] (data not shown). In response to $E_2$, there is a remarkably increased binding of both condensin I (NCAPG) and condensin II (NCAPH2) on ER-α-bound active enhancers (**Figure 1D, E, F** and **Figure S2B**), which was not present on the primed enhancers (**Figure S2A** and **Figure 1G**). Binding of condensin I and II on active enhancers was highly correlated with that of ER-α, with Pearson correlation coefficients of $\rho$=0.87 and $\rho$=0.88, respectively (**Figure S2C**). The ER-α binding sites involved in putative chromosomal looping (Fullwood et al., 2009) were found to exhibit higher NCAPG and NCAPH2 binding intensity than those ER-α binding sites without looping formation (**Figure S2D**), further suggesting condensin enrichment to functional ER-α-bound enhancers. When we compared the binding of condensins at active enhancers to

that of other known transcription factors/cofactors and some histone marks (ChIP-Seqs), we found that NCAPG and NCAPH2 exhibited the most dramatically induced recruitment in response to $E_2$, similar to that of SRC3, the classical ER-α coactivator (CoA), and ER-α itself (**Figure S2E**). A hierarchical cluster analysis (HCA) of the $E_2$-induced binding of these factors indicated that condensins exhibited the highest correlation with ER-α, similar to that of SRC3 (**Figure 1H**). Together, these data reveal that both condensin I and II complexes are preferentially recruited to ER-α-regulated, functionally active enhancers upon $E_2$ treatment; and exhibited the most dramatic induction in response to ligand.

NCAPG ChIP-Seq in MCF-7 cells without stripping or in enriched mitotic cells showed that the binding of NCAPG to typical ER-α/condensin co-bound sites in *TFF1* locus was already diminished in asynchronized MCF-7 cells without stripping, that contain ~30% mitotic cells (**Figure S3A** *vs.* **Figure S1A**), which further decreased to very minimal levels in mitosis-enriched MCF-7 cells (**Figure S3B**, pink peaks); this was observed on most of the active enhancers (**Figure S3C** *vs.* **Figure 1D**). These data indicate that the observed ChIP-Seq binding of condensins to active enhancers represent interphase-specific events.

**Condensins are *"trans"* loaded by ER-α to active enhancers in response to E2**

To test for potential interactions between condensin complexes and ER-α, we first performed gel filtration using MCF-7 nuclear extract and found highly-overlapped co-

fraction profiles of ER-α and the condensin I as well as condensin II complexes in several fractions between ~1-1.5MDa, noting that some subunits of condensins (*e.g.* SMC2 and NCAPH2) and ER-α itself also exhibited additional elution in other fractions (**Figure 2A**). Co-immunoprecipitation (IP) experiments revealed that specific antibodies to endogenous condensin subunits co-precipitate ER-α (**Figure 2B,C** and **Figure S3D**). Reciprocally, both the endogenous and the overexpressed form of ER-α could successfully pull-down many condensin subunits (**Figure S3E** and **Figure 2D**). These interactions were independent of the presence of DNA (**Figure 2C**). ChIP-Western result of NCAPG and ER-α interaction suggests that their interaction takes place on chromatin (**Figure 2E**). Importantly, condensin interaction with ER-α was not disrupted when lysine 539 of ER-α was mutated (*i.e.* L539A, **Figure 2D**), a mutation that precludes ligand-dependent binding of LxxLL-containing nuclear receptor coactivators (CoAs) and corepressors (CoRs)(Lonard et al., 2000), exemplified by failure to bind SRC3 or RIP140 (**Figure 2D**). Rather, interestingly, the DNA binding domain (DBD) of ER-α exhibited the strongest association with condensins (**Figure S3F**). These data suggested that condensins interact with ER-α in a non-canonical manner, very distinctive from those "LxxLL"-containing cofactors. Consistent with the possibility that condensins may be "*trans*" recruited to ER-α-bound enhancers by ER-α itself, rather than through a direct association with chromatin (i.e. *cis* binding), MCF-7 cells were treated with a down-regulator of ER-α - ICI 182780 (Wakeling et al., 1991); the $E_2$-induced NCAPG and NCAPH2 binding was almost completely abolished (**Figure 2F)**. Levels of condensin proteins were not obviously altered by $E_2$ or ICI treatment (**Figure 1B**). Consistent with a previous study (Ono et al.,

2003), we did not observe any direct interaction between the condensin I and condensin II complexes themselves (**Figure S3G).** This was confirmed by a mass spectrometry experiment following NCAPG IP from MCF-7 nuclear extracts, showing that NCAPG pulls down condensin I subunits and SMCs, but not condensin II constituents (**Figure S3H**). Interestingly, several E3 ubiquitin ligases, as well as ubiquitin itself, were found to co-IP with NCAPG (**Figure S3H**), suggesting that condensin complexes may associate with some previously unappreciated functional partners in breast cancer cells.

Although either condensin I or II bound some distinct sites, they co-localized on 5,253 sites in the genome (**Figure 2G**), and most of these co-bound regions were also occupied by ER-α (~94% positive). This high overlap between the chromatin localization of condensin I and II under $E_2$ signalling, apparently recruited by liganded ER-α, differs from their largely non-overlapping chromatin localization in mitosis (Green et al., 2012; Hirano, 2012; Ono et al., 2003). Two-step ChIP experiment using NCAPG or NCAPH2 antibodies for first ChIP, followed by a re-ChIP with ER-α, NCAPH2, or NCAPG antibodies revealed that ER-α co-occupied some similar chromatin region bound by condensins (**Figure 2H**), as illustrated by qPCR on classical ER-α binding sites, *TFF1* promoter (*TFF1p*), *FOXC1* enhancer (*FOXC1e*) and *NRIP1* enhancer (*NRIP1e*). Interestingly, NCAPH2 and NCAPG can also reciprocally re-ChIP each other on the same genomic regions (**Figure 2H**). These data suggested that, although condensin I and II do not directly interact (Ono et al., 2003) (**Figure S3G**), they simultaneously co-occupy ER-α-bound active enhancers. Knockdown of NCAPH subunit of condensin I

reduced the binding of NCAPG, as expected (**Figure S3J**); it also decreased the protein levels of the whole condensin I complex (**Figure S3I)**. Condensin I knockdown (i.e. *siNCAPG*) apparently did not affect either the binding or complex stability of condensin II (**Figure S3I,K**). These data, together with the lack of interaction between condensin I and II (**Figure S3G**) suggested that it is unlikely to have a mix-and-match form of condensin complex present in MCF-7 cells. But our data could not exclude if there is any sub-stoichiometric condensin complex formed in the MCF-7 cells, and/or only present in certain genomic regions, which could be an interesting future direction as has been done for cohesin (Ding et al., 2011).

**Condensins are required for $E_2$-activated gene and eRNA transcriptional program**

We used at least two different siRNAs to effectively knockdown multiple condensin subunits (**Figure S3I, S4B,C**), which resulted in a significantly dampened $E_2$ activation of many well-established target coding genes by RT-qPCR, such as *TFF1*, *FOXC1, SMAD7, SIAH2* and *PGR* (**Figure 3A** and **Figure S4D**), without reducing *ER-*$\alpha$ mRNA or protein levels (**Figure S4E,F**). GRO-Seq (Core et al., 2008a) analysis confirmed this inhibition (**Figure 3B,C**). Based on analysing the $E_2$-induced fold-change ($E_2$-FC) of the $E_2$-upregulated coding genes with a >1.5FC, there is a significant reduction of $E_2$-FC in the absence of either NCAPG or NCAPD3 compared to that in control MCF-7 cells (**Figure 3C**). Whole-gene GRO-Seq profile showed a dramatic transcriptional attenuation of $E_2$ target genes upon *NCAPG* knockdown (red *vs.* purple

line, **Figure S5A**). Correspondingly, RNA Pol II loading also decreased over the gene bodies of the same group genes by ChIP-Seq (**Figure S5B**). Of the RefSeq genes that showed reduced transcription after si*NCAPG* treatment (*i.e.* NCAPG-positively regulated genes), a high percentage were also $E_2$-upregulated targets (**Figure 3D**), suggesting that NCAPG is widely involved in the $E_2$-dependent gene activation program. ESR1 appeared as one of the top Gene Ontology (GO) terms (interaction) for this group of NCAPG-positively regulated genes (**Figure S5C**)(Heinz et al., 2010a). Similar results were observed upon *NCAPD3* knockdown, resulting in a dramatic inhibition of $E_2$-FC of estrogen target genes (**Figure 3C,D**). In estrogen-treated breast cancer cells, the two condensin complexes regulated a partially overlapping category of coding genes (**Figure 3D**), consistent with their partially overlapped chromatin localization (**Figure 2G**). Interestingly, the eRNA levels neighbouring to genes regulated by condensin I or condensin II or by both of them were found higher than those next to genes regulated by $E_2$ only, consistent with the possibility that condensins work on gene regulation via highly transcribing eRNA+ enhancers (**Figure 3E**). Representative UCSC browser images of GRO-Seq and Pol II ChIP-Seq are shown for *TFF1* locus (**Figure 3B**). Together, these data indicate that condensins play an important role in activating the expression of estrogen target genes, acting at the level of transcription.

Flow cytometry revealed no significant change of cell cycle phase distribution after condensin depletion in MCF-7 cells (**Figure S5D**), excluding the possibility that the observed transcription inhibition was caused by indirect effects on cell cycle. This is

consistent with previous results that single condensin knockdown did not obviously impact mitotic index (Ono et al., 2003).

**Condensins regulate full eRNA activation and enhancer:promoter looping**

Because only a small percentage of the large cohort of coding genes activated by either condensin I, condensin II or ER-α exhibited promoter binding of themselves (**Figure 4A**), we focused on investigating condensin effects on estrogen-dependent enhancer function. Examining eRNA transcription, a mark of active enhancers (Andersson et al., 2014a; Hah et al., 2013a; Lam et al., 2014a; Li et al., 2013a; Wu et al., 2014a), RT-qPCR result revealed clear inhibition when specific condensin I or II subunits were knocked down (**Figure 4B**), which also inhibited Pol II loading to enhancers (**Figure S5E**). Genome-wide analyses using both GRO-Seq (**Figure 4C** and **Figure S5F**) and RNA Pol II ChIP-Seq (**Figure 4D**) confirmed the quantitative but significant inhibition of enhancer transcription upon loss of condensins. The UCSC browser screen shoots of *TFF1* and *FOXC1* enhancers are shown (**Figure 3B** and **Figure S5G**). In accord with the role/contribution of eRNA to gene activation and enhancer:promoter looping (Hsieh et al., 2014a; Lai et al., 2013a; Li et al., 2013a), we found that the knockdown of a condensin subunit (*siNCAPH2*) also led to an inhibited enhancer:promoter (E:P) contact frequency in the *TFF1* locus by 3D-DSL (**Figure 4E**). The effect was quite specific to the E:P looping without clear effects on other interactions surrounding the adjacent regions of the acceptors designed to the BamHI restriction sites. The reduced E:P looping of *TFF1* locus upon condensin subunit knockdown was also

confirmed by 3C-PCR using another restriction enzyme SacI **(Figure 4F)**. A PCR product migrated at the correct size (i.e. ~1.1kb by informatic calculation) was observed only in ligated samples, which exhibited clear reduction in the presence of *siNCAPG* **(Figure 4F,G)**. This 3C-PCR product was subjected to Sanger sequencing, which confirmed its identity (**Figure 4H**). Similar reduction of specific E:P looping was also found in the *FOXC1* locus by both 3D-DSL and 3C-PCR (**Figure S5H-K**), with concomitant decrease of the eRNA (**Figure S5G)**. As a control, a condensin-independent gene *GATA3* did not exhibit obvious change of its E:P looping (**Figure S5L**). These data suggested that condensins play an important role during estrogen-induced enhancer activation, including allowing Pol II recruitment, eRNA transcription and E:P looping.

**Condensins maintain an equilibrium of CoA:CoR binding on active enhancers**

Previous studies have revealed sequential/dynamic cofactor recruitment on classical ER-α-bound sites (Metivier et al., 2003; Shang et al., 2000), upstream of pol II loading (Shang et al., 2000). To further examine which step in this sequence of events requires the actions of condensins, we performed ChIPs for critical transcription factors/cofactors, including pioneer factor FOXA1, several conventional CoAs and CoRs, and ER-α itself (Foulds et al., 2013). With knockdown of individual condensin subunits, neither FOXA1 nor ER-α binding at active enhancers exhibited significant reduction (**Figure 5B** and **Figure S6A-C**). However, $E_2$-induced increment of p300 binding to the condensin/ER-α co-regulated sites was markedly inhibited, as indicated by both ChIP-

qPCR and ChIP-Seq (**Figure 5A,B**). Reduction was also observed for recruitment of other CoAs including SRC1, SRC3 and TIP60 (**Figure S6D-F**). In accord with the fact that many of these CoAs possess histone acetyltransferase activity, we observed a significant decrease of the H3K27Ac histone modification (another indicator of enhancer activity) on the active enhancers following condensin knockdown (**Figure 5C**). Depletion of condensin also resulted in quantitatively decreased binding of MED1 to these active enhancers, consistent with the linkage of mediator complex to both transcription and E:P looping (Hsieh et al., 2014a; Kagey et al., 2010; Lai et al., 2013a)(**Figure S6G**). Interestingly, loading of condensins seemed to be a downstream event during enhancer activation after the trans recruitment and assembly of "MegaTrans" complex (Liu et al., 2014), as demonstrated by the reduction of condensin binding after dual knockdown of RARα/RARϒ, but a lack of effect on RARα binding upon depletion of condensin subunit (**Figure S6H, I**). A representative genome browser image for the *TFF1* locus (**Figure 5D**) illustrates clear reduction of p300 binding and H3K27Ac levels, without diminishing that of ER-α after depletion of either NCAPG or NCAPD3. Knockdown of p300 revealed that *sip300* and *siNCAPG* caused a similar level of inhibition of $E_2$-target coding genes and eRNAs by RT-qPCR (**Figure S6H**), although partial effect of p300 knockdown could be attributed to the reduced level of ER-α itself (**Figure S6H**). By testing for effects on two CoRs, RIP140 and CtBP1(Augereau et al., 2006; Watson et al., 2012; White et al., 2005), we found that while RIP140 displayed an $E_2$-induced binding on several ER-α/condensin co-bound sites by ChIP-qPCR (**Figure 5E**), its recruitment became further augmented when condensin was depleted (**Figure 5E**). Knockdown of

RIP140 increased several interrogated eRNA transcription by RT-qPCR (**Figure S6I**). Intriguingly, a concomitant increase of CtBP1 binding could also be detected with condensin depletion (**Figure S6J**). These observed changes of CoA and CoR binding should not be attributed to any detectable change of their protein amounts upon condensin knockdown (**Figure S6K**). These data suggest that condensins license enhancer activation by maintaining a fine balance of $E_2$-dependent recruitment of CoAs and CoRs.

**Condensin-dependent recruitment of HECTD1 licenses enhancer activation**

We next explored the finding that some E3 ubiquitin ligases were found in complex with NCAPG by mass spectrometry (**Figure S3H**). Especially as a HECT family member, E6-AP/UBE3A (Rotin and Kumar, 2009) was discovered as a CoA for nuclear receptors (Nawaz et al., 1999), we were particularly intrigued by the potential importance of HECTD1 (Sarkar and Zohn, 2012; Zhou et al., 2012) when Co-IP experiments confirmed the interaction between condensin subunits with HECTD1 in MCF-7 cells (**Figure 6A and Figure S7A**). Like condensins, HECTD1 also interacts with ER-α independent of L539A mutation and with particularly high affinity with the DBD domain (**Figure 6B and Figure S7B)**. The co-fraction profile of HECTD1 also well coincided with those of condensins (**Figure 2A**). Further mapping of interacting domain showed that the C terminus and a central fragment of HECTD1 displayed interaction with condensin (*i.e.* NCAPH, **Figure S7C,D**). ChIP-qPCR using two different commercial antibodies against HECTD1, despite different affinities, both revealed an $E_2$-

induced binding to several condensin/ER-α binding sites (**Figure S7E** and data not shown). ChIP-Seq using one of these HECTD1 antibodies identified 3,274 peaks genome-wide in liganded MCF-7 cells, about ~45% and ~41% of which overlapping the sites of ER-α and NCAPG, respectively (**Figure S7F**). Heatmap analysis revealed the presence of HECTD1 and its $E_2$-induction on the active enhancer group (**Figure 6C**), as exemplified by the *TFF1* locus (**Figure 6D**). Furthermore, HECTD1 and NCAPG binding on the active enhancers exhibited high correlation (**Figure 6E**). This is an interesting observation consistent with the finding that active ubiquitination and protein proteolysis events are enriched on active enhancers and selective promoters (Catic et al., 2013). When we knocked down *NCAPG*, the binding of HECTD1 on many ER-α/condensin co-bound sites was significantly reduced (**Figure 6F**), but the HECTD1 protein level was not affected (**Figure S6K**), suggesting that HECTD1 was recruited to ER-α-bound active enhancers in a condensin-dependent manner. Similar to condensin knockdown, siRNA depletion of *HECTD1* caused an inhibition of p300 recruitment and increase of RIP140 binding to ER-α-regulated sites (**Figure 6G,H**). This was accompanied by reduced transcription of eRNAs and coding genes in response to $E_2$ (**Figure 6I**). To elucidate if the E3 ligase activity is important for HECTD1 function, a rescue experiment were performed, which showed that an HA-tagged mouse wild-type HECTD1 (mHECTD1-WT) expression plasmid could rescue, at least in part, the eRNA inhibition resulted from HECTD1 knockdown in MCF-7 cells (**Figure 6J** and **Figure S7G, H**). In contrast, a HECTD1 mutant (C2579G) that is defective of E3 ligase activity (Sarkar and Zohn, 2012) failed to produce rescue (**Figure 6J** and **Figure S7G,H**). Further,

the overexpression of the C-terminus of HECTD1 (HECTD1-4) that still interacts with condensin (**Figure S7D**) quantitatively dampened the $E_2$ activation of eRNAs and coding genes (**Figure S7I**), suggesting a dominant-negative effect, again indicating the binding of condensin with HECTD1 is needed for full activation of eRNA transcription.

**HECTD1 polyubiquitinates and dismisses RIP140 from active enhancers**

Considering that RIP140 binding on ER-α-bound enhancers was augmented in the absence of HECTD1, we sought to determine if RIP140 might be a direct target of HECTD1. Interestingly, RIP140 was recently reported to be polyubiquitinated in macrophages to modulate inflammatory gene transcription (Ho et al., 2012). Polyubiquitination ($Ub_n$) of RIP140 *in vivo* could be detected in MCF-7 cells after $E_2$ treatment, and was enhanced by MG-132, a proteasome inhibitor (**Figure 7A,B**). $E_2$ treatment did not alter the total protein levels of RIP140 in MCF-7 cells, until the addition of cycloheximide (CHX) during $E_2$ stimulation (**Figure 7C**), suggesting a possibility that the $E_2$-induced polyubiquitination of RIP140 elicited its degradation, which was simultaneously balanced by new protein synthesis. The presence of α-amanitin also inhibited the reduction of RIP140, suggesting that its turnover may be transcription-dependent (**Figure S7J**). When HECTD1 was knocked down in presence of CHX, the $E_2$-triggered RIP140 reduction was disrupted (**Figure 7D)**. An *in vivo* ubiquitination assay was performed in 293T cells by ectopically co-expressing Flag-tagged RIP140 and HA-tagged wild-type HECTD1 or C2579G mutants in the presence of wild-type or K48R mutant ubiquitin. Wild-type but not C2579G mutant of HECTD1

promoted RIP140 polyubiquitination **(Figure 7E)**, and only in the presence of wild-type ubiquitin but not K48R mutant (**Figure 7F**). Functionally, the reduced activation of $E_2$ target genes and eRNAs due to *siHECTD1* could be at least partially rescued by RIP140 knockdown (**Figure 7G**). These data together suggested that RIP140 is one of the functional substrates of HECTD1 during $E_2$-induced enhancer activation. A model diagram is shown in **Figure 7H** to depict the role of condensins in recruiting HECTD1 to regulate the $E_2$-regulated coactivator/corepressor equilibrium and enhancer activation.

## DISCUSSION

### Enhancer binding of condensin I and condensin II

Where are interphase condensin I and condensin II on the chromatin? Our current study has revealed a previously unsuspected interphase chromatin loading of condensin I and condensin II to the ER-α-bound active enhancers, in a rapid, simultaneous and dramatic manner in response to estrogen stimulus in human cancer cells. Their binding represents probably the most robust signature of active enhancers than other interrogated factors or marks, distinctive from other structural molecules (e.g. cohesin). This dramatic enhancer enrichment is quite surprising especially for mammalian condensin I as it was considered to display low nuclear/chromatin abundance in interphase (Hirano, 2012). Intriguingly, the overall chromatin-association of condensins by biochemical fractionation did not display significant change by $E_2$ treatment, implying that the enhancer-bound portion was re-distributed from other chromatin regions, reminiscent of the relocation of cohesin on yeast chromatin after initial loading (Lengronne et al., 2004).

The quite high co-localization for the two condensin complexes in interphase is distinct from their "non-overlapping" localization in mitosis (Green et al., 2012; Hirano, 2012; Ono et al., 2003), thus extending observations in other organisms (D'Ambrosio et al., 2008; Kim et al., 2013; Kranz et al., 2013) or a recent study in murine stem cells reporting the presence of condensin II on (super-) enhancers (Dowen et al., 2013). Interestingly, condensin II binding does not seem enriched to enhancers in Drosophila (Van Bortle et al., 2014), raising a possibility that certain enhancer-based roles represent evolving functions of condensins. Importantly, our data provided a novel insight into the poorly understood process of condensin chromatin loading in interphase, that condensins could be "*trans*" recruited by interaction with a transcription factor (i.e. ER-α) to regulatory elements, rather than directly associating with chromatin (i.e. *cis*), renewed the existing models of mitotic condensin chromatin loading (Liu et al., 2010; Piazza et al., 2014; Tada et al., 2011). Of course, it is also possible that this initial recruitment by ER-α allows subsequent association of condensin with enhancer DNA by other strategies, such as topological entrapment (Piazza et al., 2014).

**Condensins activate eRNAs and coding genes**

Functionally, GRO-Seq data has revealed that condensins surprisingly activate gene expression, and this regulation occurs at the level of transcription rather than any post-transcriptional steps or by impacting RNA stability. These results are rather unexpected as condensins are long considered to "condense" chromatin, which

supposedly might attenuate transcription, as in the cases exemplified by the condensin-like dosage compensation complex (DCC) in X chromosome transcription repression in *C.elegans* (A.J. et al., 2010). Interestingly, even in DCC-defective mutant worms, while expression of X genes increased, many autosomal genes seemed reduced (Jans et al., 2009). Condensin I and condensin II regulate a partially shared category of coding genes in liganded breast cancer cells, consistent with their incompletely overlapping chromatin localization.

Mechanistically, condensins appear to modulate the activation of ER-α-bound enhancers by regulating the balanced recruitment of LxxLL motif-containing coactivators vs. specific corepressors. In turn, these events license RNA Pol II binding, eRNA transcription and enhancer full activation. The effects of condensin knockdowns on eRNA transcription were comparable to those observed with si*p300*, but appeared quantitative, likely suggesting certain redundancy or yet unknown mechanisms underlying eRNA transcription. On the basis of a role of eRNA in enhancer:promoter looping formation and gene activation (Hsieh et al., 2014a; Lai et al., 2013a; Li et al., 2013a), we suggest that, the modulation of specific enhancers by condensins is an important component of the full activation of coding target genes in response to regulatory signals. Consistent with this, condensin depletion reduced stability of *TFF1* enhancer:promoter looping event. But our data could not clearly define if the looping defect was completely or partially a consequence of reduced eRNA levels. Indeed, there could well be a possibility that condensins directly exert structural control of higher-order

chromatin architecture, potentially by regulating topological domain borders (Hirano, 2012; Jeppsson et al., 2014; Van Bortle et al., 2014).

**Condensins and ubiquitination machinery**

Mitotic condensins are thought to play structural roles in regulating chromatin, possibly through ATPase or DNA super-coiling activities (Hirano, 2012; Hudson et al., 2008; St-Pierre et al., 2009), or topological entrapment of chromosomes (Cuylen et al., 2013; Hirano, 2012). But in interphase, their regulatory mechanism on gene expression/transcription is rather elusive. Our data suggest that, at least in part, condensins could exert interphase actions based on their ability to recruit/organize specific post-translational enzymatic machinery to control transcriptional activation of regulated enhancers. This is exemplified by condensin-dependent recruitment of HECTD1, an E3 ubiquitin ligase (Sarkar and Zohn, 2012), to polyubiquitinate and dismiss corepressor RIP140 from binding to active enhancers, warranting a fine balance of CoA/CoR recruitment (Foulds et al., 2013; Liu et al., 2002). These data provided a novel insight into the long-observed dynamic/cyclic recruitment of CoAs (e.g. p300 and SRC3) and CoRs (e.g. RIP140) to nuclear receptors to allow for a proper transcriptional output (Foulds et al., 2013; Metivier et al., 2003; Shang et al., 2000). Consistently, a recent genome-wide study of transcription factor/cofactor ubiquitination revealed that active protein turnover by ubiquitination is required for gene regulation and takes place mostly on active enhancers and specific promoters (Catic et al., 2013). Based on these observations and known structural roles of condensins, one likely speculation is that the

post-translational enzymatic machinery such as ubiquitination could be organized in a sub-nuclear "structure" (Skowronska-Krawczyk et al., 2014) to exert its actions.

### Condensins/HECTD1 and cancer

Finally, our current results of condensins function in estrogen gene transcriptional program in breast cancer cells may have disease implications. Indeed, several condensin subunits have been associated with cancers (Emmanuel et al., 2011; Leiserson et al., 2014; Murakami-Tonami et al., 2014; Ryu et al., 2007); HECTD1 was found with higher levels in ER-α-positive breast cancer patients in TCGA database (**Figure S7K**), as well as important for ER-α-negative breast cancer cell invasion and metastasis (Li et al., 2013c). In addition, given the important roles of condensins acting on tightly regulated specific genomic regions (e.g. enhancers), we are tempted to propose that dysregulated temporal or spatial loading of interphase condensins may lead to aberrant gene expression, possibly involved in human diseases.

The current study therefore serve to support an enhancer-based important regulatory function exerted by interphase condensins on a specific ligand-activated gene transcriptional program, and have provided novel insights into our understanding of the regulation of eRNA transcription and enhancer activation.

## EXPERIMENTAL PROCEDURES

MCF-7 cells were initially obtained from ATCC, maintained in culture and treated as described in(Li et al., 2013a). To induce estrogen signalling, MCF-7 cells were hormone stripped for three to four days and treated or untreated with 100nM $E_2$ (Sigma) dissolved in ethanol. RT-qPCR was carried out as previously described (Li et al., 2013a), normalized to either Actin or GAPDH. siRNAs were purchased from Sigma-Aldrich, Qiagen or Dharmacon. Knockdown experiments with siRNAs were conducted as transient transfections using Lipofectamin 2000, as per manufacturer's instructions (Life Technologies). ChIP-Seqs and GRO-Seqs were performed as previously reported (Li et al., 2013a). Two-step ChIP was conducted following a published method(Ross-Innes et al., 2010). Experimental datasets of ChIP-Seqs and GRO-Seqs are deposited in GEO databases (GSE62229)

**ACKNOWLEDGEMENTS**

Chapter 1 is an adaptation of the material as it appears in Molecular Cell, 2015. The authors of this study are Wenbo Li, Yiren Hu, Soohwan Oh, Qi Ma, Daria Merkurjev, Xiaoyuan Song, Xiang Zhou, Zhijie Liu, Bogdan Tanasa, Xin He, Aaron Yun Chen, Kenny Ohgi, Jie Zhang, Wen Liu, and Michael G. Rosenfeld. The dissertation author was co-first author of the paper, contributing to this study through performing all the experiments and leading all the analysis related to condensin II, as well as intellectual input.

# Chapter 2: JMJD6 Licenses Estrogen Receptor α-Dependent Enhancer and Coding Gene Activation by Modulating the Recruitment of the CARM1/ MED12 Co-activator Complex

## INTRODUCTION

The steroid hormone estrogens (17-b-estradiol, estradiol, $E_2$) play a vital role in various biology processes, such as normal mammary gland development, brain development, and reproduction(Couse and Korach, 1999). However, prolonged exposure to high levels of estrogen can lead to breast cancer by constitutively activating the transcription of genes predominantly implicated in metabolism and cell cycle regulation. Estrogen effects on normal mammary gland development and breast tumorigenesis are mediated by two receptors, estrogen receptor alpha (ERα) and beta (ERβ), which function in the nucleus as estrogen-dependent transcription factors. Upon estrogen binding, ERα undergoes a conformational change and translocates from cytosol to nucleus to bind to specific estrogen response elements (ERE) and regulates gene expression. Estrogen-dependent gene expression requires a highly coordinated and complex interplay between various transcription factors, epigenetic enzymes involving in post-translational modifications on histones, epigenetic readers and chromatin remodelers(Hervouet et al., 2013). For instance, bromodomain-containing protein 4 (BRD4) has been shown to play an important role in promoting estrogen-regulated transcription and proliferation of ER-positive breast cancer cells(Feng et al., 2014; Nagarajan et al., 2015; Nagarajan et al., 2014; Osmanbeyoglu et al., 2013). Despite the plethora of proteins that have been

identified to play important roles in ER-positive breast cancers, a deeper understanding of the underlying molecular mechanisms is needed to uncover novel therapeutic targets and develop new drugs for treating ER-dependent breast cancers.

Enhancers, genomic regulatory elements described about forty years ago, are well established to play key roles in controlling regulated tissue-specific gene expression(Bulger and Groudine, 2011a; Heintzman et al., 2009; Ong and Corces, 2011; Plank and Dean, 2014a). Genomic features including histone modifications (e.g., H3K4me1/2, H3K27Ac), coactivators (e.g., CBP, p300, MED1, MED12), and an open chromatin architecture (e.g., DNase I hypersensitivity) have been identified as signatures of enhancers(Natoli and Andrau, 2012b). Differential decoration of enhancers with these features in a given cell may define distinct classes of enhancers that specify distinct gene expression profiles and biological outcomes. ChIP-seq analysis of ERa under estrogen stimulation revealed that majority of its genomic binding sites localized on distal enhancers(Carroll et al., 2006; Li et al., 2013b). More recently, several studies have shown that many enhancers are loaded with RNA Pol II and associated with the production of transcription, namely enhancer RNAs (eRNAs)(De Santa et al., 2010; Djebali et al., 2012; Hah et al., 2011; Heinz et al., 2013; Kim et al., 2010b; Lai et al., 2013b; Lam et al., 2013b; Melgar et al., 2011b; Melo et al., 2013b; Mousavi et al., 2013b; Natoli and Andrau, 2012b; Wang et al., 2011; Wu et al., 2014b). eRNAs have been defined as short transcripts (50-2000 nucleotides) that are transcribed bi-directionally, or sometimes uni-directionally, from enhancer regions(Kim et al., 2010b). Although whether eRNAs themselves are functional remains to be unequivocally proven, many

studies have clearly demonstrated that enhancer transcription occurs before coding gene activation and may help to create an open chromatin environment, facilitate promoter and enhancer looping, or contribute to coding gene transcriptional regulation(Heinz et al., 2013; Hsieh et al., 2014b; Lai et al., 2013b; Lam et al., 2013b; Li et al., 2013b; Melo et al., 2013b; Mousavi et al., 2013b; Pnueli et al., 2015; Schaukowitch et al., 2014; Zhao et al., 2016). In addition, enhancer transcription has been suggested to play an essential role in enhancer marker (H3K4me1/2) deposition at de novo enhancers(Kaikkonen et al., 2013b). However, the molecular machinery that controls the appropriate transcriptional output of enhancers and how it participates in subsequent activation of coding genes remains elusive.

One class of proteins that have been shown to be critical for gene transcription is the large family of JmjC domain-containing proteins. One member of this family, the Jmjc domain-containing protein 6 (JMJD6), was originally identified as a phosphatidylserine receptor on the surface of phagocytes(Bose et al., 2004; Fadok et al., 2000; Wang et al., 2003). Subsequent studies demonstrated that it was localized in the nucleus of a cell, suggesting it might possess novel nuclear functions(Cikala et al., 2004; Cui et al., 2004; Hahn et al., 2008; Hahn et al., 2010; Tibrewal et al., 2007). JMJD6 was found to function as an iron ($Fe^{2+}$)- and 2-oxoglutarate (2-OG)-dependent dioxygenase that demethylates methylated arginines as well as hydroxylates lysines on both histone and non-histone proteins(Chang et al., 2007; Gao et al., 2015; Lawrence et al., 2014; Liu et al., 2013; Mantri et al., 2011; Poulard et al., 2014; Tikhanovich et al., 2015; Unoki et al., 2013; Wang et al., 2014a; Webby et al., 2009; Wu et al., 2015). We recently reported

a new transcriptional paradigm in which JMJD6 regulates promoter-proximal Pol II pausing release in a distal manner(Liu et al., 2013). Besides its function in transcriptional control, we and others have shown that JMJD6 also interacts with multiple splicing factors, and is involved in gene splicing control(Heim et al., 2014; Liu et al., 2013; Rahman et al., 2011; Webby et al., 2009). JMJD6 has been implicated in a multitude of biological processes, including embryonic development (Bose et al., 2004; Kunisaki et al., 2004; Li et al., 2003), cell cycle control (Wang et al., 2014a), cellular proliferation and motility (Chen et al., 2014; Lee et al., 2012), adipocyte differentiation (Hu et al., 2015) and development of various types of cancers, such as breast (Aprelikova et al., 2016; Lee et al., 2012; Poulard et al., 2015), lung (Zhang et al., 2013) and colon cancer (Wang et al., 2014a). Previously, we found that expressing JMJD6 could demethylate the repressive H4R3me(2s) mark on a large cohort of ienhancers, as well as demethylating the methylated CAP of 7SK, leading to promoter pause release events at the cognate target coding gene promoter (REF).

The mediator is a large, multi-subunit complex that is conserved from yeast to humans(Malik and Roeder, 2010). The mammalian mediator complex comprises 30 individual subunits that are arranged in four modules called head, middle, tail and kinase modules(Malik and Roeder, 2010; Taatjes, 2010). MED12, a component in the kinase module, is located on X-chromosome and encodes a 2177 amino acid (aa) protein. It has been shown that *med12* gene is essential for early development in mouse and is involved in the transcriptional regulation of many signaling pathways(Philibert and Madan, 2007; Rocha et al., 2010). MED12 has been shown to be implicated in a number of neurological

disorders(Ding et al., 2008; Graham and Schwartz, 2013; Philibert and Madan, 2007; Risheg et al., 2007; Sandhu et al., 2003; Schwartz et al., 2007; Xu et al., 2011), as well as human cancers like uterine leiomyomas, melanoma, breast, prostate, colon and lung cancers(Huang et al., 2012; Schiano et al., 2014; Shalem et al., 2014; Turunen et al., 2014; Wang et al., 2015). Particularly, MED12 was linked to drug resistance in multiple cancer types including breast, colon, lung cancers and melanoma(Huang et al., 2012; Shalem et al., 2014; Wang et al., 2015). However, whether MED12 is involved in estrogen-induced transcriptional program and how its activity is regulated is not fully determined.

In the current study, we found that JMJD6 is specifically recruited onto ERa-bound active enhancers in response to estrogen stimulation, and is required for activation of these enhancers, including RNA Pol II recruitment and eRNA transcription, leading to transcriptional activation of cognate estrogen target genes, exhibiting features of promoter pause release. Affinity purification revealed that JMJD6 interacts with MED12 in the mediator complex, and is required for MED12 recruitment onto ERa-bound active enhancers. Quantitative mass spectrometry (qMS) analysis revealed that, in the absence of JMJD6, MED12 interaction with CARM1 is significantly attenuated, which is found to methylate MED12 at its c-terminus at multiple arginine sites and is required for MED12 recruitment onto ERa-bound active enhancers. Consistent with its role in estrogen/ERa-induced transcriptional program, our findings further reveal that JMJD6 serves as a critical regulator of breast cancer cell growth and tumorigenesis, with potential future therapeutic implications.

## RESULTS

### Estrogen induces JMJD6 binding on ERa-bound active enhancers

We mined breast cancer-linked gene expression data using the Gene Expression-Based Outcome for Breast Cancer Online (GOBO) tool, and found that high expression of JMJD6 was significantly associated with worse survival in estrogen receptor (ER)-positive breast cancer (**Fig. S8A**). This observation, in concert with our recent study demonstrating that JMJD6 regulates gene transcription through its actions on gene enhancers, prompted us to examine the possibility that it might exert critical roles in transcriptional programs regulated by ERa in breast cancer cells. We first examined its binding with chromatin in response to estrogen by using ChIP-seq (chromatin immunoprecipitation coupled with high throughput sequencing) in ERa-positive MCF7 breast cancer cells. MCF7 cells cultured in stripping medium for three days were treated with or without estrogen followed by ChIP-seq with anti-JMJD6 specific antibody. Consistent with our previous study in other cell lines in the absence of regulatory signals, the majority of JMJD6 binding sites without estrogen treatment were found to be localized at distal regions (non-promoter regions) (**Fig. 8A** and **Fig. S8B**). However, upon estrogen treatment, there were additional 629 JMJD6 binding sites which were strongly induced (fold induction (FC) > 2) (**Fig. 8A-8D**). The vast majority of these estrogen-induced JMJD6 binding sites (>90%) were localized at distal regions (non-promoter regions) (**Fig. 8D** and **8E**). Because estrogen effects in MCF7 cells were mainly mediated through ERa binding on distal enhancers, we first analyzed estrogen-induced JMJD6 binding sites to see their correlation with ERa binding and to see whether they

harbor the classical estrogen response element (ERE). Motif analysis revealed that ERE was the most significant enriched motif (P=1e-308) found in estrogen-induced JMJD6 binding sites (**Fig. 8F**). ERa binding was highly enriched on these sites upon estrogen treatment shown by heat map and tag density plot (**Fig. 8G**, the third column, and **Fig. S8C**, top panel on the right). We next assessed whether those estrogen-induced JMJD6 binding sites shared enhancer characteristics, including highly enriched H3K4me1/2, but low levels of H3K4me3. Heat map and tag density plots confirmed they were, indeed, ERa-bound enhancers (**Fig. 8G**, the fourth to the ninth columns, and **Fig. S8C**, the second to the fourth panels). Furthermore, it was reported recently that a group of enhancers, namely active enhancers, were essential for the transcriptional activation of estrogen-induced coding target genes(Li et al., 2013b). These enhancers were decorated with H3K27Ac histone marker and co-activator protein p300, and associated with the highest levels of ERa binding and prevalent enhancer transcripts called enhancer RNAs (eRNAs) in the presence of estrogen, but were devoid of repressive histone markers including H3K9me3 or H3K27me3. Both heat map and tag density plots revealed that H3K27Ac and p300 were indeed induced by estrogen (**Fig. 8G**, the tenth and thirteenth panels, and **Fig. S8C**, the fifth and sixth panels), and ERa levels were much higher on these estrogen-induced JMJD6 binding sites compared to that on all ERa sites (**Fig. S8C**, the top two panels). Repressive histone markers, both H3K9me3 and H3K27me3, were found to be absent (**Fig. 8G**, the fourteenth to seventeenth panels, and **Fig. S8C**, the seventh and eighth panels). Binding of JMJD6, ERa, H3K4me1/2/3, H3K27Ac, p300, H3K9me3 and H3K27me3 on representative active enhancers were shown, such as the

ones nearby classical estrogen-induced coding genes, *FOXC1*, *SIAH2*, *GREB1* and *SMAD7* (**Fig. 8H**, **8I** and **Fig. S8D, S8E**).

**JMJD6 is a determinant of transcriptional activation of ERa-bound active enhancers**

Several studies reported recently that enhancer RNAs (eRNAs) are involved in transcriptional regulation of nearby coding genes(Hsieh et al., 2014b; Kim et al., 2010b; Lai et al., 2013b; Lam et al., 2013b; Li et al., 2013b; Melo et al., 2013b; Mousavi et al., 2013b; Pnueli et al., 2015; Schaukowitch et al., 2014; Zhao et al., 2016). For instance, estrogen-induced eRNAs from ERa-bound active enhancers were critical for the transcriptional activation of cognate estrogen-induced coding genes(Li et al., 2013b). Our observation that binding of JMJD6 is induced on ERa-bound active enhancers prompted us to examine whether JMJD6 is required for enhancer activation (i.e. eRNA production), and therefore estrogen-induced cognate coding gene activation. To this end, Gro-seq (global run-on coupled with high throughput sequencing), which has been proven to be sufficiently robust to detect eRNAs, was performed in MCF7 cells transfected with control siRNA or siRNA specifically against JMJD6 in the presence or absence of estrogen treatment. It was found that eRNAs were dramatically induced bi-directionally on those estrogen-induced JMJD6 binding sites upon estrogen treatment (**Fig. 9A** and **9B**), whereas there was nearly no induction of eRNA expression on those ERa-bound enhancers without JMJD6 co-occupancy (**Fig. S9A** and **S9B**) (compare siCTL (CTL) (+) to siCTL ($E_2$) (+) and siCTL (CTL) (-) to siCTL ($E_2$) (-)), suggesting JMJD6 might be a determinant for estrogen-induced eRNA production. To support this notion, eRNA

production was attenuated on those estrogen-induced JMJD6 binding sites when JMJD6 was knocked down (**Fig. 9A** and **9B**). Significance of the change of eRNA induction by estrogen and by JMJD6 knockdown was demonstrated by box plot (**Fig. S9C** and **S9D**). Serving as a control, JMJD6 knockdown had no significant impact on eRNA production on those ERa-bound enhancers without JMJD6 co-occupancy (**Fig. S9A** and **S9B**). Furthermore, when we classified estrogen-induced JMJD6 binding sites based on ChIP-seq tag intensity into three groups, high, medium and low, it was found that eRNA induction was positively correlated with JMJD6 tag intensity (**Fig. 9C**). The knockdown efficiency of JMJD6 was examined at mRNA and protein level through RT-qPCR and immunoblotting analysis, respectively (**Fig. S9E** and **S9F**).

To validate JMJD6 effects on eRNA production, total RNA extracted from MCF7 cells transfected with control siRNA or siRNA specifically against JMJD6 in the presence or absence of estrogen treatment were subjected to RT-qPCR analysis using primers specifically targeting several ERa and JMJD6 co-bound active enhancers nearby estrogen-induced coding genes, such as *FOXC1*, *SIAH2*, *GREB1*, *NRIP1* and *SMAD7*. Consistent with our observation from meta-analysis (**Fig. 9A**), eRNA production from these active enhancers was induced by estrogen treatment, which was attenuated by *JMJD6* knockdown (**Fig. 9D**). Furthermore, JMJD6 effects on eRNA production were confirmed in *JMJD6* knockout MCF7 cells (**Fig. 9E**), which was generated by using CRISPR (clustered, regularly interspaced, short palindromic repeats)/Cas9-mediated gene editing technology (**Fig. S9G** and **S9H**).

Transcription of eRNA has been shown to be driven by RNA Polymerase II (Pol II). We thus tested whether JMJD6 is required for Pol II recruitment onto active enhancers. Pol II ChIP-seq was performed in MCF7 cells transfected with control siRNA or siRNA specifically targeting JMJD6 in the presence or absence of estrogen. As expected, estrogen induced Pol II recruitment onto those JMJD6/ERa-co-bound active enhancers, and knockdown of *JMJD6* attenuated estrogen effects, which were shown by both tag density plots and heat map analysis (**Fig. 9F** and **9G**). Statistical test for the change of Pol II recruitment by estrogen and JMJD6 effects on such change was performed (**Fig. 9H**). Serving as a control, Pol II binding was not affected on those ERa-bound enhancers that did not exhibit JMJD6 co-occupancy (**Fig. S9I** and **S9J**). Taken together, our data suggested that JMJD6 is a determinant for transcriptional activation of ERa-bound active enhancers, involving estrogen-induced Pol II recruitment and eRNA production.

**JMJD6 is required for estrogen-induced coding gene transcriptional activation**

ERa-bound active enhancers and associated eRNAs have been reported to be required for cognate coding gene transcriptional activation(Li et al., 2013b). We therefore asked whether JMJD6 is required for estrogen-induced coding gene activation based on our Gro-seq described above in MCF7 cells. Of a large cohort of 1,108 genes that were induced by estrogen (FC>1.5) (**Fig. 10A**), expression of 731 of these genes was attenuated following knockdown of JMJD6, representing 66% of all estrogen-induced genes (**Fig. 10B**). These 731 genes are referred to as estrogen-induced and JMJD6-

dependent genes. The expression of these genes in the presence of estrogen in control and *JMJD6* knockdown conditions was shown by heat map (**Fig. 10C** and **10D**). JMJD6 effects on representative estrogen-induced coding gene transcriptional activation were confirmed by RT-qPCR analysis in MCF7 cells with *JMJD6* knockdown and knockout mediated by siRNA and CRISPR/Cas9, respectively (**Fig. 10E** and **10F**).

We recently reported a new paradigm in gene transcriptional regulation, in which JMJD6 localized at distal enhancers to regulate promoter-proximal pausing release and transcriptional elongation of cognate coding genes(Liu et al., 2013). Therefore, we investigated whether those estrogen-induced and JMJD6-dependent genes experience promoter-proximal pausing regulation, and the role of JMJD6 in this process. Promoter-proximal pausing index(Zeitlinger et al., 2007) or traveling ratio (TR)(Reppas et al., 2006) is defined as the relative ratio of Pol II density in the promoter-proximal region and the gene body, which can be calculated based on Gro-seq as it detects transcripts generated in nuclear run-on reactions by RNA Pol II that are engaged in and competent for transcription, and it can precisely distinguish paused Pol II from backtracked and arrested Pol II(Adelman et al., 2005; Core et al., 2008b). Based on our Gro-seq data, vast majority of genes induced by estrogen and dependent on JMJD6 experience promoter-proximal pausing, which was released upon estrogen treatment (i.e., TR was decreased upon estrogen treatment) (**Fig. 10G**). Importantly, knockdown of *JMJD6* abolished estrogen-induced pausing release (**Fig. 10G**). The significance of the TR change caused by estrogen treatment and the impact of JMJD6 on such change was visualized by box plot analysis (**Fig. 10H**). Close examination of the tag density distribution surrounding

transcription start sites (TSSs) (6kb up- and down-stream of TSS) revealed that there was a decrease of tag density at promoter-proximal region, but an increase along the gene body upon estrogen treatment for genes induced by estrogen and dependent on JMJD6, resembling a typical pause release (**Fig. 10I**). Importantly, knockdown of *JMJD6* attenuated estrogen effects on tag density distribution/pausing release (**Fig. 10I**). Taken together, our data suggest that JMJD6 regulates promoter-proximal pausing release and transcriptional activation of a large set of estrogen-induced coding genes.

**JMJD6 regulates MED12 function in estrogen-induced transcriptional activation**

To further explore the molecular mechanisms underlying JMJD6 regulation of estrogen-induced transcription program, we purified JMJD6-associated proteins in an inducible stable MCF7 cell line expressing JMJD6 in the presence of estrogen. First, cells extracts were prepared in relatively low salt concentration (see materials and methods) and subjected to affinity purification followed by mass spectrometry (MS) analysis. Strikingly, 23 out of 30 subunits in the mediator complex were pulled down by JMJD6, with one of the subunits, MED12, had the most unique peptides identified (**Fig. S10A**). To further investigate which subunit might directly interact with JMJD6 on chromatin to regulate estrogen-induced gene transcriptional activation, chromatin-bound fraction (pellet) was extracted and subjected to affinity purification followed by MS analysis. It was found that MED12 was the only subunit in the mediator complex that still remains associated with JMJD6. MED12 has been implicated in the transcriptional regulation of a variety of signaling pathways(Philibert and Madan, 2007). We therefore focused on

investigating the potential physical and functional relationship between JMJD6 and MED12 in estrogen-induced gene transcriptional activation.

JMJD6 and MED12 interaction was confirmed by affinity purification, as described above, followed by immunoblotting with anti-MED12 specific antibodies (**Fig. 11A**). Over-expressed Myc-tagged JMJD6 was found to interact with Flag-tagged MED12 (**Fig. 11B**). The interaction between JMJD6 and MED12 appeared to be direct because purified *in vitro*-expressed proteins were also found to be associated examined by surface plasmon resonance (SPR) assay (**Fig. S10B**). We next sought to test whether MED12 is involved in estrogen-induced gene transcriptional activation, as was the case for JMJD6. MCF7 cells were transfected with control siRNA or siRNA specifically against JMJD6 or MED12 in the presence or absence of estrogen followed by RNA-seq. It was found that JMJD6 and MED12 exerted similar effects on estrogen-induced transcriptional activation (**Fig. S10C**). More specifically, the expression of 61% and 69% of estrogen-induced genes were attenuated following *JMJD6* and *MED12* knock-down, respectively (FC>1.5), with the vast majority of affected genes overlapped (**Fig. 11C**). The impact of JMJD6 or MED12 on the expression of those affected genes was shown by heat map (**Fig. 11D**), and statistical test was performed (**Fig. 11E**). Effects of MED12 on representative estrogen-induced target genes were confirmed by RT-qPCR analysis (**Fig. 4F**). The enhancer transcriptional activation/eRNA production was similarly affected by MED12 (**Fig. 4G**). The knockdown efficiency of *MED12* was examined by RT-qPCR and immunoblotting analysis (**Fig. S10D** and **S10E**). To further explore the functional connection between JMJD6 and MED12, we tested whether MED12 is similarly recruited

onto active enhancers, which might potentially confer MED12 function in estrogen-induced gene transcriptional activation, and whether its recruitment is regulated by JMJD6. To this end, MCF7 cells were transfected with control siRNA or siRNA specifically targeting *JMJD6*, in the presence or absence of estrogen, followed by ChIP-seq analysis with anti-MED12 specific antibody. MED12 binding was found to be significantly increased on those enhancers exhibiting estrogen-induced JMJD6 binding upon estrogen treatment. This was significantly attenuated following *JMJD6* knockdown (**Fig. 11H-11J**). Despite at much lower levels compared to active enhancers, MED12 binding on the promoter regions of those genes induced by estrogen and dependent on both JMJD6 and MED12 was also increased by estrogen treatment, which was attenuated by *JMJD6* knockdown (**Fig. S10F-S10H**). Knockdown of *JMJD6* did not change MED12 expression, as examined by RT-qPCR and immunoblotting analysis (**Fig. S10I** and **S10J**). Our data suggested that JMJD6 exhibits an unexpected role in the recruitment of MED12 to ERa-bound active enhancers to regulate estrogen-induced transcriptional activation.

**JMJD6 is required for MED12 association with CARM1**

We next sought to explore how JMJD6 regulates MED12 association with these enhancers. We hypothesized that JMJD6 might regulate MED12 interaction with other proteins and/or MED12 post-translational modifications, and therefore its association with chromatin on the ERa-bound enhancers. To this end, we first identified the JMJD6-interacting domain in MED12. Interaction assays with MED12 truncations revealed that JMJD6 specifically interacted with C-terminus of MED12, which has been shown to the

interacting domain for many other known MED12 partners(Philibert and Madan, 2007) (**Fig. 12A** and **12B**). The interaction between JMJD6 and c-terminus of MED12 was further confirmed by SPR assay (**Fig. S11A**). To search for the protein(s) interaction with MED12 that might be altered in the absence of JMJD6, wild type (Xu et al.) or *JMJD6* knockout cells were subjected to SILAC labeling, infected with Flag-tagged c-terminus of MED12 in the presence of estrogen, pooled and followed by affinity purification and mass spectrometry (MS) analysis (**Fig. 12C** and **12D**). In addition to known MED12 interacting partners, such as REST(Ding et al., 2008), RCOR1(Ding et al., 2008), Catenin (alpha, beta and delta)(Kim et al., 2006; Rocha et al., 2010), BRD4(Bhagwat et al., 2016) and CARM1/PRMT4(Chen et al., 1999), JMJD6 was also pulled down by MED12, independently confirming JMJD6 and MED12 interaction. Quantitative analysis revealed that the most affected interacting partner with MED12 was CARM1, which is a member in the protein arginine methyltransferase family(Chen et al., 1999). The ratio of the abundance of CARM1 in MED12 pull-downs from wild type (light label, 184.2) and JMJD6 knockout cells (heavy label, 15.8) was 11.658. Decreased binding affinity between CARM1 and MED12 in the absence of JMJD6 was confirmed by immunoblotting analysis (**Fig. 12E, upper panel**).

MED12 has recently been shown to be exclusively methylated by CARM1 at its c-terminus(Wang et al., 2014b), which was required for MED12 binding with chromatin and transcriptional regulation, sensitizing breast cancer cells to chemotherapy drugs(Wang et al., 2015). Based on our quantitative MS analysis above, we hypothesized that JMJD6 might regulate MED12 through modulating CARM1 binding with MED12,

and therefore CARM1-mediated MED12 methylation and chromatin binding. To test this hypothesis, we first confirmed previous findings that CARM1 methylated MED12 at its c-terminus (aa 1616-2177) (**Fig. 12F**). Furthermore, C-terminus of MED12 was found to be only methylated by CARM1 out of all eleven members of the protein arginine methyltransferase (PRMT) family tested (**Fig. 12G**). The activities of all PRMTs have been described in our previous report(Gao et al., 2015). Next, we attempted to identify the arginine methylation sites at c-terminus of MED12, which are presumably catalyzed by CARM1, and examine the change of such methylation in response to JMJD6 depletion by using the MS data collected above in both wild type and J*MJD6* knockout cells. MED12 was found to be heavily methylated at multiple arginine sites in its c-terminus, including arginine 1854 mono- and di-methylation (R1854me1/2), R1859me1/2, R1862me1/2, R1871me1/2, R1899me1/2, R1994me1/2 and R2015me1 (**Fig. S11B**). More importantly, the levels of R1854me1, R1871me1/2 and R1899me1/2 were decreased significantly in JMJD6 knockout cells (**Fig. 12H**), although events at R1854me2, R1859me1/2, R1862me1/2, R1994me1 and R2015me1 could not be accurately quantified. Decrease of arginine methylation on MED12 C-terminus was confirmed by immunoblotting using anti-H3R17me2 (a) antibody, which could largely recognize the methylated substrates for CARM1 (**Fig. 12E, middle panel**). MED12 c-terminus was equally pulled down in both wild type and JMJD6 knockout cells (**Fig. 12E, bottom panel**). We then examined whether knockdown of CARM1 would affect MED12 recruitment to ERa-bound active enhancers. A significant decrease of MED12 binding was observed when cells were transfected with siRNA specifically targeting CARM1,

such as enhancer regions nearby *FOXC1*, *SIAH2* and *GREB1* (**Fig. 12I**). Taken together, our data suggested that JMJD6 modulates MED12 binding with CARM1, which methylates MED12 and is required for MED12 recruitment onto JMJD6 and ERa co-occupied active enhancers.

**JMJD6 is required for estrogen-induced breast cancer cell growth and tumorigenesis.**

Due to its critical role in estrogen/ERa-induced gene transcriptional activation, we then tested whether JMJD6 regulates estrogen/ERa-induced breast cancer cell growth and tumorigenesis. Using MCF7 breast cancer cell line as a model system, we demonstrated that knockdown of JMJD6 decreased the proliferation rate of cells cultured in normal medium as well as in stripping medium followed by estrogen treatment (**Fig. 13A** and **13B**). The effects of JMJD6 on MCF7 cell proliferation in normal medium as well as stripping medium followed by estrogen treatment were confirmed in *JMJD6* knockout cells (**Fig. 13C** and **13D**), which was further demonstrated by colony formation assay (**Fig. 13E** and **13F**). We also found that *JMJD6* knockout decreased cell migration significantly compared with control cells analyzed by wound healing assay (**Fig 13G-13J**).

To test JMJD6 effects on tumor growth *in vivo*, we injected nude mice subcutaneously with control cells or JMJD6 knockout MCF7 cells, with or without estrogen administration. After six weeks, it was found that tumor volume was dramatically induced when mice were estrogen-treated compared to the control group. Importantly, JMJD6 knockout diminished the effects of estrogen-induced tumorigenesis

(**Fig. 13K-13L**). We noted that body weight of mice was decreased slightly with estrogen treatment (**Fig. S12A** and **S12B**). Taken together, our data suggested that JMJD6 is required for estrogen-induced MCF7 breast cancer cell growth *in vitro* and tumor growth in *vivo*.

## DISCUSSION

Enhancers critically regulate both the development of specific cell types, and the subsequent responses of their transcriptional programs by diverse signals, including ligands of nuclear receptors. One of the characteristics of ligand-activated actived enhancers is the production of eRNAs, which, directly or indirectly, exert functional roles in regulating their cognate coding gene transcription. However, the protein factors which govern eRNA production remain poorly characterized. Here, we report that JMJD6 is a critical regulator for estrogen/estrogen receptor (ER)-induced enhancer activation and coding target gene transcription based on its regulated recruitment to ERa-bound active enhancers, affecting both breast cancer cell growth and tumorigenesis. JMJD6 was found to be required for RNA Pol II recruitment and eRNA production on these enhancers, leading to transcriptional activation of cognate estrogen target genes. Mechanistically, JMJD6 was found to be required for MED12 recruitment, a component of the mediator complex, impacting estrogen-induced transcriptional activation.

A number of JmjC domain-containing proteins have been shown to play key roles in breast cancer growth, including LSD1/KDM1A, KDM2 subfamily, KDM3A, KDM4 subfamily, KDM5 subfamily, KDM6A, KDM6B and JMJD6(Berry and Janknecht, 2013;

Kwok et al., 2017; Ramadoss et al., 2017; Taylor-Papadimitriou and Burchell, 2017; Wang et al., 2009). Here we focused on investigating JMJD6 function in breast cancer enhancer function based on our previous observations that JMJD6 binding at enhancers plays a critical role in transcriptional pause release. Consistent with our previous finding that it is mainly localized on distal enhancers, JMJD6 was found to be specifically recruited onto ERa-bound active enhancers upon estrogen stimulation. Importantly, JMJD6 appeared to be a critical determinant for enhancer activation, including RNA Pol II recruitment and eRNA transcription, and knockdown of JMJD6 attenuated the transcriptional activation of vast majority of estrogen-induced coding genes. Specifically, JMJD6 was required for transcriptional pausing release of estrogen-induced coding genes, presumably through its interaction with P-TEFb complex(Liu et al., 2013). To further explore the molecular mechanisms underlying JMJD6 regulation of enhancer and cognate coding gene transcriptional activation, we purified JMJD6-associated proteins in the presence of estrogen. To our surprise, besides BRD4, which is required for JMJD6 binding with chromatin to regulate transcriptional pause release(Liu et al., 2013), 23 out of 30 subunits in the mediator complex were recovered in our purification. Further extraction with high salt from chromatin fraction revealed that MED12 was likely the subunit directly interacted with JMJD6. The role of BRD4 in estrogen-induced enhancer and coding gene transcriptional activation has been recently described(Nagarajan et al., 2014). As might be predicted from their physical interactions, JMJD6 and MED12 co-regulated a large program of estrogen-induced genes, and JMJD6 was required for MED12 to bind to ERa-bound active enhancers. Requirement of JMJD6 for MED12 to

bind with chromatin led us to explore whether JMJD6 might regulate MED12 affinity with its associated proteins and/or MED12 post-translational modifications. Quantitative MS analysis revealed that one of the most dramatically altered MED12 binding protein upon JMJD6 knockdown was CARM1, which has been shown to be involved in estrogen-induced transcriptional activation(Al-Dhaheri et al., 2011; Lupien et al., 2009). Intriguingly, MED12 was recently shown to be exclusively methylated by CARM1 and such methylation was required for MED12 binding with chromatin, sensitizing breast cancer cells to chemotherapy drugs(Wang et al., 2015). We investigated the JMJD6-dependent alterations in MED12 methylation by quantitative MS analysis. Seven arginine residues (R1854, R1859, R1862, R1871, R1899, R1994 and R2015) were found to be methylated with high confidence at the c-terminus of MED12, which nearly covered all the methylation sites, except R1910 and R1912, currently reported in a comprehensive protein post-translational modification database (phosphosite.org). Further analysis revealed that the levels of methylation on several sites (R1854, R1871 and R1899) were significantly reduced in the absence of JMJD6, consistent with the notion that MED12 interaction with CARM1 was attenuated in the absence of JMJD6. It should be noted that, despite the observation that arginine methylation on only three sites was found to be decreased, we can not exclude the possibility that methylation on other sites, which could not be confidently quantified, indeed also decrease in the absence of JMJD6. It should also be noted that not all arginine residues at the C-terminus of MED12 were recovered in our MS analysis. Therefore, the exact methylation site which is critical for MED12 binding with chromatin and its regulated estrogen-induced transcription remains to be

determined. The most likely scenario is that the all the methylation sites combinatorially confer MED12 function herein. Thus, a BRD4, JMJD6, CARM1 and MED12 molecular axis/network was revealed to regulate estrogen-induced transcriptional activation. Intriguingly, based on our previous and current findings along with others, the components in this axis seem to interact highly with each other (**Fig. 14**).

Our data thereby reveal that JMJD6 is required for estrogen/ER-induced transcriptional activation, breast cancer cell growth and tumorigenesis, suggesting JMJD6 might serve as a potential drug target in ER-positive and endocrine therapy-resistant breast cancer. Indeed, JMJD6 has been found to be highly expressed in clinical ERα-positive breast tumor samples(Aprelikova et al., 2016; Lee et al., 2012; Poulard et al., 2015). JMJD6 has been shown to possess, at least two types of enzymatic activities, demethylation(Chang et al., 2007; Liu et al., 2013) and hydroxylation(Webby et al., 2009), which are important for its function in gene transcription and splicing. As JMJD6 function in breast cancer is apparently dependent on its enzymatic activity, developing small molecule inhibitors targeting JMJD6 will provide an additional therapeutic adjunct for ERα-positive and endocrine therapy-resistance breast cancers. Further , small molecule inhibitor capable of interfering with the molecular axis including BRD4, JMJD6, CARM1 and MED12, and antagonizing the enhancer activation program would also be efficacious in battling ERα-positive and endocrine therapy-resistance breast cancer.

## MATERIALS AND METHODS

### Plasmids and Cloning Procedures

JMJD6 was PCR-amplified from p3XFLAG-CMV-10-JMJD6 we reported previously(Liu et al., 2013), and then cloned into pRevTRE (Clontech) or pCMV-myc (Clontech) expression vector. Flag- and HA-tag was added to the amino- and carboxy-terminus of JMJD6 when cloned into pRevTRE vector, respectively. MED12 full length (FL) or truncations were PCR-amplified from cDNAs by using Transstart fastpfu fly polymerase (TransGen Biotech) and then cloned into p3XFLAG-CMV-10 (Sigma), pBobi (Flag- and HA-tag was added to the amino- and carboxy-terminus, respectively), pET-28a (+) (Novagen) or pGEX-6P-1 (Promega) expression vectors.

### SiRNAs and Antibodies

SiRNA specifically targeting *JMJD6* has been described previously*(Liu et al., 2013)*，and siRNA specifically targeting *MED12* (GUACUUAGAUGAUUGCAAATT) was purchased from Qiagen. Anti-JMJD6 (ab10526, used for ChIP-seq, discontinued during the course of this study) and anti-H3R17me2(a) antibodies were purchased from Abcam; anti-MED12 (A300-774A) antibody was purchased from Bethyl Laboratory; anti-Flag (F1804) antibody was purchased from Sigma; anti-HA (3F10) was purchased from Roche; anti-Pol II (SC-899) and anti-Actin (SC-8432) were purchased from Santa Cruz Biotechnology; anti-CARM1 (#12495) was purchased from Cell Signaling Technology.

### SiRNA Transfection, RNA Isolation, and RT-qPCR

SiRNA transfections were performed using Lipofectamine 2000 (Invitrogen) according to the manufacturer's protocol. Total RNA was isolated using RNeasy Mini Kit (Qiagen) following the manufacturer's protocol. First-strand cDNA synthesis from total RNA was carried out using GoScript Reverse Transcription System (Promega), followed by quantitative PCR (qPCR) using AriaMx Real-Time PCR machine (Agilent Technologies). All RT-qPCRs were repeated at least three times and representative results were shown. Sequence information for all primers used to check gene expression was presented in Supplementary Table 2.

**Plasmids Transfection, Lentivirus Packaging and Infection, Immunoblotting and Immunoprecipitation**

Plasmid transfections were performed using Lipofectamine 2000 (Invitrogen) according to the manufacturer's protocol.

Lentivirus Packaging and Infection: HEK293T cells were seeded in culture plates coated with poly-D-lysine (0.1% (w/v), Sigma, P7280) and transfected with pBobi-flag-MED12 (1616-2177)-HA together with packaging vectors, pMDL, VSVG and REV, at a ratio of 10:5:3:2 using Lipofectamine 2000 for 48 hrs. Virus was collected, filtered and added to MCF7 cells in the presence of 10 mg/mL polybrene (Sigma, H9268), followed by centrifugation for 30 mins at 1,500g at 37 °C. Medium was replaced 24 hrs later.

Protein immunoprecipitation and immunoblotting were performed following the protocol described previously(Liu et al., 2013; Liu et al., 2010).

**Cell Proliferation Assay, Colony Formation Assay, Wound Healing Assay, and Tumor Xenograft Assay**

Cell proliferation assay was performed as previously reported(Liu et al., 2010). Cell viability was measured by using a CellTiter 96 AQueous one solution cell proliferation assay kit (Promega) following the manufacturer's protocol. Briefly, MCF7 cells were transfected with siRNA and maintained in normal growth medium for different time points followed by cell proliferation assay. If estrogen ($E_2$) was added, cells were maintained in stripping medium (phenol red free) for two days before treating with or without estrogen ($E_2$, $10^{-7}$ M) for different time points followed by cell proliferation assay. When JMJD6 (Xu et al.) and JMJD6 (KO) were subjected to cell proliferation assay, cells were seeded at the same density and maintained in normal growth medium for different time points followed by cell proliferation assay. If estrogen ($E_2$) was added, cells were seeded at the same density and maintained in stripping medium (phenol red free) for two days before treating with or without estrogen ($E_2$, $10^{-7}$ M) for different time points followed by cell proliferation assay. To measure cell viability, 20 ml of CellTiter 96 AQueous one solution reagent was added per 100 ml of culture medium, and the culture plates were incubated for 1 hr at 37 °C in a humidified, 5% $CO_2$ atmosphere incubator. The reaction was stopped by adding 25 ml of 10% SDS. Data was recorded at wavelength 490 nm using a Thermo Multiskan MK3 Microplate Reader.

For colony formation assays, 2,000 cells, either MCF7 (Xu et al.) or MCF7 (KO), were seeded in one well in a 6-well plate, and colonies were examined 10 days after. Briefly, colonies were fixed with methanol/acid solution (3:1) for 5 mins and stained with 0.1% crystal violet for 15 mins.

For wound-healing assay, cells were grown to confluence in 6-well plates in normal growth medium or stripping medium, and wounds were performed with a p200 pipette tip. After removing cellular debris by washing cells with PBS, three images of each well were taken. The wounded area was measured by using image J and recorded as A0. For cells maintained in stripping medium, estrogen ($E_2$, $10^{-7}$ M) was then added. The cells were then allowed to migrate back into the wounded area, and three images were taken and the wounded area was measured again 24 hrs later and recorded as A1. Cell migration was presented as wound closure (%) = (wounded area (A0-A1)/wounded area A0)×100%.

For Tumor xenograft assay, four group (4 mice/group) of female BALB/C nude mice (age 4-6 weeks) were subcutaneously implanted with $5\times10^6$ of MCF7 (Xu et al.) or MCF7 (JMJD6/KO) cells suspended in DMEM medium without FBS. To supplement the estrogen for MCF7 cell proliferation, each nude mouse was brushed with estrogen ($E_2$, $10^{-2}$ M) every 3 days for the duration of the experiments. All mice were euthanized 6 weeks after subcutaneous injection. Tumors were then excised, photographed and weighted. Animals were housed in the Animal Facility at Xiamen University under pathogen-free conditions, following the protocol approved by the Xiamen Animal Care and Use Committee.

**Generation of JMJD6 Knockout Cell Lines Using CRISPR/Cas9 Gene Editing Technology**

JMJD6 knock out (KO) MCF7 cells were generated by using CRISPR/Cas9 system. Specifically, gRNA sequence (5'-GCTCTCGTAGTAGTTGTGCCGGG-3')

targeting JMJD6 was first cloned into gRNA cloning vector (Addgene, 41824) and confirmed by sequencing. MCF7 cells were then transfected with pcDNA3.3-hCas9 (Addgene 41815) and gRNA expression vectors, followed by G418 (1 mg/mL) selection. Single colonies were subjected to immunoblotting to select knock-out ones, which were further validated by PCR using genomic DNA as template followed by Sanger sequencing. The sequencing information for primer set used was as follows: Forward (F) 5'-GTGCGTTAGTGTCAGGAAGC-3' and Reverse (R) 5'-GCCCAGAGAAAGGTGCGTA-3'.

**Chromatin Immunoprecipitation Coupled with High Throughput Sequencing (ChIP-Seq)**

ChIP was performed following the protocol described previously(Liu et al., 2013; Liu et al., 2010). Briefly, cells were maintained in stripping medium (phenol red free) for three days before treating with or without estrogen ($E_2$, $10^{-7}$ M) for 1 hr. Cells were then fixed with 1% formaldehyde (Sigma) for 10 mins at room temperature (RT) (for MED12 and Pol II ChIP), or fixed with disuccinimidyl glutarate (DSG) (2 mM) (Proteochem) for 45 mins at RT, washed twice with PBS and then double-fixed with 1% formaldehyde for another 10 mins at RT (for JMJD6 ChIP). Fixation was stopped by adding glycine (0.125 M) and incubated for 5 mins at RT, followed by washing with PBS twice. Chromatin DNA was sheared to 300~500 bp average in size through sonication. Resultant was immunoprecipitated with anti-MED12, anti-Pol II or anti-JMJD6 antibody overnight at 4 °C, followed by incubation with protein G magnetic beads (Invitrogen) for an additional 2 hrs. After washing and elution, the protein-DNA complex was reversed by

heating at 65 °C overnight. Immunoprecipitated DNA was purified by using QIAquick spin columns (Qiagen) and subjected to high throughput sequencing.

ChIP-seq sample preparation and computational analysis of ChIP-seq data were performed as described previously except that sequencing reads were aligned to hg19 Refseq database(Zhang et al., 2016). Only when fold change of ChIP-seq tag density in estrogen treatment versus control was larger than 2, this site was considered as estrogen specific. ERa ChIP-seq was from GSE45822; H3K27Ac and p300 ChIP-seq were from GSE62229; MED1 ChIP-seq was from GSE60272; H3K4me3, H3K9me3 and H3K27me3 ChIP-seq were from GSE23701. ChIP-seq data (JMJD6, Pol II and MED12) were deposited in the Gene Expression Omnibus database under accession GSE101562.

**Global Run-On Sequencing (Gro-seq)**

Gro-seq was performed following the protocol as described previously(Liu et al., 2013). Gro-Seq Analysis was performed following the protocol as described previously except that sequencing reads were aligned to hg19 Refseq database (Zhang et al., 2016). EdgeR was used to determine estrogen-regulated gene program ($P<0.001$, $FC>1.5$). Estrogen-regulated gene program was determined by fold change (FC) of gene RPKM (reads per kilobase per Million mapped reads) in control and estrogen-treated samples ($FC>1.5$). Only coding genes with RPKM larger than 0.5, either in control or estrogen-treated sample, were included in our analysis. All Gro-seq data were deposited in the Gene Expression Omnibus database under accession GSE101562.

**RNA Sequencing (RNA-seq)**

Total RNA was isolated using RNeasy Mini Kit (Qiagen) following the manufacturer's protocol. DNase I in column digestion was included to ensure the RNA quality. RNA library preparation was performed by using NEBNext® Ultra™ Directional RNA Library Prep Kit for Illumina (E7420L). Sequencing reads were aligned to hg19 Refseq database by using TopHat 2.1.1. Estrogen-regulated gene program was determined by fold change of FPKM (fragments per kilobase per million mapped reads) in control and estrogen-treated samples (FC>1.5). Only coding genes with FPKM larger than 0.5, either in control or estrogen-treated sample, were included in our analysis.

**Traveling Ratio Calculation**

Traveling ratio (TR) was calculated following the protocol described previously(Liu et al., 2013). Briefly, TR calculated based on Gro-seq tag density was defined as ratio of Gro-seq reads density at the promoter-proximal bin (from -50 to +300 bp surrounding TSS) to that at the gene body bin (from +300 bp to +30K bp). The significance of the change of TR was displayed using box plot and determined using Student's t test.

**Generation of Inducible MCF7 Cells Stably Expressing pRevTRE-Flag-JMJD6-HA and Purification of JMJD6-associated Proteins**

MCF7 cells stably expressing pTet-On-Advanced (Clontech) were transfected with pRevTRE-Flag-JMJD6-HA, and then selected with hygromycin (200 mg/mL). To induce the expression of JMJD6, doxycycline (Dox) was added at a final concentration of 1 mg/mL for 48 hrs. To purify proteins associated with JMJD6, cell extracts were prepared in a buffer containing 50 mM Tris-HCl (pH 7.4), 150 mM NaCl, 1 mM EDTA

and 1% Triton X-100, and then subjected to affinity purification by using anti-Flag M2-agarose, washed extensively and eluted with 3XFlag peptides. Elutes were then subjected to in solution digestion and LC-MS/MS analysis following the protocol described below. To further purify proteins associated with JMJD6 on chromatin, resultant pellets as described above were further extracted with a buffer containing 50 mM Tris-HCl (pH 7.4), 420 mM NaCl, 1 mM EDTA and 1% Triton X-100, and subjected to affinity purification, elution, in solution digestion and LC-MS/MS analysis.

**Stable Isotope Labeling by Amino Acids in Cell Culture (SILAC), Affinity Purification, In Solution Digestion and LC-MS/MS Analysis**

Wild type and JMJD6 KO MCF7 cells were grown in SILAC DMEM (Invitrogen) supplemented with L-lysine/arginine and L-lysine/arginine-U-13C6 (Cambridge Isotope Laboratories), respectively, together with 10% dialyzed FBS, L-glutamine and penicillin/streptomycin for 2 weeks followed by infection with Lenti-viral vectors expressing pBobi-Flag-MED12 (1616-2177)-HA for 48 hrs before adding estrogen ($10^{-7}$ M) for 1 hr. Cells were then lysed in a buffer containing 50 mM Tris-HCl (pH 7.4), 420 mM NaCl, 1 mM EDTA and 1% Triton X-100, pooled and subjected to affinity purification by using anti-Flag M2-agarose, washed extensively with a buffer containing 50 mM Tris-HCl (pH 7.4), 420 mM NaCl, 1 mM EDTA and 1% Triton X-100, and eluted with 3X Flag peptides. Elutes were then subjected to in solution digestion and LC-MS/MS analysis following the protocol described below. The elutes after IP were firstly reduced in 20 mM dithiothreitol (DTT) (Sigma) at 95 °C for 5 mins, and subsequently alkylated in 50 mM iodoacetamide (IAA) (Sigma) for 30 mins in the dark at room

temperature (RT). After alkylation, the samples were transferred to a 10 kD centrifugal spin filter (Millipore) and sequentially washed with 200 μL of 8 M urea for three times and 200 μL of 50 mM ammonium bicarbonate for two times by centrifugation at 14,000 g. Next, tryptic digestion was performed by adding trypsin (Promega) at 1:50 (enzyme/substrate, m/m) in 200 μL of 50 mM ammonium bicarbonate at 37 °C for 16 hrs. Peptides were recovered by transferring the filter to a new collection tube and spinning at 14,000 g. To increase the yield of peptides, the filter was washed twice with 100 μL of 50 mM ammonium bicarbonate. Peptides were desalted by StageTips. MS experiments were performed on a nanoscale UHPLC system (EASY-nLC1000, Proxeon Biosystems) connected to an Orbitrap Q-Exactive equipped with a nanoelectrospray source (Thermo Fisher Scientific). The peptides were dissolved in 0.1% formic acid (FA) with 2% acetonitrile (Cao et al.) and separated on a RP-HPLC analytical column (75 μm´15 cm) packed with 2 mm C18 beads (Thermo Fisher Scientific) using a 4 hrs gradient ranging from 5% to 35% ACN in 0.1% FA at a flow rate of 300 nL/min. The spray voltage was set at 2.5 kV and the temperature of ion transfer capillary was 275 °C. A full MS/MS cycle consisted of one full MS scan (resolution, 70,000; automatic gain control (AGC) value, 1e6; maximum injection time, 100 ms) in profile mode over a mass range between m/z 350 and 1800, followed by fragmentation of the top twenty most intense ions by high energy collisional dissociation (HCD) with normalized collision energy at 28% in centroid mode (resolution, 17,500; AGC value: 1e5, maximum injection time: 100 ms). The dynamic exclusion window was set at 30 s. One microscan was acquired for each MS and MS/MS scan. Unassigned ions or those with a charge of 1+ and >7+ were

rejected for MS/MS. Raw data was processed using Proteome Discoverer (PD, version 2.1), and MS/MS spectra were searched against the reviewed Swiss-Prot human proteome database. All searches were carried out with precursor mass tolerance of 10 ppm, fragment mass tolerance of 0.02 Da, oxidation (Met) (+15.9949 Da), methylation (Arg, Lys) (+14.0266 Da), dimethylation (Arg, Lys) (+28.0532 Da) and acetylation (protein N-terminus) (+42.0106 Da) as variable modifications, carbamidomethylation (Hannedouche et al.) (+57.0215 Da) as fixed modification and three trypsin missed cleavages allowed. Only peptides with at least six amino acids in length were considered. The peptide and protein identifications were filtered by PD to control the false discovery rate (FDR) <1%. At least one unique peptide was required for protein identification.

**Protein Purification from Bacterial Cells or HEK293T Cells**

GST- and His-tagged proteins were expressed in BL21 (DE3) bacterial cells (Stratagene) and purified by using Glutathione agarose (Sigma) and Ni-NTA agarose (Qiagen), respectively, following the protocol described previously(Liu et al., 2013). Flag–tagged proteins were expressed in HEK293T cells and cells were lysed in lysis buffer containing 50 mM Tris-HCl, pH 7.4, 150 mM NaCl, 1 mM EDTA, 1% Triton X-100. Flag–tagged proteins were then affinity-purified by using anti-Flag M2 agarose and washed extensively with washing buffer containing 50 mM Tris-HCl, pH 7.4, 420 mM NaCl, 1 mM EDTA, 1% Triton X-100 before elution with 3X Flag peptides (Sigma).

**Surface Plasmon Resonance**

The binding kinetics between JMJD6 and MED12 was analyzed at room temperature (RT) on a Biacore T200 machine. A CM5 sensorchip (GE Healthcare) was

chemically activated by injecting 100 ml of N-ethyl-N′-3-(diethylaminopropyl) carbodiimide (EDC) (200 mM) and N-hydroxysuccinimide (NHS) (50 mM) (v/v 1:1). *In vitro* purified bacterially-expressed JMJD6 in 10 mM sodium acetate (pH 5) was immobilized on the pre-activated CM5 chip using amine coupling according to the manufacturer's instructions. The remaining ester groups were blocked by injecting 100 μL of 1 M ethanolamine-HCl (pH 9.5). The amount of immobilized JMJD6 was detected by mass concentration-dependent changes in the refractive index on the sensorchip surface, and corresponded to about 10000 resonance units (RU). A serial concentration of MED12 ranging from 1.25 to 20 nM was added at a flow rate of 20 μL/min. When the data collection was finished in each cycle, the sensor surface was regenerated with glycine-HCl (10 mM, pH 2.5). Sensorgrams were fit globally with BIAcore T200 analysis using 1:1 Langmuir binding mode.

***In vitro* Methylation Assay**

*In vitro* methylation assay was performed in methylation buffer (50 mM Tris-HCl, pH 8.0, 20 mM KCl, 5 mM DTT, 4 mM EDTA) in the presence of 2mCi L-[*methyl*-$^{3}$H]-methionine at 37 °C for 1 hr. The reaction was stopped by adding SDS sample buffer followed by SDS-PAGE gel and autoradiogram.

**ACKNOWLEDGEMENTS**

Chapter 2 is an adaptation of a manuscript that is being submitted for publication. The authors of this study are Weiwei Gao, Rongquan Xiao, Wenjuan Zhang, Yiren Hu, Yaohui He, Bingling Peng, Haifeng Shen, Wenjuan Li, Jiancheng Ding, Ying Li, Zhiying

Liu, Michael G. Rosenfeld, and Wen Liu. The dissertation author was co-first author of the paper, contributing to this study through performance of experiments related to Gro-seq, Pol II ChIP-seq, Med12 ChIP-seq, as well as intellectual input.

# Chapter 3: KDM2B and ERα Function as Dual Transcription Brakes to Curb Inflammation

## INTRODUCTION

As a first line of defense against pathogen infections and tissue traumas, inflammation is an innate immune response that needs to be tightly regulated (Smale and Natoli, 2014). Correspondingly, acute inflammation is normally self-resolved and tissue homeostasis is restored after elimination of "alarming" stimuli. However, chronic, unresolved inflammation "fired" by diverse tumor-infiltrating immune cells, activated fibroblasts and local adipose tissue constitutes a tumor promoting microenvironment. By secreting inflammatory mediators like cytokines and chemokines, pro-inflammatory signaling ultimately activates the NFκB pathway in surrounding cells. Upon stimulation, the transcription factor NFκB subunits (p65 and p50) enter the nucleus and bind to NFκB promoter and enhancer elements to regulate target gene transcription, the outcome of which facilitates angiogenesis, cancer initiation, invasion and metastasis(Grivennikov et al., 2010) . Thus, inflammation has been recognized as an enabling characteristic of cancer (Hanahan and Weinberg, 2011). The cancer promoting effects of inflammation depends on the activation of a complex transcriptional program that is both cell-type- and stimulus-specific and involves the dynamic regulation of hundreds of genes (Grivennikov et al., 2010; Smale and Natoli, 2014). Understanding the specific molecular mechanism controlling pro-inflammatory transcription program would help taming it for cancer treatment.

In breast cancer cells, estrogen signaling pathway mediated by estrogen receptor alpha (ERα) plays key growth-promoting roles. Upon binding with estrogen, ERα undergoes conformational changes, translocates into the nucleus, and binds to thousands of estrogen responsive elements (ERE) across the genome, a subset of which are enriched for enhancer-associated histone marks (e.g. H3K27Ac, H3K4me1 and H3K4me2 marks) (Carroll et al., 2006; Hah et al., 2011; Li et al., 2013b). At these putative enhancers, ERα fosters recruitment of co-activators, epigenetic enzymes, and general transcription machinery to activate transcription of enhancer RNAs (eRNAs) as well as corresponding target coding genes involved in cell cycle regulation and metabolism control (Dasgupta et al., 2014; Hah et al., 2013b; Li et al., 2015; Shang et al., 2000). At the same time, ligand-bound ERα is capable of repressing a subset of gene expression, though the molecular mechanism is not fully understood.

As ERα is found in about 75% of breast cancer tumors at the time of diagnosis, it makes these patients appropriate recipients for anti-hormone endocrine therapies (Frasor et al., 2015; Ignatiadis and Sotiriou, 2013). However, the breast cancer cells with hyper active inflammatory signaling exhibit a more aggressive phenotype associated with endocrine therapy resistance, chemotherapy failure, reduced apoptosis and increased metastatic recurrence (Baumgarten and Frasor, 2012). In both patients-derived tumor samples and breast cancer cell lines, cellular ERα concentration is inversely correlated with NFκB activation and DNA binding (Biswas et al., 2000; Zhou et al., 2005). Moreover, NFκB target genes expression is higher in breast tumor samples with lower

ERα expression (Van Laere et al., 2007), indicating that a transrepressive interaction may exist between estrogen and inflammation signaling pathways. While analysis with single genes like TNFα and IL6 have shown that estrogen-ERα impairs NFκB signaling (Galien and Garcia, 1997; Hsu et al., 2000), the effects of estrogen-ERα exerts on pro-inflammatroy genes transcription on a genome-wide scale and the molecular events involved in this regulation are still not completely clear.

As NFκB-mediated inflammation signaling plays such essential roles in breast cancer progression, we are quite interested in finding the molecular "brakes" that are responsible to hold inflammation at bay. Using MCF-7 breast cancer cells as a model, we set to uncover the global impacts estrogen-ERα has on shaping the pro-inflammatory transcription and the molecular mechanism involved. We discovered that estrogen bound ERα specifically repress pro-inflammatory genes transcription upon acute treatment of TNFα. This repression is achieved by tethering of ERα to NFκB enhancer elements to quench the enhancer activity while not affecting NFκB association with DNA. In an effort to find partner molecules for ERα repressive function, we found that ERα recruits GRIP1 as a corepressor to suppress NFκB target genes upon estrogen and TNFα co-treatment. We also uncovered that at basal condition many pro-inflammatory genes are occupied by KDM2B-PRC1 complex and that KDM2B-PRC1 deficiency leads to derepression of a subset of genes normally activated by NFκB. Similar effects of KDM2B deficiency were observed in other ERα-positive breast cancer cells and macrophage as well. Our findings revealed a two-layer transcriptional "brakes" for pro-

inflammatory program: KDM2B functions as a guardian against unwanted pro-inflammatory transcription at basal condition; ligand-bound ERα recruits co-repressor to further inactivate NFκB enhancers.

## RESULTS

### E2-ERα Signaling Represses Pro-inflammatory Gene Activation Program

To investigate how pro-inflammatory response may be affected by estrogen at transcription level, we treated ERα positive MCF-7 breast cancer cells with estradiol (E2), TNFα or both for 1 hour and assayed with global run-on coupled with deep sequencing (Gro-seq). From three biological replicate samples, we identified that 1722 genes are significantly induced by TNFα treatment (fold change>1.5, FDR<0.01,p<0.05). Overall activation of these genes is greatly dampened under simultaneous treatment of E2 and TNFα, as exemplified by the boxplot analysis (Figure 1A). Representative Gro-seq examples of estrogen-ERα repress pro-inflammatory gene activation are shown in Figure 1B. Moreover, the effect on pro-inflammatory gene mRNA level was confirmed by RT-qPCR experiments (Figure S1A).

Further analysis of TNFα activated genes shows that they can be divided into three groups: 1) about 70% of TNFα up-regulated genes (n=1231) are significantly less activated when treated with E2 and TNFα together 2) 269 genes are transcribed at similar level under both conditions 3) the rest 222 genes can be synergistically activated by E2 and TNFα signals (Figure 1C). Gene ontology analysis shows that genes responding to LPS or cytokine stimulus and inflammatory response are predominantly represented in

group 1, suggesting that E2 preferentially down-regulates pro-inflammatory genes (Figure 1D).

To verify that the estrogen repressive effect is mediated by ERα, we "knocked down" ERα by specific siRNA, and examined pro-inflammatory gene expression using RT-qPCR. Indeed, knockdown of ERα abolished E2 repression on pro-inflammatory genes (Figure S1B). Moreover, we found that ERα-negative breast cancer cells exhibit higher expression of pro-inflammatory genes (Figure S1C), consistent with findings that ERα-negative breast tumors compared with ER-positive breast tumors display more active NFκB (Biswas et al., 2004). By transfecting ERα expressing vectors into MDA-MB231 (ERα negative) cells, we were able to repress pro-inflammatory genes expression, indicating the potent anti-inflammatory effects of ERα (Figure S1D).

**ERα is Tethered to NFκB Active Enhancers Upon E2 and TNFα Treatment**

To understand how ERα represses pro-inflammatory gene expression, we performed chromatin immunoprecipitation assays coupled with next-generation sequencing (ChIP-seq) using antibodies specific for ERα and p65 (a key subunit of NFκB) respectively. Following TNFα treatment, NFκB enters into the nucleus and binds to DNA cis-regulatory elements at enhancers to promote pro-inflammatory transcription(Kaikkonen et al., 2013b). Focusing on the group 1 genes which were activated by TNFα but repressed upon addition of E2, we identified ~1200 NFκB enhancers which are intergenic regulatory elements exhibiting TNFα-induced p65 binding and the enhancer histone mark H3K4me2 enrichment(Heinz et al., 2010b). Upon E2 and TNFα co-stimulation, ERα was recruited to these NFκB enhancers as detected by

ChIP-seq experiment (Figure 2A). Interestingly, genomic regions that gained ERα binding exhibit highly significant enrichment for motifs recognized by NFKB1/p65, FOXA1 but not ERα itself (Figure 2B), leading to the hypothesis that ERα is tethered to NFκB enhancers independent of its own DNA binding ability. To test if this is the case, we generated HA-tagged ERα inducible cell lines with or without DNA binding domain mutations (Figure S2A and S2B) and performed ChIP-seq using antibody targeting the HA-tag. From ChIP-seq analysis, we found that P-Box mutations substantially reduce ERα binding at active estrogen responsive ERE-containing enhancers (Figure S2C), which is consistent with previous reports that E203G/G204S/A207V mutations in P-Box would disrupt binding of ERα to its cis-DNA binding motif (ERE) (Mader et al., 1989; Stender et al., 2010). On the other hand, ERα binding to NFκB enhancers is largely preserved regardless of the mutations, indicating that ERα recruitment to NFκB enhancers is through a tethering mechanism (Figure 2C).

**Tethered ERα Represses NFκB Enhancers Activity**

Interestingly, upon E2 and TNFα co-stimulation, p65 or p50 binding doesn't change much as compared to TNFα treatment condition (Figure S2D). Similarly, the histone H3K4me2 level stays the same at previously identified NFκB Enhancers (Figure 2D). However, in response to ERα tethering, we observed significant decrease of active enhancer histone marks H3K27ac as well as H4K20ac at NFκB enhancers, suggesting that enhancer activity decreases following addition of E2 (Figure 2E). The histone acetyl transferase p300 binding was markedly inhibited as well (Figure 2E). Correspondingly, the transcripts from the putative NFκB enhancers (eRNAs) decreased upon ERα tethering

(Figure 2F). To test if the enhancers we identified are responsible for transcription changes at nearby coding gene, we constructed inducible dCas9-KRAB MCF-7 cell line to specifically shut-down target enhancer transcription and observe its effects on neighboring coding gene. By designing sgRNA targeting NFκB enhancers (e.g. IL6, IL8), we were not only able to repress eRNA production at target loci but also capable of repress the neighboring pro-inflammatory genes (Figure S2E). These further support that tethering to NFκB enhancers underlies ERα repressive effects on pro-inflammatory transcription program.

**KDM2B Prevents Inflammatory Gene Transcription at Basal Condition**

Intrigued to solve the question how ERα tethering may lead to NFκB enhancers inactivation, we first searched for potential co-repressors that ERα might utilize. We conducted a siRNA-based small-scale screening with classical nuclear receptor co-repressors, histone deacetylases and histone demethylases as candidates. We found that both GRIP1 and histone demethylase KDM2B knockdown were able to reverse ERα repressive effects on target genes (Figure 3A and 3B). While GRIP1 has been recognized as a co-repressor for GR in repressing LPS-induced inflammation in macrophage (Chinenov et al., 2012), we decided to investigate the KDM2B functional mechanism first.

After knocking down KDM2B with two different siRNAs respectively, we used RNA-seq to examine the resulting E2 repressive effects on pro-inflammatory genes. We found that both siRNAs targeting KDM2B were able to reverse the anti-inflammation effects of E2-ERα (Figure S3A). More interestingly, pro-inflammatory genes like IL6

and CCL2 became actively transcribed after KDM2B knockdown without external TNFα stimulation (Figure S3B), suggesting that KDM2B functions as a "gatekeeper" for pro-inflammatory genes expression even at basal condition. Indeed, for the TNFα activated genes, knocking down KDM2B elevated the expression level as shown by RNA-seq analysis (Figure S3C). To check if the regulation happens at transcription or post-transcription steps, we performed Gro-seq experiment with control siRNA and siRNA targeting KDM2B. We found that knockdown of KDM2B activated more than half of the previously identified TNFα activated genes (Figure 3C). Moreover, we also observed an up-regulation of neighboring enhancer transcription exemplified by the eRNA level (Figure 3D). Gene Ontology analysis shows that the group of genes activated by KDM2B knockdown is enriched for cytokine response or NFκB signaling (Figure S3D) while genes repressed by siKDM2B do not show such enrichment (Figure S3E). Correspondingly, when we analyze p65 binding at the up-regulated gene loci, we found an induced recruitment of p65 after knockdown of KDM2B, suggesting that activation of pro-inflammatory gene in KDM2B deficient cells is NFκB-dependent (Figure 3E). Representative examples of siKDM2B effects on pro-inflammatory genes transcription are shown in Figure 3F. Additionally, knockdown of KDM2B in other ERα positive breast cancer cells, for example, T47D and ZR75-1 cells, induced inflammatory genes expression to a similar level, suggesting that KDM2B prevents unwanted onset of pro-inflammatory transcription may be a general protective mechanism against inflammation (Figure S3F).

**KDM2B Nucleates PRC1 Complex to Repress Inflammation**

Interested in how KDM2B functions as a 'gatekeeper' to prevent inflammation, we first explored KDM2B binding with chromatin by using ChIP-seq in MCF-7 cells. While using commercial KDM2B antibodies could not generate robust ChIP-seq result, we turned to a HA-tag-based approach to overcome the technical limitations. To this aim, we engineered the MCF-7 cells to stably express HA-tagged KDM2B, and used antibody specific for HA peptide to perform ChIP-seq. In total we identified around 25,000 KDM2B binding sites, 5324 of which overlap with TNFα-treated p65 binding loci (Figure 4A). The p65 and KDM2B co-occupied sites include previously identified NFκB enhancers (Figure 4D), which correlate with enhancer RNA transcription up-regulation after KDM2B knock down (Figure 3E).

While previously KDM2B has been recognized as an H3K36 specific demethylase(He et al., 2008), we performed H3K36me2 ChIP with or without siRNA targeting KDM2B. Exemplified by the qPCR result, H3K36me2 level didn't change much after KDM2B knock down, indicating that KDM2B anti-inflammation function is independent of its H3K36 demethylase activity (Figure S4A). Furthermore, when we performed "gain-of-function" analysis by overexpressing KDM2B in MCF-7 cells, we found that both wild type KDM2B and demethylase mutant (H242A, I243A, D244A) were able to repress pro-inflammatory gene expression at basal condition as well as after TNFα treatment as shown by RT-qPCR (Figure S4B and S4C). Altogether, these suggest that KDM2B represses inflammation independent of its demethylase activity.

To explore the molecular partners of KDM2B in mediating the repressive effects, we performed immunoprecipitation followed by mass spectrometry (IP-MS) experiment

with MCF-7 nuclear lysate stably expressing HA-tagged KDM2B. Besides KDM2B itself, we also pulled down several components of a variant Polycomb group Repressive Complex 1 (PRC1) like BCOR, PCGF1, Ring1A and Ring1B (Figure 4B), which is consistent with previous findings that KDM2B may form a variant PRC1 complex in mouse embryonic stem cells (Blackledge et al., 2014; Farcas et al., 2012; He et al., 2013; Lagarou et al., 2008). We next pulled down KDM2B with antibody specific for KDM2B and examined by western blot for its association with polycomb group proteins. Indeed, KDM2B could interact with BCOR and Ring1A of PRC1 complex (Figure 4C). Pull down of PRC1 components and EZH2 also confirmed the interaction (Figure S4D). Moreover, heat map analysis of ChIP-seq data demonstrated that 1) the KDM2B-p65 co-occupied sites are enriched for Ring1A and Ring1B binding 2) while the p65 binding sites not bound by KDM2B are devoid of PRC1 components. This leads to the hypothesis that KDM2B nucleates PRC1 complex and potentially further recruits PRC2 complex to repress inflammatory gene transcription.

To test if polycomb group proteins are involved repressing inflammation, we knocked down BCOR, Ring1A, and EZH2 using specific siRNAs and assessed pro-inflammatory genes expression by RNA-seq. Indeed, knockdown of each of these polycomb proteins, just like knockdown of KDM2B, induced the expression of pro-inflammatory genes (Figure 4E). Similarly, RT-qPCR analysis confirmed the finding (Figure S4E). Moreover, we checked the polycomb group proteins binding at NFκB sites with siRNA control or siRNA targeting KDM2B. By ChIP-qPCR analysis, we found that polycomb group proteins binding to inflammatory gene enhancers and promoters

decreased upon KDM2B knockdown, indicating that KDM2B recruits polycomb group proteins to repress inflammation at basal condition (Figure 4F).

**KDM2B Represses Cytokine Production in Macrophage**

Obsessed by the discovery that KDM2B and ERα form a two-layer restrictive mechanism to precisely control inflammatory gene transcription program in ER positive breast cancer, we wondered if similar mechanism exists in other tissue or organism, for example, immune cells. Interestingly, employing qRT-PCR to examine the kinetics of KDM2B expression in mouse macrophage RAW 264.7 cells (RAW cells) exposed to LPS, we identified that KDM2B mRNA was suppressed to half just 2 hours after LPS treatment (Figure 5A). Furthermore, the KDM2B protein level decreases at 4 hours post LPS stimulation (Figure S5A). By mining the RNA-seq data of bone marrow-derived dendritic cells (BMDC) and bone marrow-derived macrophage (BMDM) with or without LPS treatment (Bhatt et al., 2012; Das et al., 2015; Zhang et al., 2015), we found that KDM2B levels in dendritic cells as well as macrophages are also down regulated in response to LPS treatment (Figure S5B).

To test our hypothesis that KDM2B regulates inflammation responsive genes in immune cells, we knocked down KDM2B in RAW cells using two different shRNAs respectively and compared cytokine gene expression with shCTL cells. By RT-qPCR, we found that efficient knockdown of KDM2B leads to enhanced basal expression of pro-inflammatory genes like IL6 and CCL2 (Figure 5B). To assess the impact of KDM2B deficiency on pro-inflammatory genes expression in macrophages, we performed transcriptome analysis using RNA-seq in resting RAW cells with the above-mentioned

two shKDM2Bs. With two biological replicates, we were able to capture 1624 genes up-regulated by both shRNAs targeting KDM2B and 880 genes down-regulated by both shRNAs (Figure 5C). With gene ontology enrichment analysis, we found that genes activated by KDM2B knockdown are enriched for regulation of response to external stimulus, cell migration, cytokine production and response to cytokine (Figure 5D, complete list see supplementary table), suggesting that KDM2B regulates part of pro-inflammatory genes expression in resting macrophages as well.

Next, we performed "gain-of-function" analysis by overexpressing KDM2B in RAW cells and stimulated cells with LPS to check its impacts on LPS-responsive genes expression. Compared to lentiviral vector control, overexpression of KDM2B squelched activation of cytokine genes like IL6, CCL2 (Figure S5C), which further supports the hypothesis that KDM2B is a negative regulator of pro-inflammatory gene expression in macrophage.

**GRIP1 is a Co-repressor for ERα in Repressing Pro-inflammatory Genes**

Subsequently, we moved on to investigate the second layer of inflammation repression—GRIP1 functions as a co-repressor partner for ERα. Previously, GRIP1 has been implicated in mediating ERα repressive effect on single genes like TNFα (An et al., 1999; Cvoro et al., 2006). To get a comprehensive assessment of the repressive effects of GRIP1 on TNFα induced transcriptome, we performed RNA-seq on MCF-7 samples with siRNA CTL or siRNA specific for GRIP1 under TNFα or E2 plus TNFα conditions. We found that indeed siGRIP1 caused de-repression of ERα suppressed pro-inflammatory genes as shown by boxplot analysis as well as heat map (Figure 6A and 6B).

Next, we explored the chromatin binding profile of GRIP1 through ChIP-seq analysis. We found that in response to E2 plus TNFα GRIP1 gains binding to our previously defined NFκB enhancers similar to ERα (Figure 6C). While knock down of GRIP1 does not affect ERα binding on NFκB enhancers, knock down of ERα decreases GRIP1 loading on pro-inflammatory gene loci (Figure 6D), suggesting that GRIP1 is recruited by ERα as a co-repressor to suppress pro-inflammatory genes. Furthermore, through comparing Pol II ChIP-seq at siCTL condition with siGRIP1 condition, we found that E2 would trigger a genome wide promoter-proximal pausing of Pol II at NFκB target genes and that knockdown of GRIP1 would lead to release of the paused Pol II (data not shown),suggesting that GRIP1 repressive functions may in part dependent on RNA polymerase II pausing machinery.

Altogether, our study uncovered an intricate two-layer mechanism controlling pro-inflammatory genes transcription. On the basal layer, KDM2B nucleates PRC1 complex at NFκB sites to prevent pro-inflammatory gene expression. With the addition of E2 and TNFα, ERα is tethered to inflammatory gene enhancers and recruits co-repressor GRIP1 to induce Pol II promoter proximal pausing such that suppression of pro-inflammatory genes is achieved.

ACKNOWLEDGEMENTS

Chapter 3 and 4 are currently being prepared for submission for publication. Yiren Hu, Yuliang Tan, Jia Shen, Wubin Ma, Feng Yang, Haifeng Shen, Kenny Ohgi, Jie

Zhang and Michael G. Rosenfeld are participants of the project. The dissertation author was the primary investigator and author of this paper.

# Chapter 4: Discussion

Chronic, unresolved inflammation fuels breast cancers to develop endocrine therapy resistance, chemotherapy failure and high recurrence of metastasis (Baumgarten and Frasor, 2012). About 75% of breast tumors express ERα. The expression level of ERα inversely correlates with inflammation activity in breast cancer cell lines as well as patients tumor samples. Does ERα have anti-inflammatory activity? If so, how is NFκB transcription program being shaped by estrogen-ERα signaling pathway? Our current study unveiled the global effects estrogen-ERα exerts on pro-inflammatory transcription program. Through transcriptome analysis, we found that estrogen treatment would specifically repress about 70% of TNFα stimulated genes, which are enriched for inflammatory response pathway. Furthermore, genome wide ChIP-seq results show that ERα is tethered to NFκB enhancers to "decommission" the enhancers thus represses corresponding target genes transcription. Using siRNA-based screening strategy, we uncovered two distinct inflammation repressors: KDM2B and GRIP1. GRIP1 is a corepressor recruited by ERα. Upon binding to NFκB enhancers, ERα-GRIP1 induced promoter-proximal pausing of Pol II in target coding genes. On the other hand, we found that KDM2B nucleates PRC1 complex at NFκB sites to prevent pro-inflammatory genes activation at the basal condition. Moreover through RNA-seq analysis, we found that KDM2B functions as a checkpoint for cytokine genes expression in macrophage, suggesting that the two-layer inflammatory restriction mechanism we found here may have broader impacts in other cell types as well.

**Estrogen-bound ERα is Tethered to Repress NFκB-dependent Pro-inflammatory Transcription Program**

The anti-inflammation activity of ERα has been observed before based on single gene expression analysis. Our study provides a global picture of how ERα-mediated estrogen signaling shapes the transcriptional landscape of NFκB-orchestrated inflammatory pathway using human breast cancer MCF-7 cells as a model. While majority (70%) of the NFκB stimulated genes are suppressed by ERα, there are about 200 genes synergistically regulated by both signaling pathways, consistent with previous findings (Franco et al., 2015; Frasor et al., 2009; Pradhan et al., 2010). Furthermore, through ChIP-seq experiments for ERα and p65, we found that ERα is tethered to NFκB enhancers to repress pro-inflammatory genes expression and that ERα binds to ERE motif-containing regulatory elements near the synergistically regulated genes to activate target genes (data not shown). This suggests a model that tethered ERα (or trans-bound ERα) leads to transcription silencing while direct-DNA binding of ERα is associated with transcription activator function, which is in line with transrepression activity described for nuclear receptors like PPARγ and LXRs (Glass and Saijo, 2010). This puts structural analysis of nuclear receptors transcription activity switch under cis- or trans- DNA binding condition an interesting direction for future investigation. Also, to circumvent inflammation induced aggressive breast cancer progression, structure-based screening for non-steroid ligands that enable ERα transrepression of inflammation but avoid activating the ERα cell proliferation pathways may provide appealing alternatives for current anti-estrogen therapies.

**GRIP1 Functions as a Transcriptional Corepressor for ERα to Suppress Inflammation**

Different hypothesis about the mechanism contributing to ERα repressive activities have been proposed: 1) activated ERα inhibits NFκB nuclear translocation (Ghisletti et al., 2005) 2) ERα prevents NFκB (especially p65) DNA binding (Paimela et al., 2007) 3) competition between ERα and NFκB for transcription coactivators (Nettles et al., 2008) 4) ERα interacts with transcription repressors which leads to less potent activation of pro-inflammatory genes (Cvoro et al., 2006). Here, we found that in response to acute inflammation, NFκB nuclear translocation or binding at target gene promoters and enhancers is not affected by ERα. Furthermore, through RNA-seq analysis we found that GRIP1 is recruited by ERα to the NFκB enhancers and functions as a corepressor to suppress pro-inflammatory gene expression on a global scale. These observations support the model that ERα interacts with transcriptional corepressor(s) to exert anti-inflammatory effects.

GRIP1, together with NCOA1 and NCOA2 belong to the p160 nuclear receptor coregulators family. Members of p160 family exhibit roughly 60% similarity to each other and are transcriptional coactivators for nuclear receptors like GR, ERs, LXRs and PPARs (Rollins et al., 2015). Surprisingly, GRIP1 has been identified to participate in GR-mediated repression of inflammatory genes in macrophage. And the repression activity is dependent on a repression domain (RD) located between GRIP1's Nuclear Receptor Interaction domain and Activation Domain (AD), which is absent from other p160 family proteins (Rogatsky et al., 2002; Rogatsky et al., 2001). In our unpublished

data, we found through immunoprecipitaion followed by mass spec (IP-MS) experiment that RD of GRIP1 could interact with NELF-A, an essential component of the Negative Elongation Factor (NELF) complex. This may help explain the promoter proximal pausing of Pol II upon ERα and GRIP1 binding. Interestingly, recently GRIP1 has been found to be a substrate of CDK9, and phosphorylation of GRIP1 potentiates its coactivator but not corepressor activities (Rollins et al., 2017). These indicate that unphosphorylated GRIP1 with tethered ERα may repress transcription through stabilizing NELF and other negative regulators association with pro-inflammatory gene promoters. Thus, it is interesting for future study that how enhancer-bound ERα/GRIP1 promotes neighboring target gene PolII promoter proximal pausing. Moreover, our study may shed light on the underlying molecular mechanisms of estrogen's beneficial effects in bone, cardiovascular tissues, and neural system.

**KDM2B Functions as a Checkpoint for NFκB induced Gene Transcription**

Intricate molecular mechanisms have been discovered to control pro-inflammatory gene transcription at activation, amplification and resolution stages, while little is known about the "safeguards" against unwanted onset of inflammatory gene activation at basal condition. Unexpectedly, in an effort to find molecular partners for ERα repressive activity, we found that KDM2B premarks the NFκB regulatory elements at basal condition and prevents pro-inflammatory genes from active transcription. The anti-inflammation activity of KDM2B is independent of its demethylase function but relies on nucleating the PRC1 complex proteins onto NFκB enhancers. Previously,

KDM2B-PRC1 has been found to mark and silent the bivalent promoters of developmental genes to maintain murine embryonic stem cell status (Farcas et al., 2012; He et al., 2013). Our findings suggest that this conserved safeguard mechanism is not only important for maintaining stem cell identity but also extends to protect somatic cells like breast epithelial cells and macrophages against pro-inflammatory cytokine challenges. Recently, a long noncoding RNA named lincRNA-EPS has been found to repress pro-inflammatory gene transcription (Atianand et al., 2016). Next step, it is interesting to investigate if KDM2B-PRC1 repression function has a lincRNA component. And more intriguingly, what determines the target specificity of KDM2B-PRC1 towards pro-inflammatory genes? Further analysis with transcription factors binding profile and epigenetic landscape at pro-inflammatory genes regulatory elements may lead to deeper understanding of the "gatekeepers" that repress inflammation transcription at basal condition, which ultimately will help us taming the inflammatory responses to re-establish body homeostasis.

ACKNOWLEDGEMENTS

Chapter 3 and 4 are currently being prepared for submission for publication. Yiren Hu, Yuliang Tan, Jia Shen, Wubin Ma, Feng Yang, Haifeng Shen, Kenny Ohgi, Jie Zhang and Michael G. Rosenfeld are participants of the project. The dissertation author was the primary investigator and author of this paper.

**Figure 1: Estrogen-Induced Loading of Condensins to ER-α-Bound Active Enhancers, Continued**

(A) A cartoon diagram showing the subunit constituents of the condensin I and condensin II complexes.
(B) Chromatin fractionation followed by western blots showing the localization of condensin subunits in MCF-7 cells upon $E_2$ or ICI treatment.
(C) Venn diagram showing the genome-wide ChIP-seq peak numbers of NCAPG and NCAPH2 and their overlap with that of ER-α in $E_2$-treated MCF-7 cells.
(D) Heatmaps showing ChIP-seq data of condensin I (NCAPG, NCAPH, NCAPG [Y.K.]) and condensin II (NCAPH2) together with p300, RNA Pol II, and active histone marks H3K4me$^2$ and H3K27Ac on active enhancers (n = 1,248) in MCF-7 cells (±$E_2$), with scales indicated. The map was sorted vertically by the binding intensity of ER-α.
(E) A snapshot of the UCSC genome browser (hg18) showing the ChIP-seq tracks of condensin subunits, ER-α, input control, and GRO-seq (+ and − denote the transcription of two strands) in *TFF1*locus (signals under ± $E_2$ treatment are represented by two colors).
(F and G) Profile plots showing normalized ChIP-seq or GRO-seq tag intensities (±$E_2$) of ER-α, NCAPG, NCAPH2, p300, RNA Pol II, and eRNAs on the active enhancer group (n = 1,248) compared to "primed enhancers" (n = 5,763). See Figure S2A for other features of these two groups. *TFF1e*, *TFF1* enhancer (an intronic enhancer localized in the *TMPRSS3* gene).
(H) Hierarchical cluster analysis showing the correlation between the $E_2$-induced recruitment of the interrogated transcription factors and histone modifications on the 1,248 active enhancers. Pairwise Pearson correlation coefficients (PCC, scaled on top of the heatmap) between samples are shown. The heatmap with red-green gradient denotes the fold (log2) of induction in response to $E_2$ (scale indicated). All heatmaps and profiles are centered on ER-α binding sites in +$E_2$ situation.

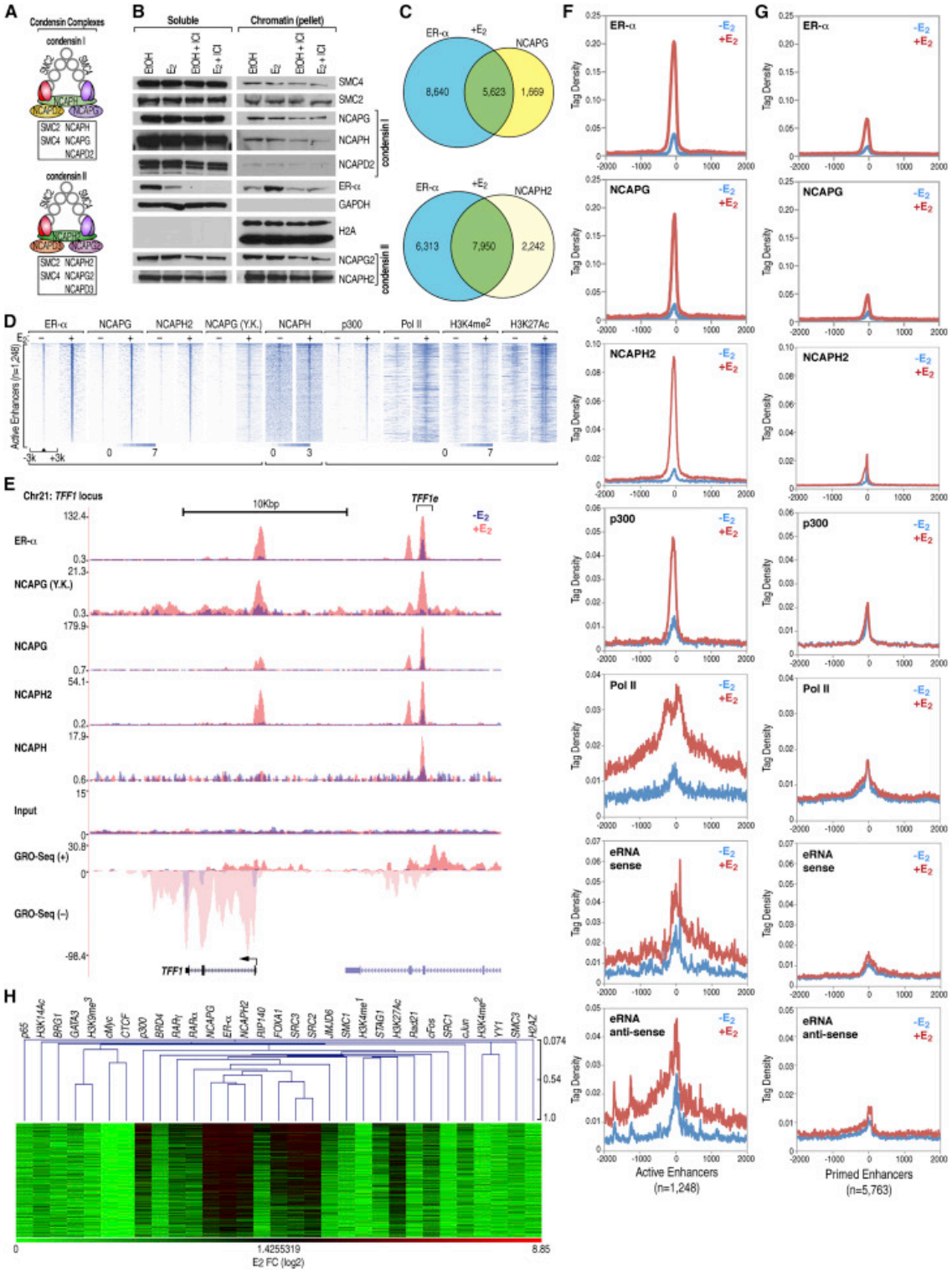
A
Condensin Complexes
condensin I
SMC2 NCAPH
SMC4 NCAPG
NCAPD2
condensin II
SMC2 NCAPH2
SMC4 NCAPG2
NCAPD3
B
Soluble
Chromatin (pellet)
EtOH
E2
EtOH + ICI
E2 + ICI
SMC4
SMC2
NCAPG
NCAPH
NCAPD2
condensin I
ER-α
GAPDH
H2A
NCAPG2
NCAPH2
condensin II
C
ER-α
+E2
NCAPG
8,640
5,623
1,669
ER-α
+E2
NCAPH2
6,313
7,950
2,242
D
ER-α
NCAPG
NCAPH2
NCAPG (Y.K.)
NCAPH
p300
Pol II
H3K4me2
H3K27Ac
E2:
Active Enhancers (n=1,248)
-3k
+3k
E
Chr21: TFF1 locus
10Kbp
TFF1e
-E2
+E2
ER-α
NCAPG (Y.K.)
NCAPG
NCAPH2
NCAPH
Input
GRO-Seq (+)
GRO-Seq (–)
TFF1
H
p65
H3K14Ac
BRG1
GATA3
H3K9me3
cMyc
CTCF
p300
BRD4
RARγ1
RARα
NCAPG
ER-α
NCAPH2
RIP140
FOXA1
SRC3
SRC2
JMJD6
SMC1
H3K4me1
STAG1
H3K27Ac
Rad21
cFos
SRC1
cJun
H3K4me2
YY1
SMC3
H2AZ
0.074
0.54
1.0
0
1.4255319
8.85
E2 FC (log2)
F
ER-α
NCAPG
NCAPH2
p300
Pol II
eRNA sense
eRNA anti-sense
Tag Density
-E2
+E2
Active Enhancers
(n=1,248)
G
ER-α
NCAPG
NCAPH2
p300
Pol II
eRNA sense
eRNA anti-sense
Tag Density
-E2
+E2
Primed Enhancers
(n=5,763)

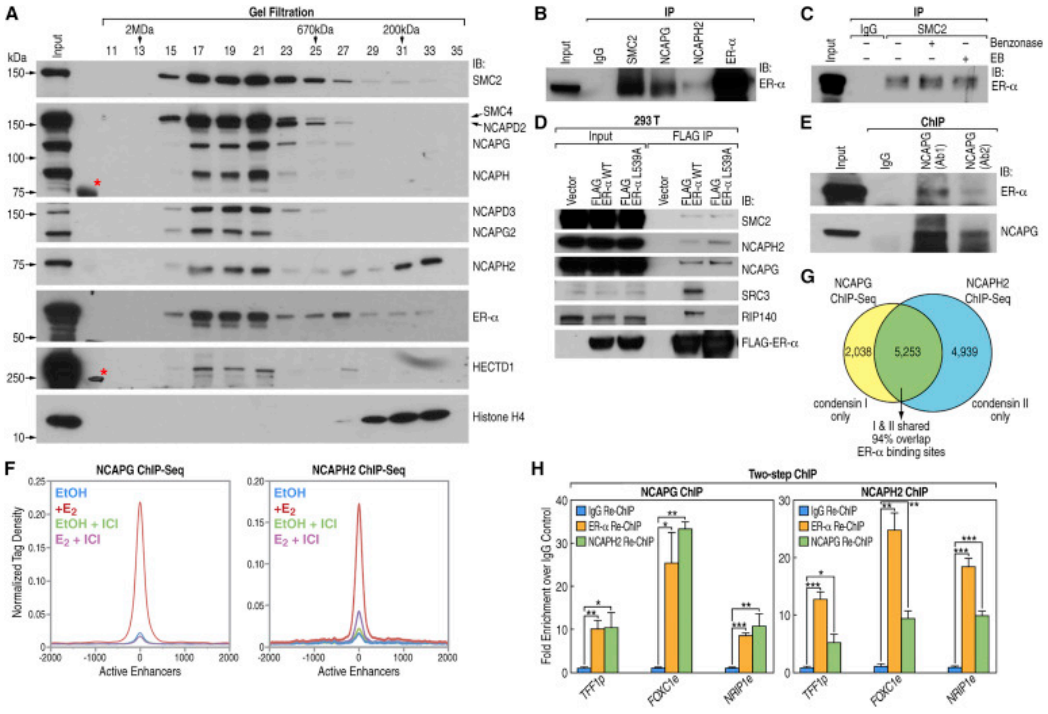


**Figure 2: ER-α Interacts with Condensins**

(A) Gel filtration of $E_2$-treated MCF-7 nuclear extracts followed by western blots showing the elution profiles of target proteins as indicated, with histone H4 as a control. Red asterisks denote irrelevant bands.
(B) CoIP in the whole-cell lysate followed by western blots showing that endogenous condensin subunits co-precipitated with ER-α (without benzonase).
(C) The presence of benzonase or ethidium bromide (EB) did not cause detectable change of condensin/ER-α interaction.
(D) CoIP followed by western blots showing that overexpressed FLAG-tagged ER-α pulls down condensin subunits (benzonase added). The L539A mutant of ER-α interacts with condensin subunits, but not with canonical coregulators SRC3 and RIP140. WT: wild type.
(E) ChIP-western data showing that two antibodies against NCAPG pull down ER-α.
(F) ChIP-seq profile plots (centered on ER-α binding peaks in $+E_2$ situation) showing the binding to active enhancers of both condensin I (NCAPG) and condensin II (NCAPH2) in presence of $E_2$ or ICI treatments.
(G) Venn diagram showing the genome-wide overlap of ChIP-seq peaks of condensin I (i.e., NCAPG) and condensin II (i.e., NCAPH2) in $E_2$-liganded MCF-7 cells.
(H) Two-step ChIP-qPCR results are shown using antibodies against condensin I and II (NCAPG and NCAPH2) and ER-α in liganded cells; experiment was repeated three times; "p" and "e" after gene names denote promoter and enhancer, respectively. Data are presented as mean ± SD. $^{*}p < 0.05$, $^{**}p < 0.01$, $^{***}p < 0.001$ (two-tailed Student's t test). IP/coIP experiments were performed in MCF-7 cells unless otherwise indicated.

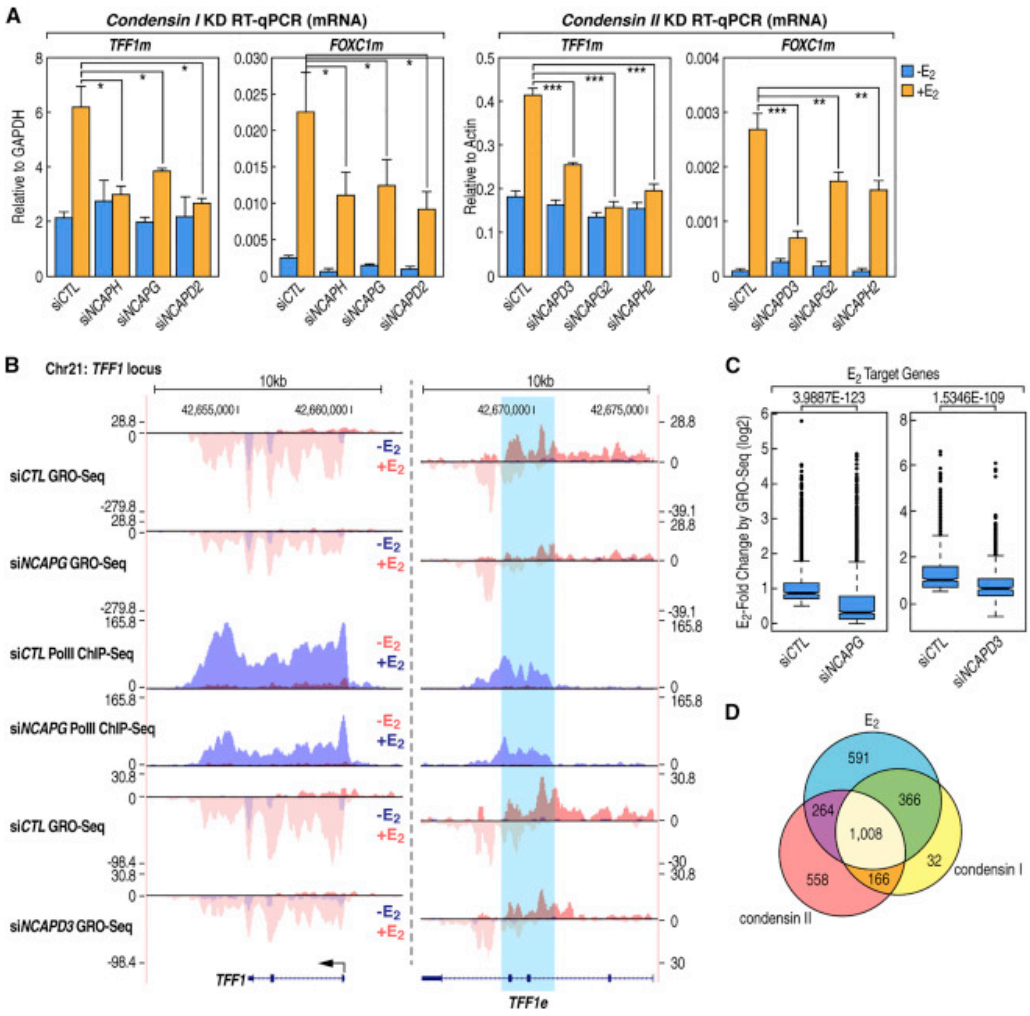


**Figure 3: Condensin I and Condensin II Control ER-α-Regulated Gene Activation in a Partially Overlapping Manner**

(A) RT-qPCR data showing the expression of *TFF1* and *FOXC1* mRNA levels in the wild-type or in cells with condensin I or condensin II knockdown ("m" after gene names denotes mRNA) (n = 5). KD, knockdown. Data are presented as mean ± SD. $^{*}p < 0.05$, $^{**}p < 0.01$, $^{***}p < 0.001$ (two-tailed Student's t test).

(B) Genome browser image showing the results of GRO-seq and Pol II ChIP-seq at *TFF1* locus in the presence of condensin knockdown (*siNCAPG* or *siNCAPD3*) versus *siCTL* transfected cells. (*TFF1e*, highlighted area).

(C) Boxplots showing the $E_2$-induced fold changes ($E_2$-FC) of all the $E_2$-upregulated coding genes in the *siCTL* group and *siNCAPG* or *siNCAPD3* groups. p values were calculated by two-tailed Student's t test.

(D) Venn diagram showing the overlap of gene groups regulated by condensin I, condensin II, and $E_2$, as calculated from GRO-seq data.

**Figure 4: Condensins Are Needed for Full eRNA Activation and Enhancer:Promoter Looping, Continued**

(A) Bar graphs showing the percentage (green colored) of the RefSeq genes upregulated by condensin I, condensin II, or ER-α that possesses direct promoter-binding of the respective factor.
(B) RT-qPCR data indicating the levels of representative $E_2$-induced eRNAs when either condensin I or condensin II subunit was knocked down ("e" after gene names denotes eRNA) (n = 5). KD, knockdown. Data are presented as mean ± SD. $^{*}p < 0.05$, $^{**}p < 0.01$, $^{***}p < 0.001$ (two-tailed Student's t test).
(C) Boxplots of normalized GRO-seq tags showing levels of $E_2$-induced eRNAs on the active enhancers in *siCTL* or *siNCAPG* transfected cells, from both sense and antisense directions (two-tailed Student's t test).
(D) Boxplot of normalized ChIP-seq tags showing RNA Pol II recruitment to active enhancers in same group of cells as in (C) (two-tailed Student's t test).
(E) Results from 3D-DSL assay showing detected chromatin interactions in the displayed region of *TFF1* locus in the presence of either *siCTL* or *siNCAPH2* (blue) (plotted by GGbio). The normalized intensities of interaction counts are plotted on the y axis, and the x axis depicts coordinates from UCSC browser (hg19). Interaction data are overlaid with positions of the Donor (D, yellow) and Acceptor (A, green) BamHI sites. The pertinent E:P interactions are shown in solid lines and other interactions are shown in dotted lines. The interactions are quantitatively coded by height. Highlighted areas denote E: enhancer, P: promoter.
(F and G) A 3C-PCR assay showing the intensities of a specific E:P looping in the *TFF1* locus upon either *siCTL* or *siNCAPG* treatment (±$E_2$). The positions of SacI sites and the 3C primers are indicated in (F). The arrow in (G) points to specific PCR product. Control 3C samples without T4 ligase are shown in (G)MW, molecular weight.
(H) Sanger sequencing of the 3C-PCR product from (G) (arrow) showing that the ligated fragment comprises regions from *TFF1* promoter and enhancer.

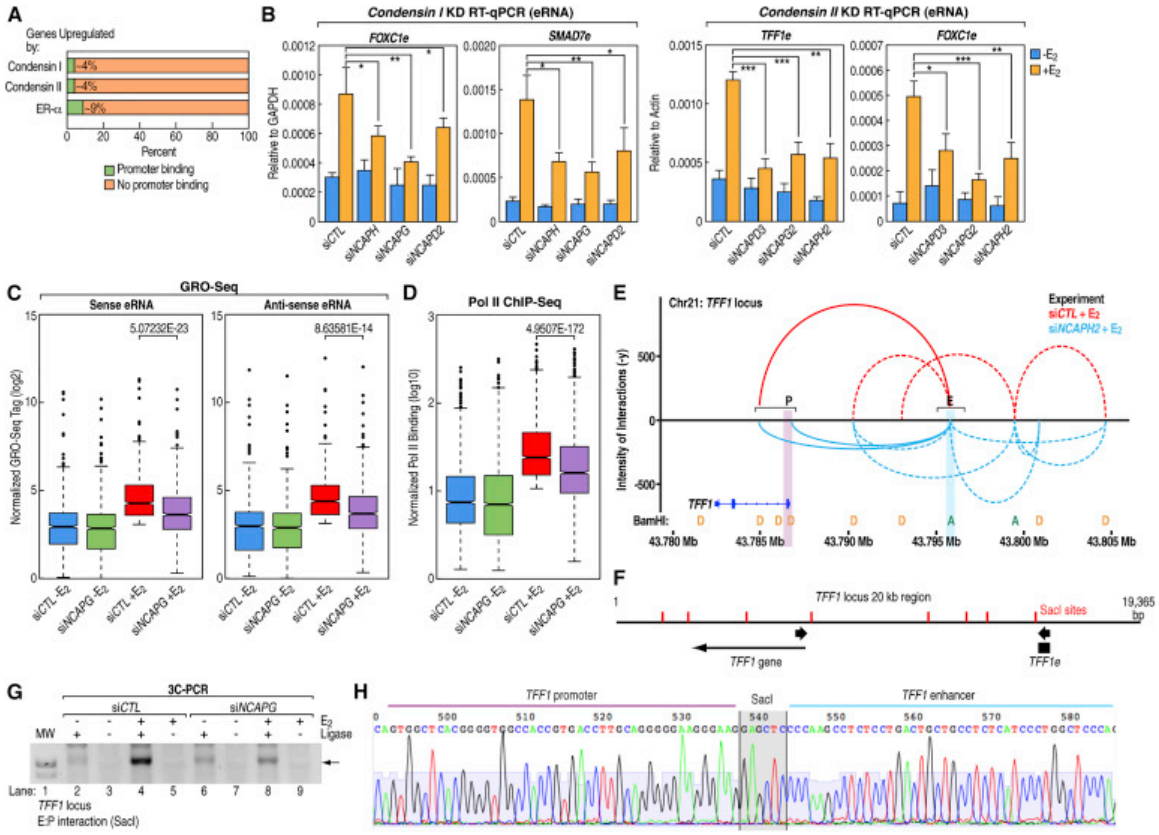
A
Genes Upregulated by:
Condensin I
Condensin II
ER-α
~4%
~4%
~9%
Percent
Promoter binding
No promoter binding
B
Condensin I KD RT-qPCR (eRNA)
FOXC1e
SMAD7e
Relative to GAPDH
siCTL
siNCAPH
siNCAPG
siNCAPD2
Condensin II KD RT-qPCR (eRNA)
TFF1e
FOXC1e
Relative to Actin
siNCAPD3
siNCAPG2
siNCAPH2
-E2
+E2
C
GRO-Seq
Sense eRNA
Anti-sense eRNA
5.07232E-23
8.63581E-14
Normalized GRO-Seq Tag (log2)
siCTL -E2
siNCAPG -E2
siCTL +E2
siNCAPG +E2
D
Pol II ChIP-Seq
4.9607E-172
Normalized Pol II Binding (log10)
E
Chr21: TFF1 locus
Experiment
siCTL + E2
siNCAPH2 + E2
Intensity of Interactions (-y)
TFF1
BamHI:
43.780 Mb
43.785 Mb
43.790 Mb
43.795 Mb
43.800 Mb
43.805 Mb
F
TFF1 locus 20 kb region
SacI sites
19,365 bp
TFF1 gene
TFF1e
G
3C-PCR
siCTL
siNCAPG
E2 Ligase
MW
Lane: 1 2 3 4 5 6 7 8 9
TFF1 locus
E:P interaction (SacI)
H
TFF1 promoter
SacI
TFF1 enhancer

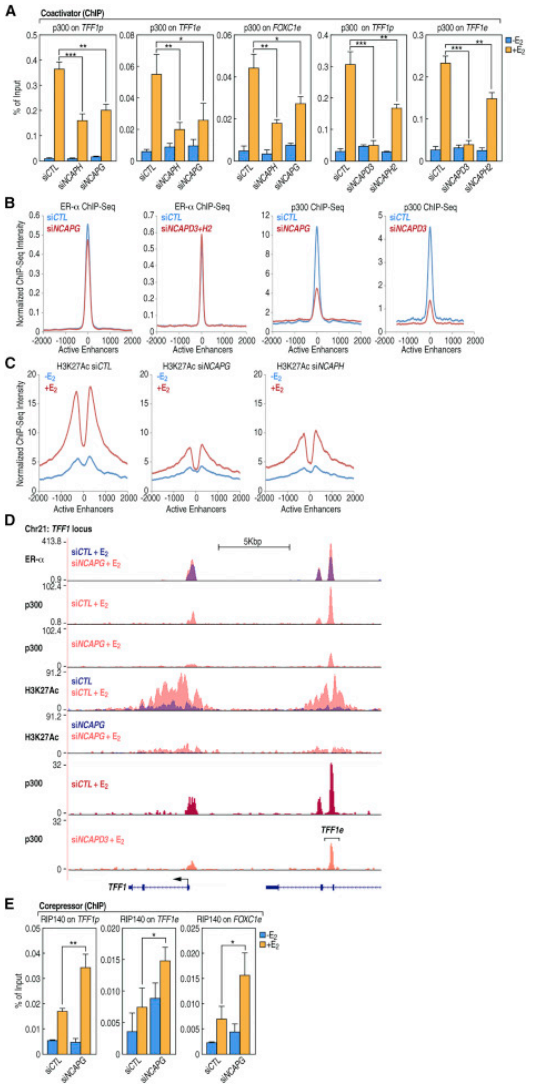

**Figure 5: Condensins License Appropriate Coactivator and Corepressor Recruitment during Enhancer Activation**

(A and B) ChIP-qPCR (n = 3) and ChIP-seq profile data showing the effects of condensin knockdown on binding of p300 or ER-α.
(C) ChIP-seq profile plots showing the levels of H3K27Ac histone modification on active enhancers in control or knockdown conditions as indicated.
(D) Genome browser image showing the binding of p300 and deposition of H3K27Ac, as well as ER-α in *TFF1* locus in the presence or absence of NCAPG or NCAPD3.
(E) ChIP-qPCR results of RIP140 showing its levels of recruitment to indicated ER-α binding sites upon *siCTL* or *siNCAPG* treatment (n = 3). Profiles in (B) and (C) are centered on ER-α binding sites in $+E_2$ situation. Experiments were repeated as indicated; data are presented as mean ± SD; $^{*}p < 0.05$, $^{**}p < 0.01$, $^{***}p < 0.001$ (two-tailed Student's t test).

**Figure 6: Condensin-Dependent Recruitment of HECTD1 Is Required for E2-Induced eRNA Activation, Continued**

(A) Endogenous coIP followed by western blots showing condensin and HECTD1 interaction using indicated antibodies. Long and Short Expo indicate the lengths of exposure time.
(B) Similar to the experiment in Figure 2D, this panel shows the western blots of HECTD1 following coIPs in 293T cells transfected with FLAG-tagged ER-α or its L539A mutant. Benzonase was added.
(C) A heatmap showing HECTD1 ChIP-seq result centered at ER-α binding active enhancers with a scale as indicated.
(D) A representative genome browser image from *TFF1* locus showing HECTD1 binding to ER-α binding sites (*TFF1e*, *TFF1* enhancer).
(E) ChIP-seq intensity plots ranked by NCAPG peaks showing the binding of NCAPG (red) and HECTD1 (green) at active enhancers, with the Pearson correlation coefficient shown.
(F) ChIP-qPCR results showing the binding of HECTD1 with and without *siNCAPG* treatment ($+E_2$) (n = 3).
(G and H) ChIP-qPCR results showing the recruitment of p300 and RIP140 to interrogated regions in control cells or *siHECTD1* transfectants (n = 3).
(I) RT-qPCR data showing the expression levels of interrogated mRNAs and eRNAs in cells with and without si*HECTD1* knockdown (n = 4).
(J) RT-qPCR data showing the levels of interrogated eRNAs upon HECTD1 knockdown and/or rescues by overexpression of wild-type mouse HECTD1 (mHECTD1-WT) or its catalytically defective mutant (mHECTD1-C2579G) (n = 3). Experiments were repeated as indicated; data are presented as mean ± SD; $^{*}p < 0.05$, $^{**}p < 0.01$, $^{***}p < 0.001$ (two-tailed Student's t test).

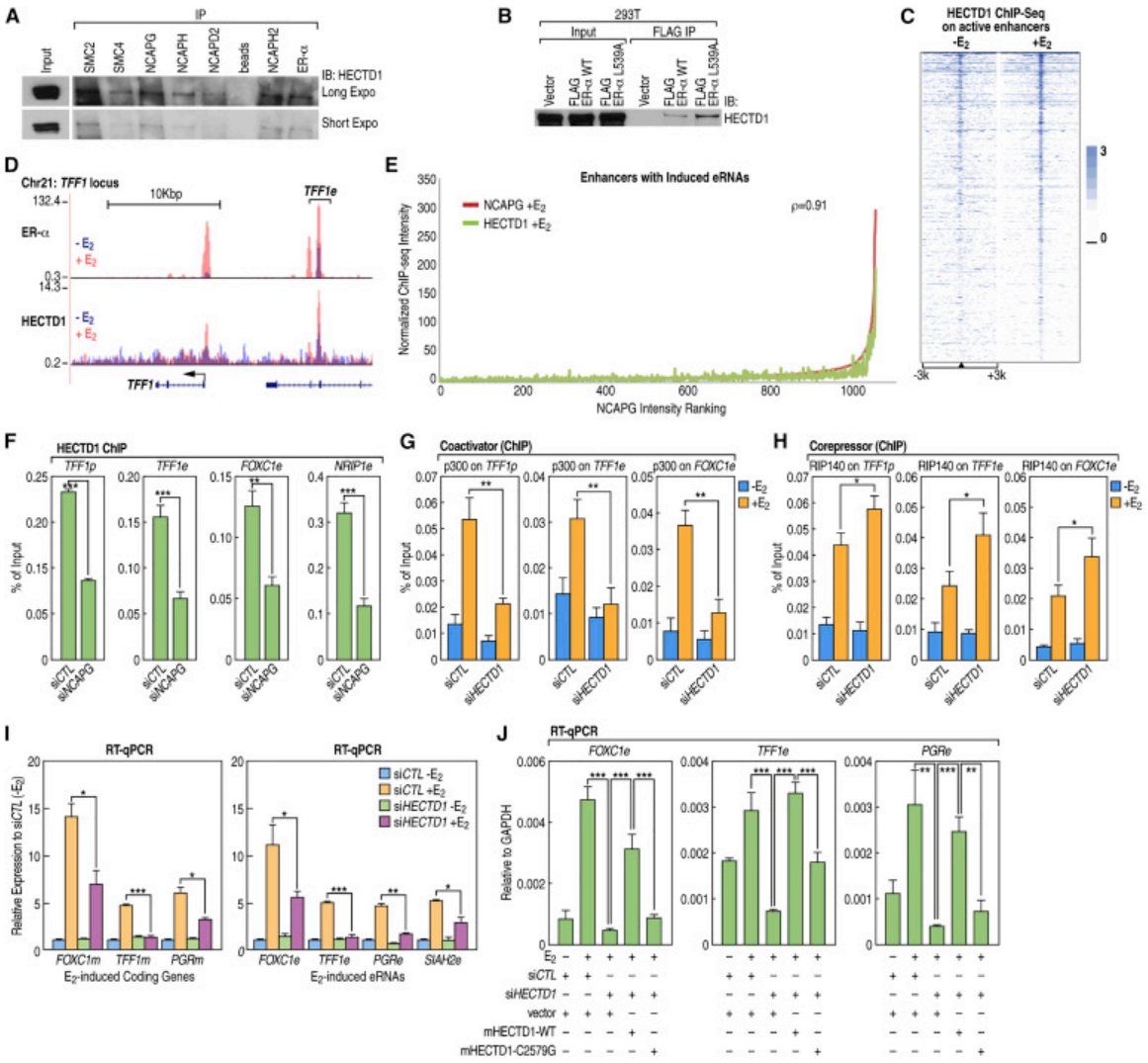
A
IP
Input
SMC2
SMC4
NCAPG
NCAPH
NCAPD2
beads
NCAPH2
ER-α
IB: HECTD1
Long Expo
Short Expo
B
293T
Input
FLAG IP
Vector
FLAG ER-α WT
FLAG ER-α L539A
IB: HECTD1
C
HECTD1 ChIP-Seq on active enhancers
-E2
+E2
3
0
-3k
+3k
D
Chr21: TFF1 locus
10Kbp
TFF1e
ER-α
HECTD1
TFF1
E
Enhancers with Induced eRNAs
NCAPG +E2
HECTD1 +E2
ρ=0.91
Normalized ChIP-seq Intensity
NCAPG Intensity Ranking
F
HECTD1 ChIP
TFF1p
TFF1e
FOXC1e
NRIP1e
% of Input
siCTL
siNCAPG
G
Coactivator (ChIP)
p300 on TFF1p
p300 on TFF1e
p300 on FOXC1e
% of Input
siCTL
siHECTD1
-E2
+E2
H
Corepressor (ChIP)
RIP140 on TFF1p
RIP140 on TFF1e
RIP140 on FOXC1e
% of Input
siCTL
siHECTD1
-E2
+E2
I
RT-qPCR
Relative Expression to siCTL (-E2)
FOXC1m
TFF1m
PGRm
E2-induced Coding Genes
siCTL -E2
siCTL +E2
siHECTD1 -E2
siHECTD1 +E2
FOXC1e
TFF1e
PGRe
SIAH2e
E2-induced eRNAs
J
RT-qPCR
FOXC1e
TFF1e
PGRe
Relative to GAPDH
E2
siCTL
siHECTD1
vector
mHECTD1-WT
mHECTD1-C2579G

**Figure 7: Evidence Suggesting RIP140 as a Polyubiquitination Substrate of HECTD1, Continued**

(A and B) Immunoblotting with indicated antibodies showing IP results using a native RIP140 antibody in wild-type MCF-7 cells (A) or cells transfected with a HA-Ub plasmid (B), revealing the polyubiquitination ((Ub)n) of RIP140.
(C) Western blots showing total protein levels of HECTD1, NCAPG, and RIP140 in MCF-7 cells upon different lengths of $E_2$ treatment with or without cycloheximide (CHX, 10 μg/ml) or MG132. Red boxes highlight the changes of RIP140.
(D) Western blots showing that knockdown of HECTD1 in MCF-7 cells blocked the reduction of RIP140 protein levels after $E_2$ treatment in the presence of CHX. Levels of other interrogated proteins are shown, too.
(E and F) Western blots with indicated antibodies showing results from in vivo ubiquitination assays by ectopically co-expressing FLAG-tagged RIP140 and HA-tagged HECTD1 or C2579G mutants in the presence of wild-type or K48R mutant ubiquitin. Long Expo and Short Expo represent exposure time.
(G) RT-qPCR data showing the expression levels of interrogated mRNAs and eRNAs upon HECTD1 knockdown with or without co-depletion of RIP140 ($n = 3$). Data are presented as mean ± SD; $^{*}p < 0.05$, $^{**}p < 0.01$ (two-tailed Student's t test). Biochemical experiments were performed in MCF-7 cells unless otherwise indicated.
(H) A proposed model of the role(s) of condensins on estrogen-regulated active enhancers.

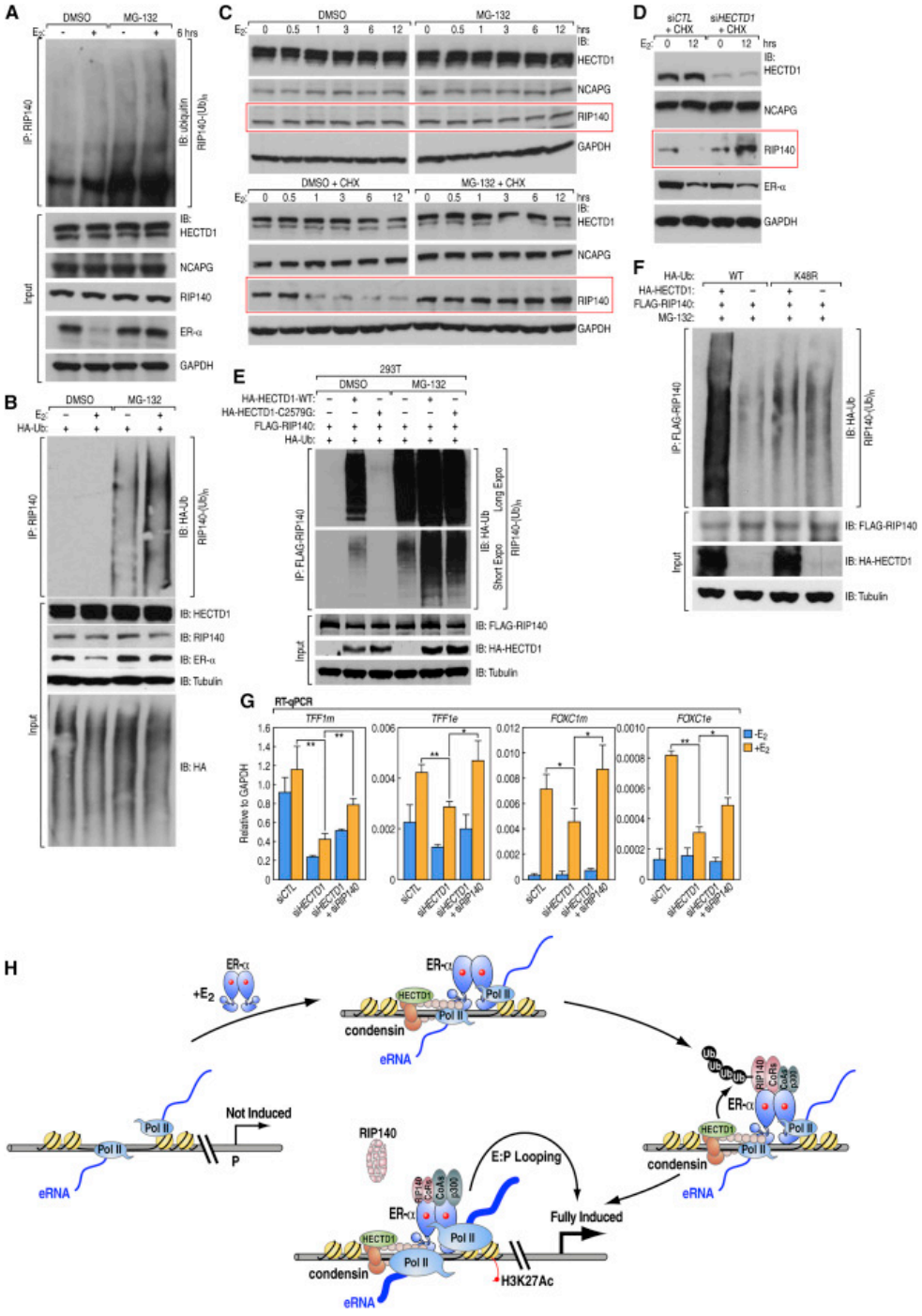
A
DMSO
MG-132
6 hrs
IP: RIP140
IB: ubiquitin
RIP140-(Ub)n
Input
IB: HECTD1
NCAPG
RIP140
ER-α
GAPDH
B
HA-Ub:
IB: HA-Ub
IB: RIP140
IB: Tubulin
IB: HA
C
hrs
DMSO + CHX
MG-132 + CHX
D
siCTL + CHX
siHECTD1 + CHX
E
293T
HA-HECTD1-WT:
HA-HECTD1-C2579G:
FLAG-RIP140:
IP: FLAG-RIP140
IB: HA-Ub
Long Expo
Short Expo
IB: FLAG-RIP140
IB: HA-HECTD1
F
HA-Ub:
WT
K48R
HA-HECTD1:
FLAG-RIP140:
MG-132:
G
RT-qPCR
TFF1m
TFF1e
FOXC1m
FOXC1e
Relative to GAPDH
-E2
+E2
siCTL
siHECTD1
siHECTD1 + siRIP140
H
ER-α
+E2
HECTD1
Pol II
condensin
eRNA
Not Induced
P
RIP140
E:P Looping
Fully Induced
H3K27Ac
CoRs
CoAs
p300
Ub

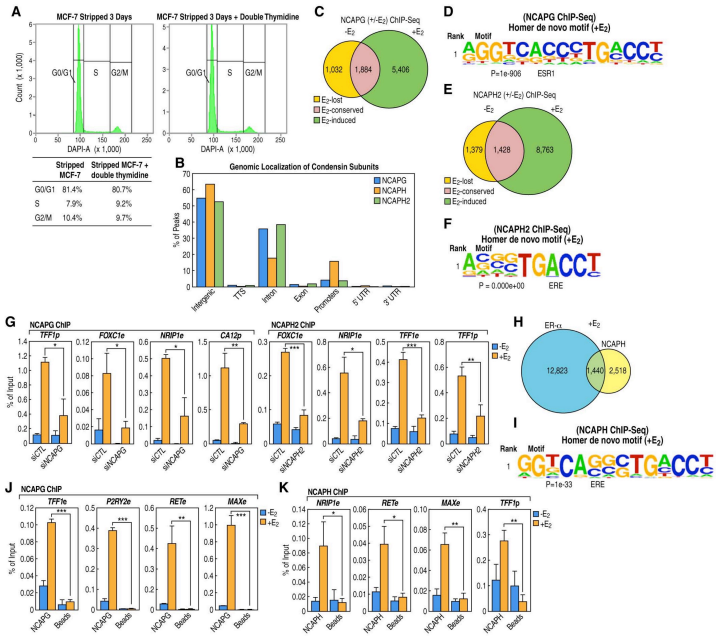

**Figure S1: Additional descriptive data of condensins localization in the genome**

**(**A) Flow cytometry data of wild-type MCF-7 cells cultured for 3 days in deficient MEM medium (stripped), in comparison to MCF-7 cells stripped for 3days after two rounds of thymidine block (12hrs each, 2mM), indicating very minimal difference and that double thymidine block did not further enrich cells in G1/S, suggesting that stripped MCF-7 cells were mostly blocked in G0/G1 phase, consistent with literature (Villalobos et al., 1995). (**B**) Bar graphs showing the genomic distribution of condensin subunits, NCAPG, NCAPH and NCAPH2; majority of which located in intergenic and intronic regions. (**C**,**E**) Venn diagrams from NCAPG and NCAPH2 ChIP-Seqs in -/+$E_2$ conditions showing that both of them were induced by $E_2$ treatment to lose, gain and maintain a cohort of binding sites, with the gained events being the most prominent.
(**D**,**F**) Motif analyses using HOMER revealed the most enriched motifs for both NCAPG and NCAPH2 peaks genome-wide were ESR1/ERE, with p values indicated.
(**G**) ChIP-qPCR data showing that the knockdown of NCAPG and NCAPH2 subunits clearly abolished their binding to several representative ER-α/condensin co-bound sites, validating the specificity of the antibodies used, (n=3).
(**H**) Venn diagram showing the co-localization of NCAPH peaks with those of ER-α in MCF-7 cells (+$E_2$).
(**I**) Motif analysis using HOMER revealed that the most enriched motif for NCAPH peaks in the intergenic regions was ESR1/ERE after $E_2$ treatment, with p value indicated.
(**J**,**K**) ChIP-qPCRs were performed to confirm many of the $E_2$-induced binding events observed by ChIP-Seq for NCAPG and NCAPH ("e" and "p" after gene names denote enhancer and promoter regions of that gene, respectively); (n=4). Experiments were repeated for indicated times; Data are represented as mean ± s.d.; *p<0.05, **p<0.01, ***p<0.001, (Two-tailed students' T-test).

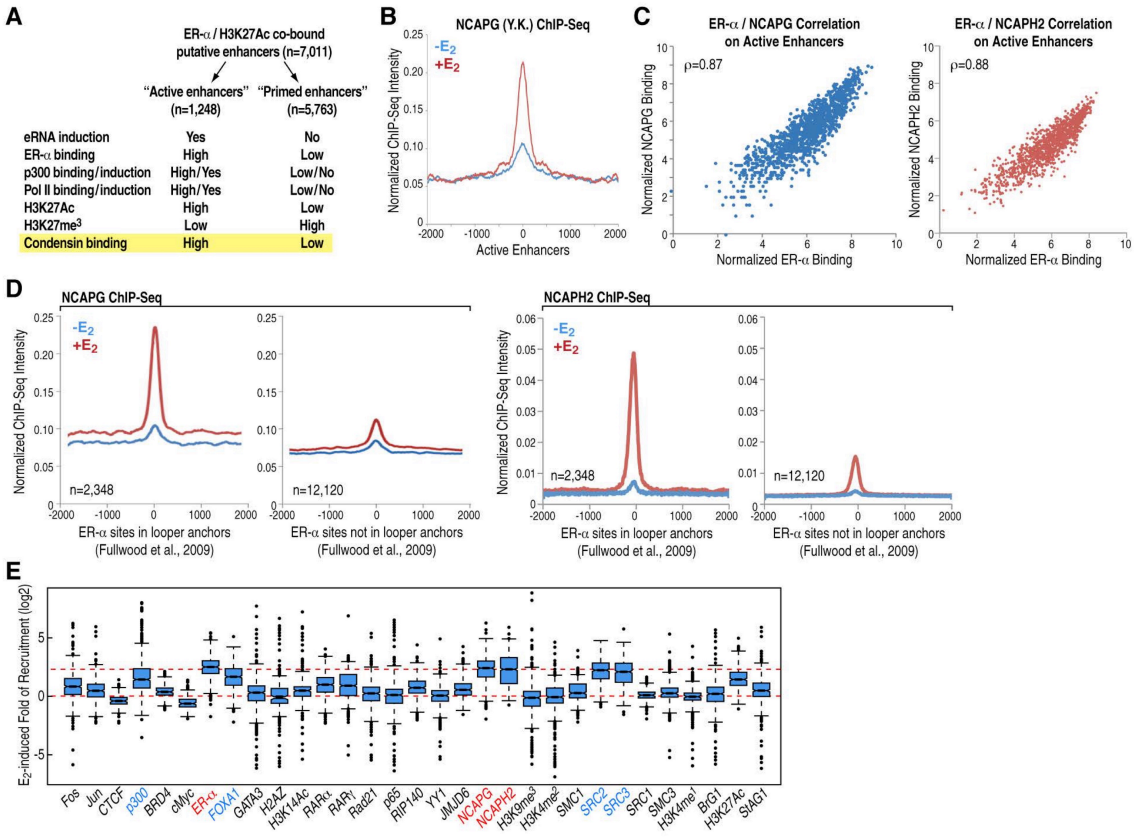


**Figure S2: Additional descriptions of condensins ChIP-Seqs and their localization to active enhancers.**

(**A**) A diagram summarizing features of active and "primed"/inactive enhancers groups used in this study.
(**B**) Profile plot from ChIP-Seq data using another antibody for NCAPG (Y.K.) also revealed a clear induction of binding to active enhancers.
(**C**) Correlation plots showing that NCAPG (blue) or NCAPH2 (Di Ruscio et al.) and ER-α binding exhibited high correlation on the active enhancers, with Pearson correlation coefficients indicated.
(**D**) ChIP-Seq profile plots showing that those ER-α binding sites that can form chromosomal interactions tend to have higher NCAPG and NCAPH2 binding intensity than those ER-α binding sites that did not exhibit interactions, based on analysis of a published ChIA-PET dataset in MCF-7 cells (Fullwood et al., 2009).
(**E**) Fold change of $E_2$-induced binding of multiple transcription factors/cofactors and histone modifications on 1,248 active enhancers were plotted using available ChIP-Seqs in MCF-7 cells.The scale indicates $E_2$-induced fold of binding (log2), with a red line indicating a log2 value of 2.3 to provide a better visual comparison of the induction. All profiles are centered on ER-α binding sites in $+E_2$ situation.

**Figure S3: Localization of condensins in mitotic MCF-7 cells, condensin/ER-α interaction and condensin I / II relationship, Continued.**

(A) Flow cytometry results showing the cell cycle indexes of asynchronized (Asyn.) MCF-7 cells cultured in complete medium (without stripping) in comparison to those enriched in mitosis by colcemid treatment followed by shake-off (refer to Supplemental Experimental Procedures).
(B) UCSC browser snapshots of NCAPG ChIP-Seq in TFF1 locus in the two stages of MCF-7 cells as shown in panel A.
(C) Heatmap of NCAPG ChIP-Seq showing its binding on active enhancers in mitotic MCF-7 cells (in panel A) with a scale as indicated, showing minimal NCAPG binding in mitosis. Heatmap was centered on ER-α binding sites in +E2 situation.
(D) Co-IP followed by Western blots using native antibodies against NCAPG and SMC2 showed that there was interaction between condensin and ER-α in MCF-7 cells, which increased upon E2 treatment (more obvious increase is seen for NCAPG).
(E) Co-IP followed by Western blots using a native antibody against ER-α (HC-20, Santa Cruz) showed its co-precipitation with condensin subunits.
(F) IP following by Western blots to map the ER-α domains interacting with condensins in 293T cells showing that the DNA binding domain (DBD) displayed the highest affinity, contrasting the interaction between ER-α and other LxxLL-containing cofactors, e.g. RIP140 and SRC3 that bind the AF2 domain. Red arrowhead points to a non-specific band.
(G) Co-IP followed by Western blots showing that condensin I subunits and condensin II subunits do not interact with each other in MCF-7 cells. Benzonase was added in the experiments for panel F but not for D,E,G. IP/Co-IP experiments were performed in MCF-7 cells unless otherwise indicated.
(H) A partial list of NCAPG-interacting partners detected from NCAPG IP followed by mass-spectrometry, refer to Tables S2 and S3 for details.
(I) Western blots showing the protein levels of condensin I or II subunits upon the knockdown of condensin I subunits NCAPH or NCPAG.
(J,K) ChIP-qPCR with indicated antibodies upon treatment with siRNA to one subunit of condensin I (siNCAPH) in panel J and to another subunit of condensin I (siNCAPG) in panel K, (n=2). Experiments were repeated for indicated times; Data are represented as mean ± s.d.; N.S. not significant; **$p<0.01$, ***$p<0.001$, (Two-tailed students' T-test).

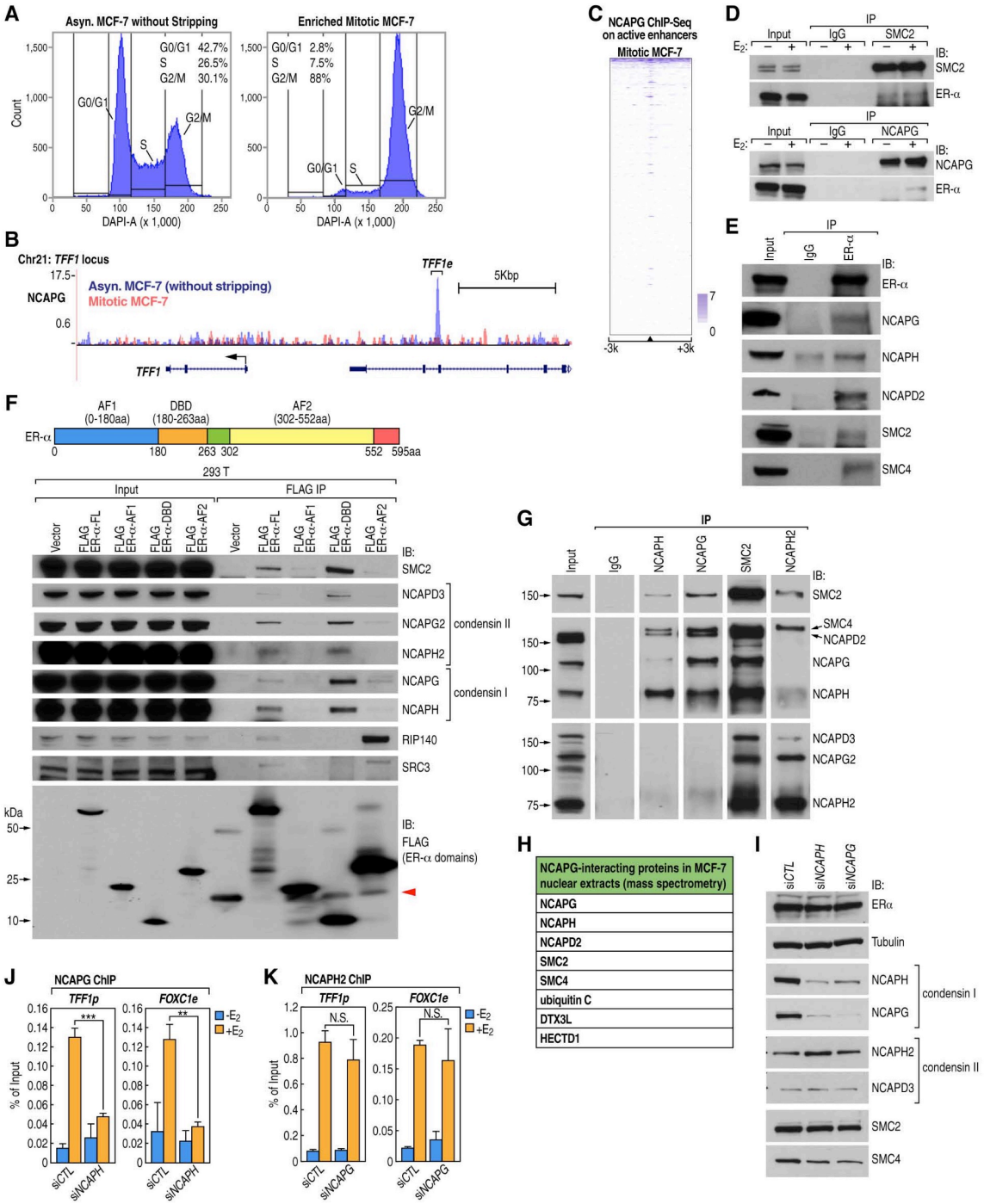
A
Asyn. MCF-7 without Stripping
Enriched Mitotic MCF-7
G0/G1 42.7%
S 26.5%
G2/M 30.1%
G0/G1 2.8%
S 7.5%
G2/M 88%
Count
DAPI-A (x 1,000)
B
Chr21: TFF1 locus
NCAPG
Asyn. MCF-7 (without stripping)
Mitotic MCF-7
TFF1e
5Kbp
TFF1
C
NCAPG ChIP-Seq on active enhancers
Mitotic MCF-7
-3k
+3k
D
IP
Input
IgG
SMC2
NCAPG
IB:
ER-α
E
NCAPH
NCAPD2
SMC4
F
AF1 (0-180aa)
DBD (180-263aa)
AF2 (302-552aa)
293 T
Input
FLAG IP
Vector
FLAG ER-α-FL
FLAG ER-α-AF1
FLAG ER-α-DBD
FLAG ER-α-AF2
NCAPD3
NCAPG2
NCAPH2
condensin II
condensin I
RIP140
SRC3
kDa
IB: FLAG (ER-α domains)
G
IP
Input
IgG
NCAPH
NCAPG
SMC2
NCAPH2
SMC4
NCAPD2
NCAPD3
NCAPG2
H
NCAPG-interacting proteins in MCF-7 nuclear extracts (mass spectrometry)
NCAPG
NCAPH
NCAPD2
SMC2
SMC4
ubiquitin C
DTX3L
HECTD1
I
siCTL
siNCAPH
siNCAPG
IB:
ERα
Tubulin
NCAPH
NCAPG
condensin I
NCAPH2
NCAPD3
condensin II
SMC2
SMC4
J
NCAPG ChIP
TFF1p
FOXC1e
% of Input
-E2
+E2
siCTL
siNCAPH
K
NCAPH2 ChIP
N.S.
siNCAPG

**Figure S4: Efficient knockdown of condensins and its effects on estrogen regulated transcription, Continued**

(**A**) A diagram showing the procedure of the siRNA knockdown performed in this study. (**B,C**) Western blots and RT-qPCR results showing efficient knockdown of condensin I and II subunits as well as HECTD1 and p300 in this study. The results were confirmed by at least two different siRNAs. (n>5).
(**D**) Additional RT-qPCR data showing the expression levels of estrogen target coding genes (*i.e. SMAD7*, *SIAH2* and *PGR*) when either condensin I or condensin II subunit was knocked down ("m"" after gene names denotes mRNA). (n=5). KD, knockdown. (**E**,**F**) RT-qPCR and Western blots showing the expression of ER-α at both protein and mRNA levels after indicated siRNA treatment. (n=4). (**G**) Normalized whole-gene GRO-Seq profile plots in *siCTL*-transfected MCF-7 cells versus in *siNCAPG* treated cells. It was calculated by counting the tags on three fragments (-2kb to 0kb upstream of transcription start sites (TSS), whole gene bodies and 0 to +3kb downstream of transcription termination sites (Guttman et al.)) of the $E_2$-upregulated genes with FC>1.5 (-/+$E_2$, light blue *v.s.* red).
(**H**) Whole-gene profiles using Pol II ChIP-Seq datasets were plotted for the same group of genes in panel **G**, The y-axis of panel **B** was set as a log2 scale to allow a better appreciation of the altered Pol II binding.
(**I**) GO term (interaction) analysis using HOMER of all NCAPG positively regulated genes; ESR1 was one of the highly enriched terms. Interestingly, ubiquitin or SUMO related terms were also observed. Experiments were repeated for indicated times; Data are represented as mean ± s.d.; *p<0.05, **p<0.01, ***p<0.001, (Two-tailed students' T-test).

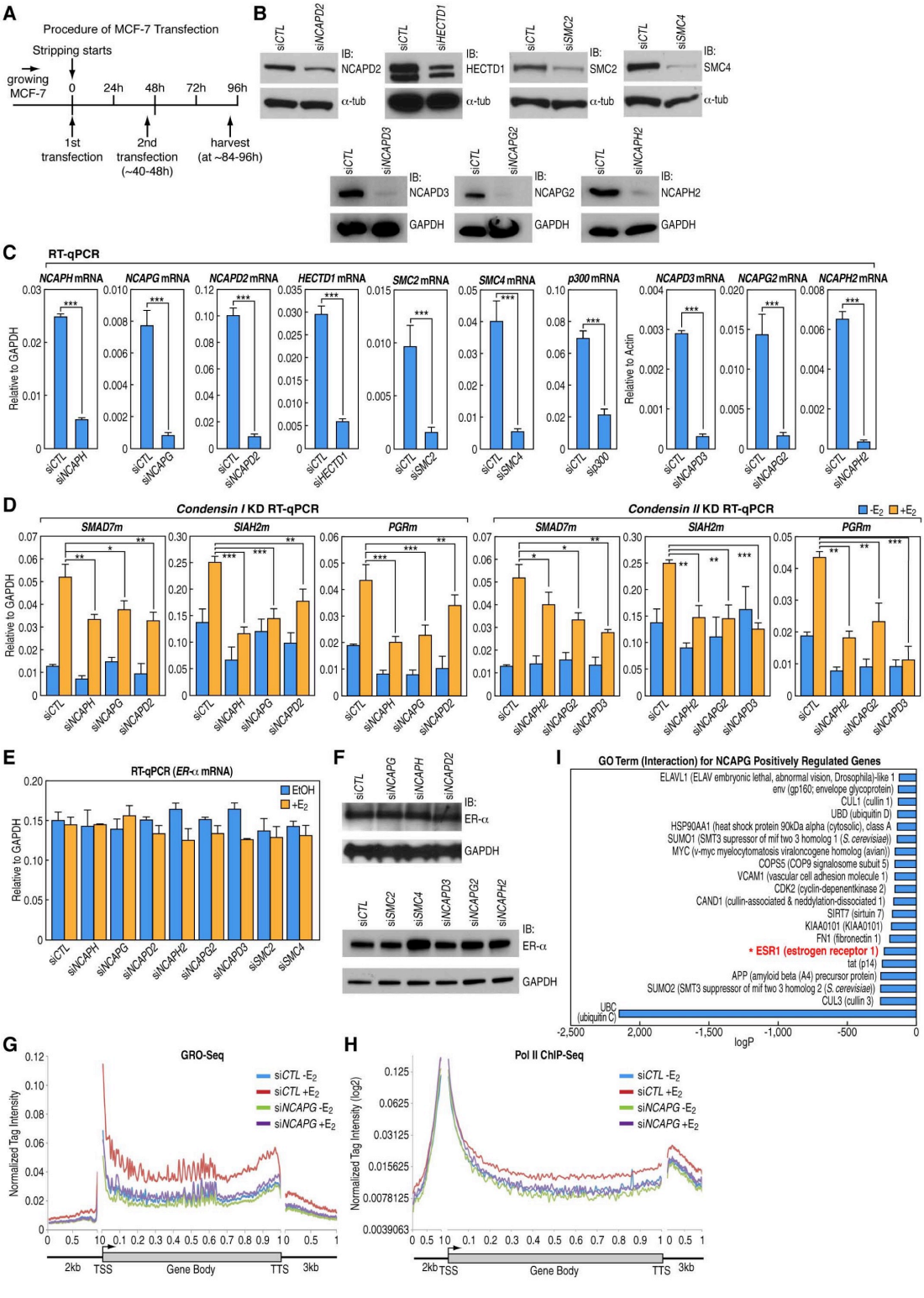
A
Procedure of MCF-7 Transfection
Stripping starts
growing MCF-7
0
24h
48h
72h
96h
1st transfection
2nd transfection (~40-48h)
harvest (at ~84-96h)
B
siCTL
siNCAPD2
IB: NCAPD2
α-tub
siHECTD1
IB: HECTD1
siSMC2
IB: SMC2
siSMC4
IB: SMC4
siNCAPD3
siNCAPG2
siNCAPH2
GAPDH
C
RT-qPCR
NCAPH mRNA
NCAPG mRNA
NCAPD2 mRNA
HECTD1 mRNA
SMC2 mRNA
SMC4 mRNA
p300 mRNA
NCAPD3 mRNA
NCAPG2 mRNA
NCAPH2 mRNA
Relative to GAPDH
Relative to Actin
siNCAPH
siNCAPG
siHECTD1
siSMC2
siSMC4
sip300
D
Condensin I KD RT-qPCR
Condensin II KD RT-qPCR
-E2
+E2
SMAD7m
SIAH2m
PGRm
siNCAPH2
siNCAPG2
siNCAPD3
E
RT-qPCR (ERα mRNA)
EtOH
+E2
siSMC2
siSMC4
F
IB: ER-α
GAPDH
I
GO Term (Interaction) for NCAPG Positively Regulated Genes
ELAVL1 (ELAV embryonic lethal, abnormal vision, Drosophila)-like 1
env (gp160; envelope glycoprotein)
CUL1 (cullin 1)
UBD (ubiquitin D)
HSP90AA1 (heat shock protein 90kDa alpha (cytosolic), class A
SUMO1 (SMT3 supressor of mif two 3 homolog 1 (S. cerevisiae))
MYC (v-myc myelocytomatosis viraloncogene homolog (avian))
COPS5 (COP9 signalosome subuit 5)
VCAM1 (vascular cell adhesion molecule 1)
CDK2 (cyclin-depenentkinase 2)
CAND1 (cullin-associated & neddylation-dissociated 1)
SIRT7 (sirtuin 7)
KIAA0101 (KIAA0101)
FN1 (fibronectin 1)
• ESR1 (estrogen receptor 1)
tat (p14)
APP (amyloid beta (A4) precursor protein)
SUMO2 (SMT3 suppressor of mif two 3 homolog 2 (S. cerevisiae))
CUL3 (cullin 3)
UBC (ubiquitin C)
logP
G
GRO-Seq
Normalized Tag Intensity
siCTL -E2
siCTL +E2
siNCAPG -E2
siNCAPG +E2
2kb
TSS
Gene Body
TTS
3kb
H
Pol II ChIP-Seq
Normalized Tag Intensity (log2)

**Figure S5: Depletion of condensins inhibits ER-α enhancer transcription, Continued.**

(A) Flow cytometry data showing the cell cycle phase distribution upon the knockdown of condensin subunits in MCF-7 cells.
(B) ChIP-qPCRs of RNA Pol II binding on TFF1p, TFF1e and FOXC1e sites with and without knockdown of condensin subunits (siNCAPH and siNCAPG). (n=2). Data are represented as mean ± s.d.; *p<0.05, **p<0.01, (Two-tailed students' T-test).
(C) Genome browser image from FOXC1 enhancer showing that condensin knockdown (siNCAPG) quantitatively but significantly reduced the typical bi-directional eRNA (GRO-Seq) and RNA Pol II recruitment (ChIP-Seq) in the FOXC1 enhancer region. ER-α peak indicates the "center" of this enhancer.
(D) Normalized GRO-Seq profile plots denoting levels of E2-induced eRNA on the active enhancers after siNCAPD3 treatment, from both sense and antisense direction. (Two-tailed students' T-test).
(E) Boxplots showing the normalized eRNAs levels (GRO-Seq) from the enhancer groups that are in the vicinity of the gene groups described in Figure 3D. Colors for the grouping of genes and enhancers were matched in this panel and in Figure 3D.
(F) 3D-DSL results for FOXC1 locus in presence or absence of condensin knockdown (siNCAPG) are shown as a plot generated by GGbio, similar to that in Figure 4E. Bundling of interactions was performed for interactions stemming from the enhancer Acceptor sites (green). The interaction involving Donor sites (yellow) closest to FOXC1 gene was considered E:P looping (solid line). The two brackets were used to denote the enhancer and gene regions.
(G,H) A 3C-PCR assay showing specific E:P looping in the FOXC1 locus, similarly as that shown in Figure 4F,G,. The positions of SacI sites and the 3C primers are indicated in panel G. The arrow in panel H points to the specific E:P looping PCR product. Control 3C samples without T4 ligase are shown in H.
(I) Sanger sequencing showing the sequence of the 3C-PCR product from panel H (arrow), which comprises on FOXC1 enhancer and promoter regions ligated by a SacI site.
(J) 3D-DSL data plotted similarly as in panel F, but for a condensin-independent gene locus (i.e. GATA3) showing a lack of clear change of its E:P looping. The interactions falling in regions closer than 20kb from each other were bundled.

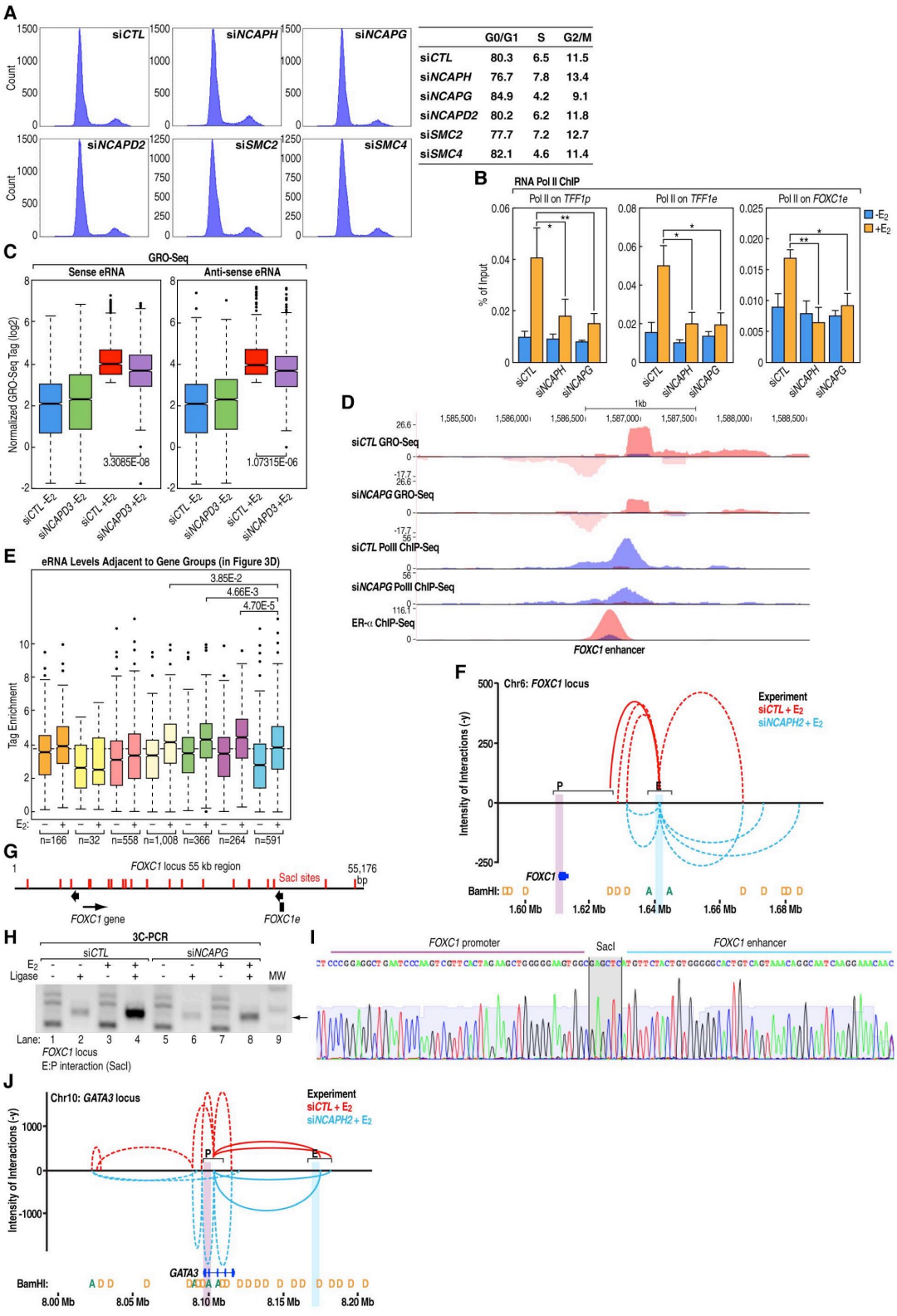
A
siCTL
siNCAPH
siNCAPG
siNCAPD2
siSMC2
siSMC4
Count
G0/G1 S G2/M
siCTL 80.3 6.5 11.5
siNCAPH 76.7 7.8 13.4
siNCAPG 84.9 4.2 9.1
siNCAPD2 80.2 6.2 11.8
siSMC2 77.7 7.2 12.7
siSMC4 82.1 4.6 11.4
B
RNA Pol II ChIP
Pol II on TFF1p
Pol II on TFF1e
Pol II on FOXC1e
% of Input
-E2
+E2
C
GRO-Seq
Sense eRNA
Anti-sense eRNA
Normalized GRO-Seq Tag (log2)
3.3085E-08
1.07315E-06
siCTL -E2
siNCAPD3 -E2
siCTL +E2
siNCAPD3 +E2
D
1kb
siCTL GRO-Seq
siNCAPG GRO-Seq
siCTL PolII ChIP-Seq
siNCAPG PolII ChIP-Seq
ER-α ChIP-Seq
FOXC1 enhancer
E
eRNA Levels Adjacent to Gene Groups (in Figure 3D)
3.85E-2
4.66E-3
4.70E-5
Tag Enrichment
E2:
n=166 n=32 n=558 n=1,008 n=366 n=264 n=591
F
Chr6: FOXC1 locus
Experiment
siCTL + E2
siNCAPH2 + E2
Intensity of Interactions (-y)
FOXC1
BamHI:
1.60 Mb 1.62 Mb 1.64 Mb 1.66 Mb 1.68 Mb
G
FOXC1 locus 55 kb region
SacI sites
55,176 bp
FOXC1 gene
FOXC1e
H
3C-PCR
siCTL
siNCAPG
E2
Ligase
MW
Lane: 1 2 3 4 5 6 7 8 9
FOXC1 locus
E:P interaction (SacI)
I
FOXC1 promoter
SacI
FOXC1 enhancer
J
Chr10: GATA3 locus
Experiment
siCTL + E2
siNCAPH2 + E2
Intensity of Interactions (-y)
GATA3
BamHI:
8.00 Mb 8.05 Mb 8.10 Mb 8.15 Mb 8.20 Mb

**Figure S6: Depletion of condensins abolished the equilibrium of CoA/CoR recruitment to active enhancers, Continued.**

(**A**,**B**) Heatmap analyses of ER-α ChIP-Seq on active enhancers did not show significant change upon knockdown of NCAPG or NCAPD3; the scales are indicated.
(**C-F**) ChIP-qPCR data showing that loss of condensin subunits did not significantly impact on the binding of pioneer factor FOXA1, but quantitatively and significantly reduced the binding of the CoAs examined, including that of SRC1, SRC3, TIP60, to the ER-α-bound sites tested. (n=2).
(**G**) ChIP-qPCR data showing the binding of MED1 to several tested sites after *siNCAPG* transfection. (n=2).
(**H**) ChIP-qPCR data examining the binding of RARα to several ER-α-bound sites upon the knockdown of condensin subunit NCAPD3. (n=2).
(**I**) ChIP-qPCR data showing that dual depletion of RARα/RARϒ reduced binding of condensin subunit NCAPH2 to tested ER-α-bound sites. (n=2).
(**J**) RT-qPCR data showing the knockdown effects of *sip300* and *siNCAPG* on some examined $E_2$ target genes and eRNAs; note that *p300* knockdown reduced the level of *ER-α* mRNA by ~50%, which might be responsible for part of the *sip300* effects. ("m" after gene names denotes mRNA, and "e" eRNA); (n=3).
(**K**) RT-qPCR data showing the expression of several tested genes and eRNAs upon *RIP140* knockdown by siRNAs in MCF-7 cells. (n=2).
(**L**) ChIP-qPCR of CtBP1 binding to the sites indicated upon *siNCAPG* treatment to MCF-7 cells (15min $E_2$). (n=2).
(**M**) Western blots data of the interrogated transcriptional cofactors, Pol II or ER-α after the knockdown of HECTD1 or NCAPG. Experiments were repeated for indicated times; Data are represented as mean ± s.d.; N.S., not significant; *p<0.05, **p<0.01, ***p<0.001, (Two-tailed students' T-test).

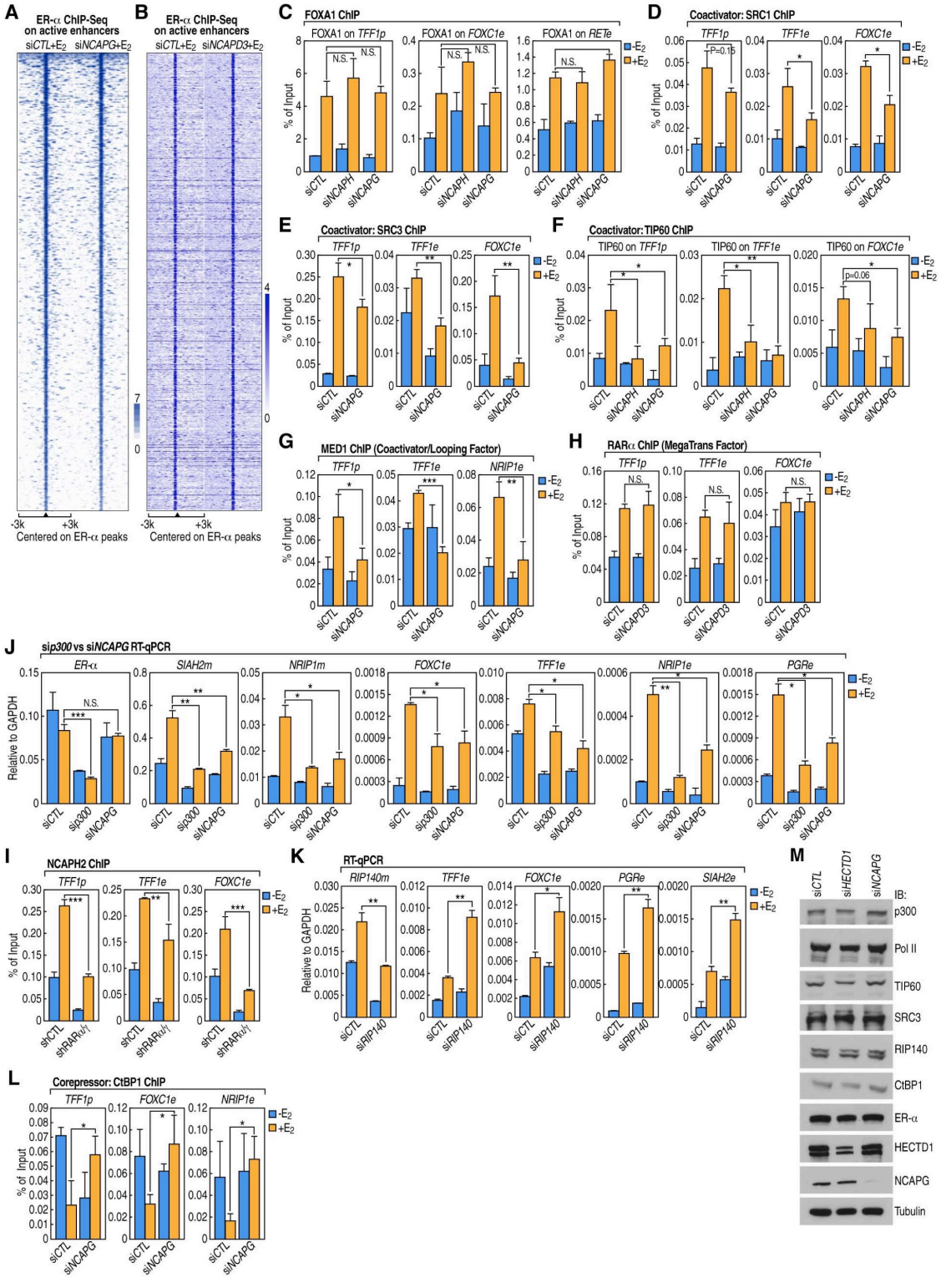
A
ER-α ChIP-Seq on active enhancers
siCTL+E2
siNCAPG+E2
Centered on ER-α peaks
B
ER-α ChIP-Seq on active enhancers
siCTL+E2
siNCAPD3+E2
Centered on ER-α peaks
C
FOXA1 ChIP
FOXA1 on TFF1p
FOXA1 on FOXC1e
FOXA1 on RETe
% of Input
-E2
+E2
siCTL
siNCAPH
siNCAPG
D
Coactivator: SRC1 ChIP
TFF1p
TFF1e
FOXC1e
P=0.15
E
Coactivator: SRC3 ChIP
F
Coactivator: TIP60 ChIP
p=0.06
G
MED1 ChIP (Coactivator/Looping Factor)
NRIP1e
H
RARα ChIP (MegaTrans Factor)
siNCAPD3
J
sip300 vs siNCAPG RT-qPCR
ER-α
SIAH2m
NRIP1m
FOXC1e
TFF1e
NRIP1e
PGRe
Relative to GAPDH
sip300
I
NCAPH2 ChIP
shRARα/γ1
K
RT-qPCR
RIP140m
SIAH2e
siRIP140
L
Corepressor: CtBP1 ChIP
M
siCTL
siHECTD1
siNCAPG
IB:
p300
Pol II
TIP60
SRC3
RIP140
CtBP1
ER-α
HECTD1
NCAPG
Tubulin

**Figure S7: Additional results for HECTD1 function, Continued.**

**(A)** Western blots following IP of HA-tagged condensin subunits (transient transfection) in MCF-7 cells using indicated antibodies; IgG was used as a control.
(**B**) Similar to **Figure S3F**, IP followed by western blots using different fragment of ER-α showing that ER-α DBD exhibits the highest affinity with HECTD1 (with Benzonase).
(**C**) A diagram showing the fragments of HECTD1 (HA-tagged) utilized for mapping its interaction with a condensin subunit (3xFLAG tagged NCAPH).
(**D**) Mapping of interaction between HECTD1 and NCAPH in 293T cells showing that the C terminus and a central fragment of HECTD1 exhibited interaction with NCAPH. The third fragment of HECTD1 (HECTD1-3, 1181-1980aa) could not be expressed at high level (no Benzonase).
(**E**) ChIP-qPCR results showing that HECTD1 (Bethyl) was induced to bind tested condensin/ER-α co-bound sites. (n=2).
(**F**) Venn diagram showing the genome-wide overlaps between ChIP-Seq peaks of HECTD1 and those of NCAPG or ER-α in MCF-7 cells (+$E_2$).
(**G**) Additional RT-qPCR data from HECTD1 knockdown and rescue experiment shown in **Figure 6J**; (n=3).
(**H**) Western blots data showing the expression of endogenous HECTD1, the HA-tagged forms of HECTD1 or its C2579G mutant in the rescue experiment.
(**I**) Two representative studies listed in Oncomine databases showed that the mRNA levels of *HECTD1* were higher in patient samples with ER-α-positive breast cancer than in ER-α-negative samples. Experiments were repeated for indicated times; Data are represented as mean ± s.d.; N.S., not significant, *p<0.05, **p<0.01, ***p<0.001, (Two-tailed students' T-test).

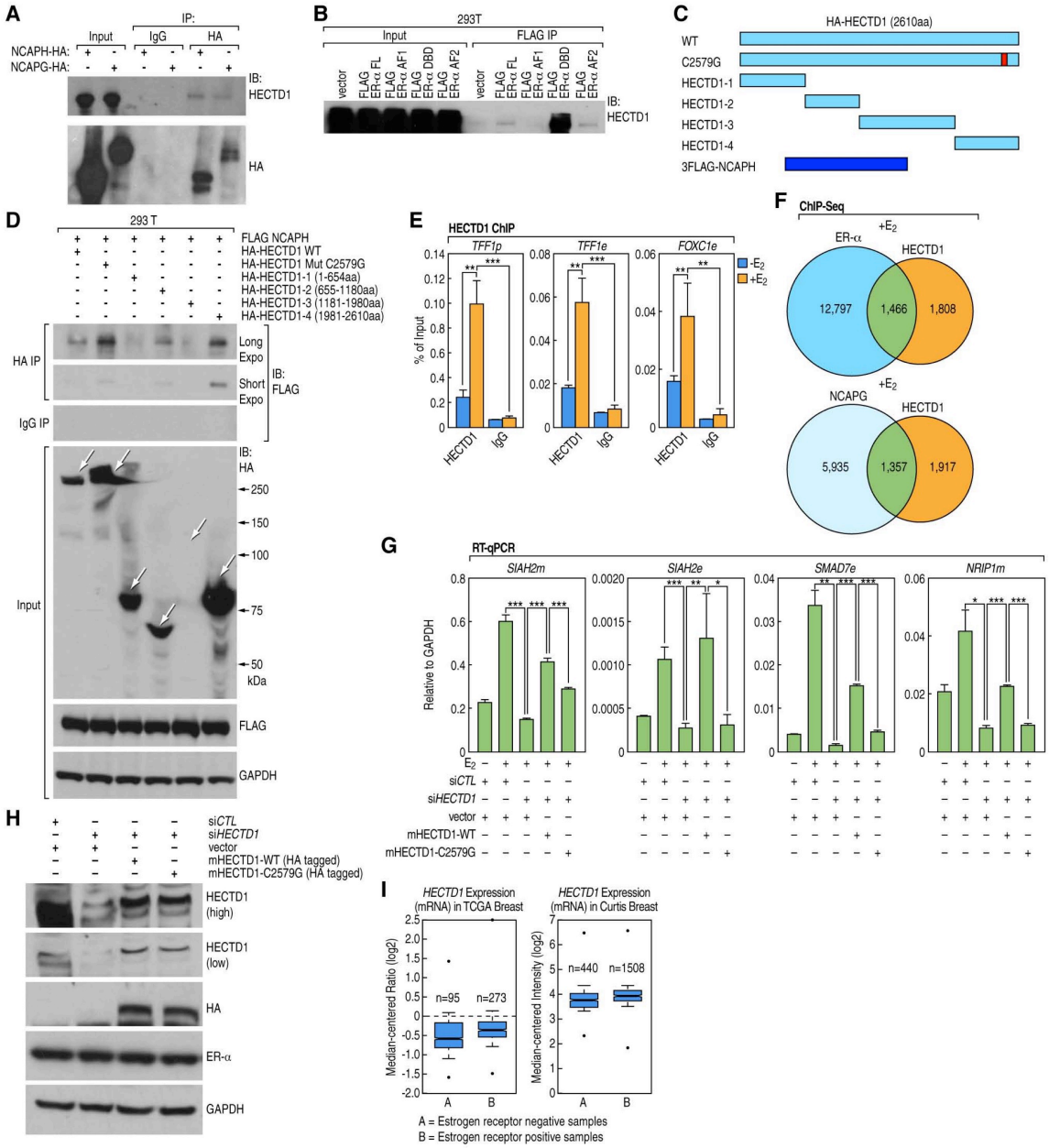
A
Input
IP:
IgG
HA
NCAPH-HA:
NCAPG-HA:
IB:
HECTD1
HA
B
293T
Input
FLAG IP
vector
FLAG ER-α FL
FLAG ER-α AF1
FLAG ER-α DBD
FLAG ER-α AF2
IB:
HECTD1
C
HA-HECTD1 (2610aa)
WT
C2579G
HECTD1-1
HECTD1-2
HECTD1-3
HECTD1-4
3FLAG-NCAPH
D
293 T
FLAG NCAPH
HA-HECTD1 WT
HA-HECTD1 Mut C2579G
HA-HECTD1-1 (1-654aa)
HA-HECTD1-2 (655-1180aa)
HA-HECTD1-3 (1181-1980aa)
HA-HECTD1-4 (1981-2610aa)
HA IP
Long Expo
Short Expo
IB: FLAG
IgG IP
Input
IB: HA
250
150
100
75
50
kDa
FLAG
GAPDH
E
HECTD1 ChIP
TFF1p
TFF1e
FOXC1e
% of Input
-E2
+E2
HECTD1
IgG
F
ChIP-Seq
+E2
ER-α
HECTD1
12,797
1,466
1,808
NCAPG
5,935
1,357
1,917
G
RT-qPCR
SIAH2m
SIAH2e
SMAD7e
NRIP1m
Relative to GAPDH
E2
siCTL
siHECTD1
vector
mHECTD1-WT
mHECTD1-C2579G
H
siCTL
siHECTD1
vector
mHECTD1-WT (HA tagged)
mHECTD1-C2579G (HA tagged)
HECTD1 (high)
HECTD1 (low)
HA
ER-α
GAPDH
I
HECTD1 Expression (mRNA) in TCGA Breast
HECTD1 Expression (mRNA) in Curtis Breast
Median-centered Ratio (log2)
Median-centered Intensity (log2)
n=95
n=273
n=440
n=1508
A
B
A = Estrogen receptor negative samples
B = Estrogen receptor positive samples

**Figure 8: JMJD6 Binding was Induced by Estrogen on ERα-Bound Active Enhancers, Continued.**

(A) MCF7 cells treated with or without estrogen (E2, 10-7 M, 1 hr) were subjected to ChIP-seq with anti-JMJD6 specific antibody, and overlapping between JMJD6 ChIP-seq binding sites in the presence or absence of estrogen was shown by venn diagram (FC>2).
(B) JMJD6 ChIP-seq tag distribution, both with and without estrogen, centered on estrogen-induced JMJD6 sites (± 3,000 bp).
(C) Box plots displaying the change of tag density induced by estrogen shown in (B).
(D) Heatmap representation of JMJD6 ChIP-seq tag density centered on estrogen-induced JMJD6 sites (± 3,000 bp). JMJD6 ChIP-seq binding sites were first categorized as 3' UTR (untranslated regions) exons, 5' UTR exons, CDS (coding sequencing) exons, intergenic, introns, non-coding, promoter (TSS, transcription start site) and TTS (transcription termination site) based on genomic location, then ChIP-seq binding sites were rank ordered from high to low tag density in each category.
(E) Genomic distribution of estrogen-induced JMJD6 sites.
(F) Motif analysis for estrogen-induced JMJD6 sites (± 100 bp from the center of ChIP-seq binding sites).
(G) Heat map representation of JMJD6, ERa, H3K4me1, H3K4me2, H3K4me3, H3K27Ac, p300, H3K9me3, H3K27me3 ChIP-seq tag density centered on estrogen-induced JMJD6 sites (± 3,000 bp).
(H, I) Genome browser views of JMJD6, ERa, H3K4me1, H3K4me2, H3K4me3, H3K27Ac, p300, MED1, MED12, H3K9me3, H3K27me3 ChIP-seq on selected active enhancer regions, such as the ones nearby estrogen-induced coding gene FOXC1 (H) and SIAH2 (I), were shown. Boxed regions indicated active enhancers.

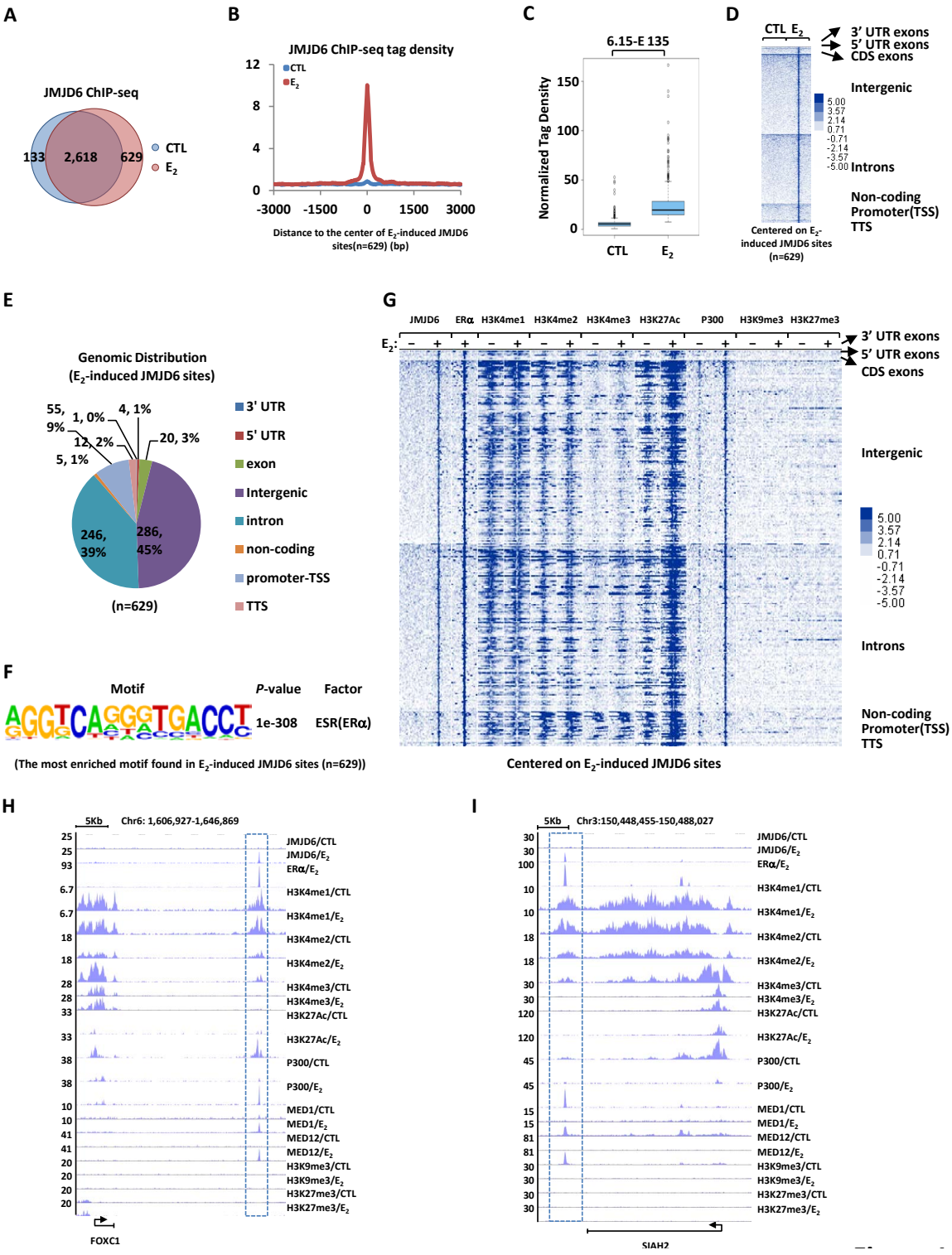
A
JMJD6 ChIP-seq
133
2,618
629
CTL
E2
B
JMJD6 ChIP-seq tag density
CTL
E2
12
8
4
0
-3000
-1500
0
1500
3000
Distance to the center of E2-induced JMJD6 sites(n=629) (bp)
C
6.15-E 135
Normalized Tag Density
150
100
50
0
CTL
E2
D
CTL E2
3' UTR exons
5' UTR exons
CDS exons
Intergenic
5.00
3.57
2.14
0.71
-0.71
-2.14
-3.57
-5.00
Introns
Non-coding
Promoter(TSS)
TTS
Centered on E2-induced JMJD6 sites (n=629)
E
Genomic Distribution
(E2-induced JMJD6 sites)
55, 9%
1, 0%
4, 1%
12, 2%
20, 3%
5, 1%
246, 39%
286, 45%
(n=629)
3' UTR
5' UTR
exon
Intergenic
intron
non-coding
promoter-TSS
TTS
F
Motif
P-value
Factor
1e-308
ESR(ERα)
(The most enriched motif found in E2-induced JMJD6 sites (n=629))
G
JMJD6
ERα
H3K4me1
H3K4me2
H3K4me3
H3K27Ac
P300
H3K9me3
H3K27me3
E2:
3' UTR exons
5' UTR exons
CDS exons
Intergenic
5.00
3.57
2.14
0.71
-0.71
-2.14
-3.57
-5.00
Introns
Non-coding
Promoter(TSS)
TTS
Centered on E2-induced JMJD6 sites
H
5Kb
Chr6: 1,606,927-1,646,869
JMJD6/CTL
JMJD6/E2
ERα/E2
H3K4me1/CTL
H3K4me1/E2
H3K4me2/CTL
H3K4me2/E2
H3K4me3/CTL
H3K4me3/E2
H3K27Ac/CTL
H3K27Ac/E2
P300/CTL
P300/E2
MED1/CTL
MED1/E2
MED12/CTL
MED12/E2
H3K9me3/CTL
H3K9me3/E2
H3K27me3/CTL
H3K27me3/E2
FOXC1
I
5Kb
Chr3:150,448,455-150,488,027
JMJD6/CTL
JMJD6/E2
ERα/E2
H3K4me1/CTL
H3K4me1/E2
H3K4me2/CTL
H3K4me2/E2
H3K4me3/CTL
H3K4me3/E2
H3K27Ac/CTL
H3K27Ac/E2
P300/CTL
P300/E2
MED1/CTL
MED1/E2
MED12/CTL
MED12/E2
H3K9me3/CTL
H3K9me3/E2
H3K27me3/CTL
H3K27me3/E2
SIAH2

**Figure 9: JMJD6 is Required for Transcriptional Activation of ERα-Bound Active Enhancers, Continued.**

(A) MCF7 cells were transfected with control siRNA or siRNA specific against JMJD6, and treated with or without estrogen (E2, 10-7 M, 1 hr), followed by Gro-seq. Gro-seq tag distribution, both sense (+) and anti-sense (-), centered on estrogen-induced JMJD6 sites were shown (± 5,000 bp).
(B) Heat map representation of Gro-seq tag density as shown in (A).
(C) Estrogen-induced JMJD6 sites were divided into three groups, high, medium and low, based on ChIP-seq tag density, and Gro-seq tag distribution, both sense (+) and anti-sense (-), centered on estrogen-induced JMJD6 sites , were shown (± 5,000 bp).
(D) MCF7 cells were transfected with control siRNA or siRNA specific against JMJD6, and treated with or without estrogen (E2, 10-7 M, 1 hr), followed by RNA extraction and RT-qPCR analysis to examine the expression of selected enhancer RNAs (eRNAs) nearby estrogen-induced coding genes as indicated (± s.e.m., *P<0.05, **P<0.01, ***P<0.001).
(E) WT and JMJD6 (KO) MCF7 cells were maintained in stripping medium for three days before treating with or without estrogen (E2, 10-7 M, 1 hr), followed by RNA extraction and RT-qPCR analysis to examine the expression of selected enhancer RNAs (eRNAs) nearby estrogen-induced coding genes as indicated (± s.e.m., *P<0.05, **P<0.01, ***P<0.001).
(F) MCF7 cells were transfected with control siRNA or siRNA specific against JMJD6, and treated with or without estrogen (E2, 10-7 M, 1hr) followed by ChIP-seq with anti-Pol II specific antibody. Pol II ChIP-seq tag distribution centered on estrogen-induced JMJD6 sites (± 6,000 bp) was shown.
(G, H) Heat map (G) and box plots (H) representation of Pol II ChIP-seq tag density centered on estrogen-induced JMJD6 sites.

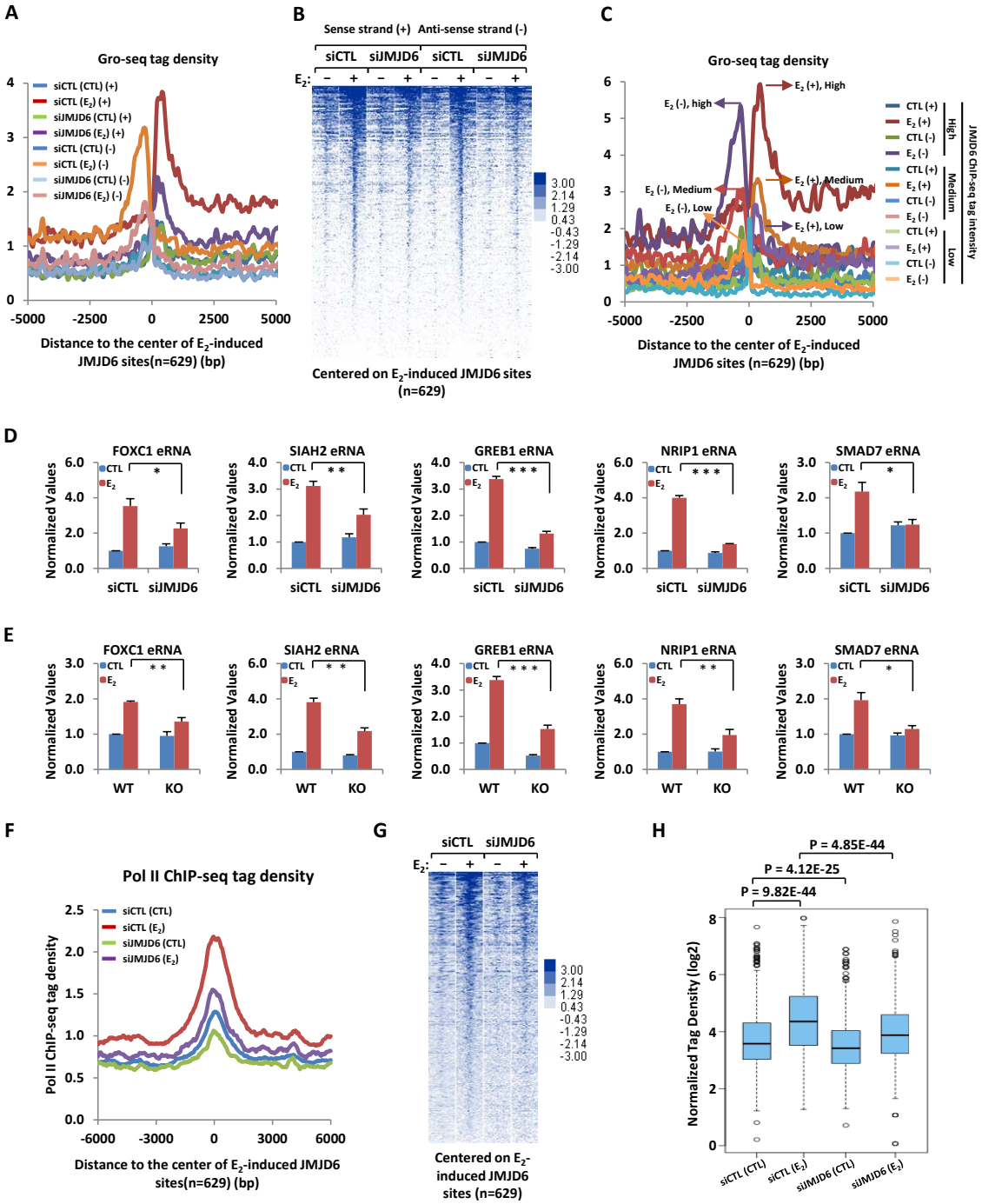
A
Gro-seq tag density
siCTL (CTL) (+)
siCTL (E2) (+)
siJMJD6 (CTL) (+)
siJMJD6 (E2) (+)
siCTL (CTL) (-)
siCTL (E2) (-)
siJMJD6 (CTL) (-)
siJMJD6 (E2) (-)
Distance to the center of E2-induced JMJD6 sites(n=629) (bp)
B
Sense strand (+) Anti-sense strand (-)
siCTL siJMJD6 siCTL siJMJD6
E2:
Centered on E2-induced JMJD6 sites (n=629)
C
Gro-seq tag density
E2 (-), high
E2 (+), High
E2 (-), Medium
E2 (+), Medium
E2 (-), Low
E2 (+), Low
JMJD6 ChIP-seq tag intensity
High
Medium
low
Distance to the center of E2-induced JMJD6 sites (n=629) (bp)
D
FOXC1 eRNA
SIAH2 eRNA
GREB1 eRNA
NRIP1 eRNA
SMAD7 eRNA
Normalized Values
siCTL siJMJD6
E
FOXC1 eRNA
SIAH2 eRNA
GREB1 eRNA
NRIP1 eRNA
SMAD7 eRNA
Normalized Values
WT KO
F
Pol II ChIP-seq tag density
Pol II ChIP-seq tag density
Distance to the center of E2-induced JMJD6 sites(n=629) (bp)
G
siCTL siJMJD6
E2:
Centered on E2-induced JMJD6 sites (n=629)
H
P = 4.85E-44
P = 4.12E-25
P = 9.82E-44
Normalized Tag Density (log2)
siCTL (CTL)
siCTL (E2)
siJMJD6 (CTL)
siJMJD6 (E2)

**Figure 10: JMJD6 Regulates Estrogen-induced Coding Gene Transcription, Continued.**

(A) MCF7 cells were transfected with control siRNA or siRNA specific against JMJD6, and treated with or without estrogen (E2, 10-7 M, 1 hr) followed by Gro-seq. Pie chart showed genes positively- and negatively-regulated by estrogen based on Gro-seq (FC (siCTL (E2)/siCTL (CTL))≥1.5).
(B) Venn diagram showing genes induced by estrogen and dependent on JMJD6 for expression based on Gro-seq as described in (A) (FC (siCTL (E2)/siJMJD6 (E2))≥1.5).
(C, D) Heat map (C) and box plots (D) representation of the expression levels (RPKM) for genes induced by estrogen and dependent on JMJD6 in the presence of estrogen as described in (B) in both control siRNA (siCTL) and JMJD6 siRNA (siJMJD6) transfected conditions.
(E) MCF7 cells were transfected with control siRNA or siRNA specific against JMJD6, and treated with or without estrogen (E2, 10-7 M, 1 hr), followed by RNA extraction and RT-qPCR analysis to examine the expression of selected estrogen-induced coding genes as indicated (± s.e.m., **P<0.01, ***P<0.001).
(F) WT and JMJD6 (KO) MCF7 cells were maintained in stripping medium for three days before treating with or without estrogen (E2, 10-7M, 1h), followed by RNA extraction and RT-qPCR analysis to examine the expression of selected estrogen-induced coding genes as indicated (± s.e.m., **P<0.01, ***P<0.001).
(G) Traveling ratio (TR) distribution calculated based on Gro-seq for genes induced by estrogen and dependent on JMJD6.
(H) Box plots displaying the change of TR as shown in (G).
(I) Gro-seq tag distribution, both sense (+) and anti-sense (-), centered on TSSs (transcription start sites) of genes induced by estrogen and dependent on JMJD6 (± 6,000 bp).

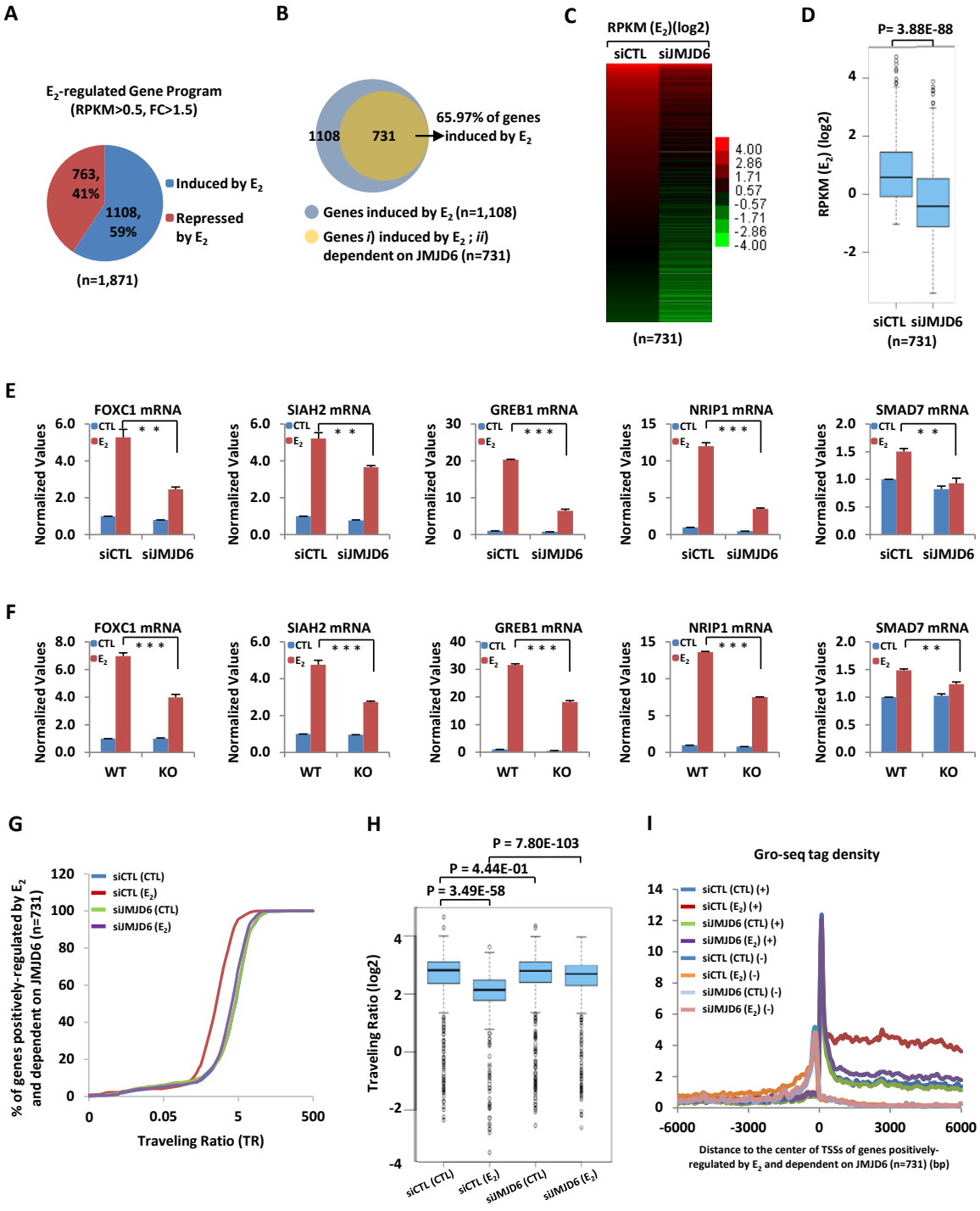
A
E2-regulated Gene Program
(RPKM>0.5, FC>1.5)
763, 41%
1108, 59%
Induced by E2
Repressed by E2
(n=1,871)
B
1108
731
65.97% of genes induced by E2
Genes induced by E2 (n=1,108)
Genes i) induced by E2 ; ii) dependent on JMJD6 (n=731)
C
RPKM (E2)(log2)
siCTL siJMJD6
4.00
2.86
1.71
0.57
-0.57
-1.71
-2.86
-4.00
(n=731)
D
P= 3.88E-88
RPKM (E2) (log2)
siCTL siJMJD6
(n=731)
E
FOXC1 mRNA
SIAH2 mRNA
GREB1 mRNA
NRIP1 mRNA
SMAD7 mRNA
Normalized Values
CTL
E2
siCTL siJMJD6
F
FOXC1 mRNA
SIAH2 mRNA
GREB1 mRNA
NRIP1 mRNA
SMAD7 mRNA
Normalized Values
WT KO
G
% of genes positively-regulated by E2 and dependent on JMJD6 (n=731)
siCTL (CTL)
siCTL (E2)
siJMJD6 (CTL)
siJMJD6 (E2)
Traveling Ratio (TR)
H
P = 7.80E-103
P = 4.44E-01
P = 3.49E-58
Traveling Ratio (log2)
siCTL (CTL)
siCTL (E2)
siJMJD6 (CTL)
siJMJD6 (E2)
I
Gro-seq tag density
siCTL (CTL) (+)
siCTL (E2) (+)
siJMJD6 (CTL) (+)
siJMJD6 (E2) (+)
siCTL (CTL) (-)
siCTL (E2) (-)
siJMJD6 (CTL) (-)
siJMJD6 (E2) (-)
Distance to the center of TSSs of genes positively-regulated by E2 and dependent on JMJD6 (n=731) (bp)

**Figure 11: JMJD6 Regulates MED12 Function in Estrogen-Induced Transcriptional Activation, Continued.**

(A) Inducible stable MCF7 cells expressing flag-tagged JMJD6 were treated with doxycycline (Dox) (+: 0.5 mg/mL; ++: 1 mg/mL) for 48 hrs and subjected to immunoprecipitation (IP) with anti-flag antibody followed by immunoblotting (IB) with antibodies as indicated.
(B) HEK293T cells transfected with myc-tagged JMJD6 in the presence or absence of flag-tagged MED12 were subjected to immunoprecipitation (IP) with anti-myc antibody followed by immunoblotting (IB) with antibodies as indicated.
(C) MCF7 cells were transfected with control siRNA, siRNA specific against JMJD6 or MED12, maintained in stripping medium for three days before treating with or without estrogen (E2, 10-7 M, 6 hrs) followed by RNA-seq analysis. Estrogen-positively regulated genes (FC (siCTL (E2)/siCTL (CTL))≥1.5) which were dependent on both JMJD6 and MED12 were shown by Pie chart.
(D, E) Heat map (D) and box plots (E) representation of the expression levels (RPKM) for genes induced by estrogen and dependent on JMJD6 and MED12 in the presence of estrogen as described in (C) in control siRNA (siCTL), JMJD6 siRNA (siJMJD6) and MED12 siRNA (siMED12) transfected conditions.
(F, G) MCF7 cells as described in (C) were subjected to RT-qPCR analysis to examine the expression of selected estrogen-induced coding genes (F) and cognate enhancer RNAs (eRNAs) (G) as indicated.
(H) MCF7 cells were transfected with control siRNA or siRNA specific against JMJD6, maintained in stripping medium for three days before treating with or without estrogen (E2, 10-7 M, 1 hr) followed by ChIP-seq with anti-MED12 specific antibody. MED12 ChIP-seq tag distribution centered on estrogen-induced JMJD6 sites (± 3,000 bp) was shown.
(I, J) Heat map (I) and box plot (J) representation of MED12 ChIP-seq tag density centered on estrogen-induced JMJD6 sites (± 3,000 bp). JMJD6 ChIP-seq binding sites were first categorized as 3' UTR exons, 5' UTR exons, CDS exons, intergenic, introns, non-coding, promoter (Andersson et al.) and TTS based on genomic location, then ChIP-seq binding sites were rank ordered from high to low tag density in each category.

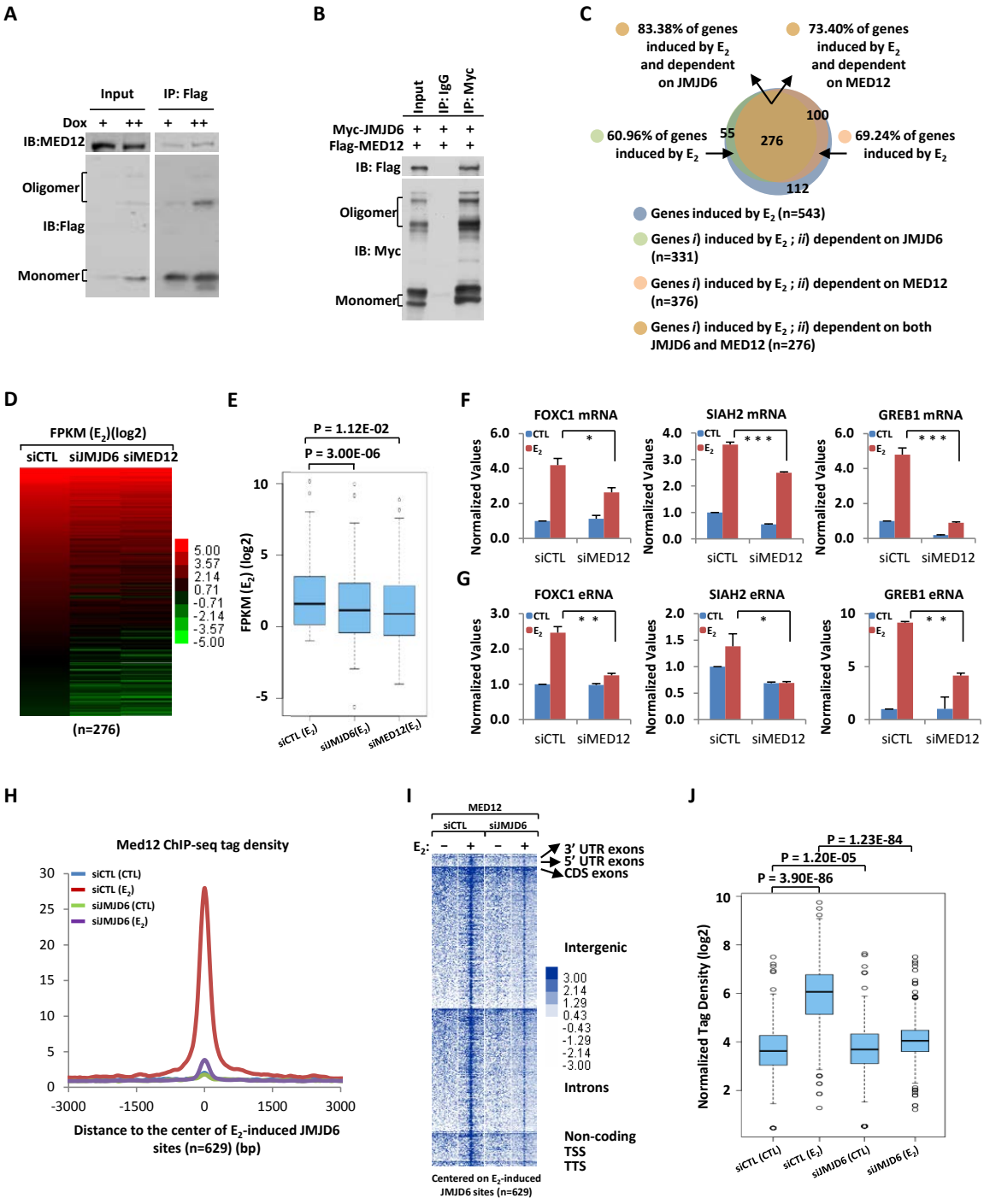
A
Input
IP: Flag
Dox + ++ + ++
IB:MED12
Oligomer
IB:Flag
Monomer
B
Input
IP: IgG
IP: Myc
Myc-JMJD6 + + +
Flag-MED12 + + +
IB: Flag
Oligomer
IB: Myc
Monomer
C
83.38% of genes induced by E2 and dependent on JMJD6
73.40% of genes induced by E2 and dependent on MED12
60.96% of genes induced by E2
69.24% of genes induced by E2
100
55
276
112
Genes induced by E2 (n=543)
Genes i) induced by E2 ; ii) dependent on JMJD6 (n=331)
Genes i) induced by E2 ; ii) dependent on MED12 (n=376)
Genes i) induced by E2 ; ii) dependent on both JMJD6 and MED12 (n=276)
D
FPKM (E2)(log2)
siCTL siJMJD6 siMED12
5.00
3.57
2.14
0.71
-0.71
-2.14
-3.57
-5.00
(n=276)
E
P = 1.12E-02
P = 3.00E-06
FPKM (E2) (log2)
siCTL (E2)
siJMJD6(E2)
siMED12(E2)
F
FOXC1 mRNA
SIAH2 mRNA
GREB1 mRNA
Normalized Values
CTL
E2
siCTL
siMED12
G
FOXC1 eRNA
SIAH2 eRNA
GREB1 eRNA
H
Med12 ChIP-seq tag density
siCTL (CTL)
siCTL (E2)
siJMJD6 (CTL)
siJMJD6 (E2)
Distance to the center of E2-induced JMJD6 sites (n=629) (bp)
I
MED12
siCTL siJMJD6
E2: - + - +
3' UTR exons
5' UTR exons
CDS exons
Intergenic
3.00
2.14
1.29
0.43
-0.43
-1.29
-2.14
-3.00
Introns
Non-coding
TSS
TTS
Centered on E2-induced JMJD6 sites (n=629)
J
P = 1.23E-84
P = 1.20E-05
P = 3.90E-86
Normalized Tag Density (log2)
siCTL (CTL)
siCTL (E2)
siJMJD6 (CTL)
siJMJD6 (E2)

**Figure 12: JMJD6 Regulates MED12 Interaction with CARM1 and hence MED12 Methylation and Chromatin Binding, Continued.**

(A) Schematic representation of the domain architecture of MED12 protein. Leucine-rich (L) domain (light green); Leucine-serine-rich (LS) domain (yellow); Proline-glutamine-leucine (PQL) domain (light blue); Poly-glutamine (Opa) domain (purple).
(B) HEK293T cells transfected with myc-tagged JMJD6 and flag-tagged MED12 (1-597), MED12 (598-964), MED12 (959-1718) or MED12 (1616-2177) were subjected to immunoprecipitation (IP) with anti-myc antibody followed by immunoblotting (IB) with antibodies as indicated.
(C) Schematic representation of the protocol applied for detecting differential binding proteins and post translational modifications (PTMs) of c-terminus of MED12 (1616-2177) in wild type (Xu et al.) or JMJD6 (KO) MCF7 cells. Wild type (Xu et al.) and JMJD6 (KO) MCF7 cells were subjected to SILAC labeling and then infected with lenti-viral vectors expressing Flag-HA-tagged MED12 c-terminus (1616-2177). Cells were then lysed and cell lysates were pooled and subjected to affinity purification using anti-Flag M2 agarose followed by mass spectrometry (MS) analysis.
(D) Cell lysates as described in (C) were subjected to immunoblotting (IB) analysis with antibodies as indicated.
(E) Cells lysates as described in (C) were subjected to immunoprecipitation (IP) with anti-flag antibody followed by immunoblotting (IB) with antibodies as indicated.
(F) In vitro methylation assay was performed by mixing purified bacterially-expressed CARM1 with flag-tagged MED12 truncations purified from over-expressed HEK293T cells (upper panel). The expression of MED12 truncations was examined by immunoblotting using anti-flag antibody (bottom panel).
(G) In vitro methylation assay was performed by mixing purified bacterially-expressed MED12 c-terminus (1616-2177) with flag-tagged PRMTs purified from over-expressed HEK293T cells (upper panel). The expression of all PRMTs was examined by immunoblotting using anti-flag antibody and indicated by white arrows (bottom panel). Star indicates methylation of MED12.
(H) Methylated arginine residues which methylation decreased upon JMJD6 depletion were identified following the protocol as described in (C), which were shown as indicated.
(I) MCF7 cells were transfected with control siRNA or siRNA specific against CARM1, maintained in stripping medium for three days before treating with or without estrogen (E2, 10-7 M, 1 h) followed by ChIP-seq with anti-MED12 specific antibody. Fold induction of MED12 binding in response to estrogen treatment on selected active enhancer regions, such as the ones nearby estrogen-induced coding gene FOXC1, SIAH2 and GREB1, were shown (± s.e.m., **P<0.01; N.S: not significant). P: promoter; E: enhancer.

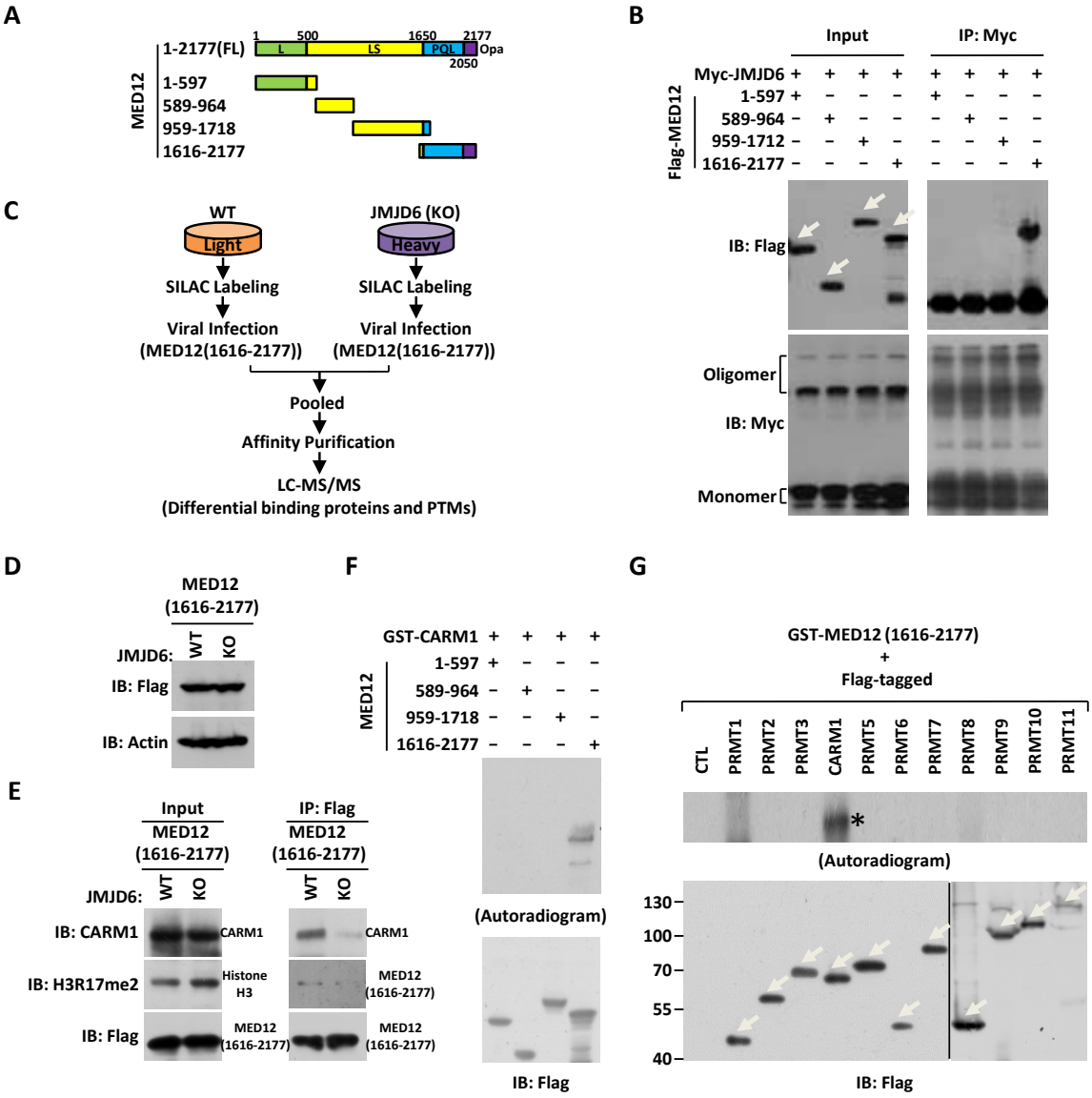


H

Methylated arginine residues which methylation decreased upon JMJD6 depletion

| Identified peptides with arginine methylation | Type of methylation | Abundance (WT) | Abundance (JMJD6 KO) |
|---|---|---|---|
| QGSIGLYTQNQPLPAGGPR(me1) | R1854me1 | 128.6 | 71.4 |
| LPTR(me1)PTYPGVLPTTMTGVMGLEPSSYK | R1871me1 | 132.3 | 67.7 |
| LPTR(me2)PTYPGVLPTTMTGVMGLEPSSYK | R1871me2 | 115 | 85 |
| TSVYR(me1)QQQPAVPQGQR | R1899me1 | 130.6 | 69.4 |
| TSVYR(me2)QQQPAVPQGQR | R1899me2 | 116.2 | 83.8 |

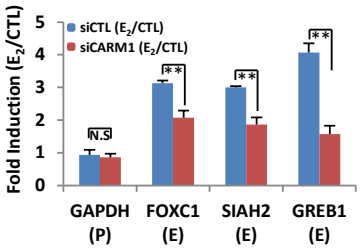

**Figure 13:JMJD6 is Required for Estrogen-Induced Breast Cancer Cell Growth and Tumorigenesis, Continued.**

(A, B) MCF7 cells were transfected with control siRNA (siCTL) or siRNA specifically targeting JMJD6 (siJMJD6) and maintained in normal growth medium (A) or stripping medium (phenol red free) for two days before treating with or without estrogen (E2, 10-7 M) (B) followed by cell proliferation assay (± s.e.m., *P<0.05, **P<0.01, ***P<0.001).
(C, D) WT and JMJD6 (KO) MCF7 cells were maintained in normal growth medium (C) or stripping medium for two days before treating with estrogen (E2, 10-7M) (D) followed by cell proliferation assay (± s.e.m., *P<0.05, **P<0.01, ***P<0.001).
(E, F) WT and JMJD6 (KO) MCF7 cells were maintained in normal growth medium (E) or stripping medium in the presence of estrogen (E2, 10-7 M) (F) for 10 days for colony formation, and cell colonies were fixed and stained with crystal violet.
(G, I) WT and JMJD6 (KO) MCF7 cells were grown to confluence in normal growth medium (G) or stripping medium before treating with estrogen (E2, 10-7 M) (I) followed by wound-healing assay.
(H, J) Quantification of wound closure shown in panel G (H) and I (J).
(K) WT and JMJD6 (KO) MCF7 cells were injected subcutaneously into female BALB//C nude mice, and brushed with or without estrogen (E2, 10-2 M) on the neck every three days for six weeks. Mice were then euthanized and tumors were excised, photographed and weighted.
(L) Significance test for tumor weight shown in (K) was performed (± s.e.m., ***P<0.001).

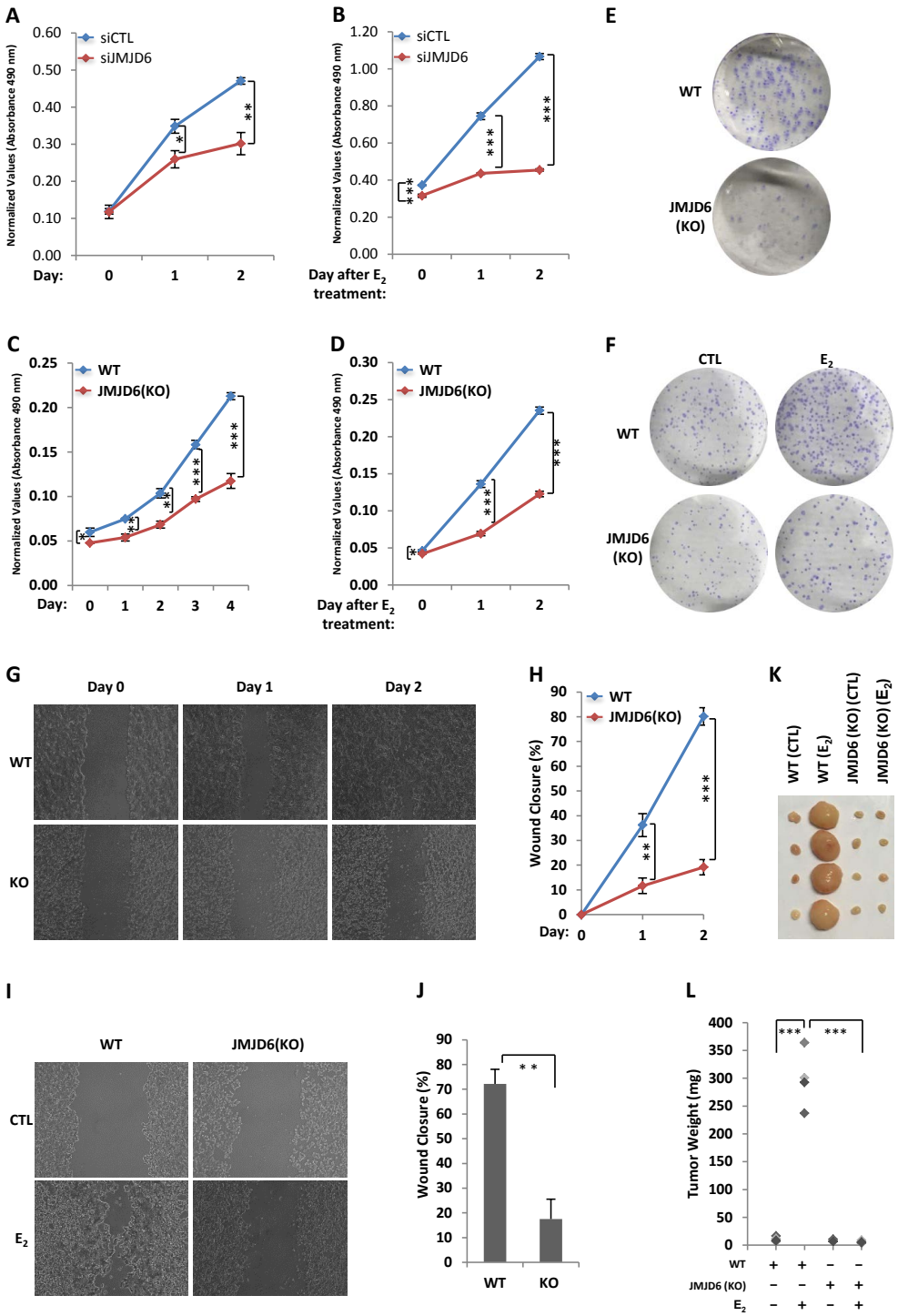
A
siCTL
siJMJD6
Normalized Values (Absorbance 490 nm)
Day:
B
Day after E2 treatment:
E
WT
JMJD6 (KO)
C
WT
JMJD6(KO)
D
F
CTL
E2
G
Day 0
Day 1
Day 2
H
Wound Closure (%)
K
WT (CTL)
WT (E2)
JMJD6 (KO) (CTL)
JMJD6 (KO) (E2)
I
J
L
Tumor Weight (mg)

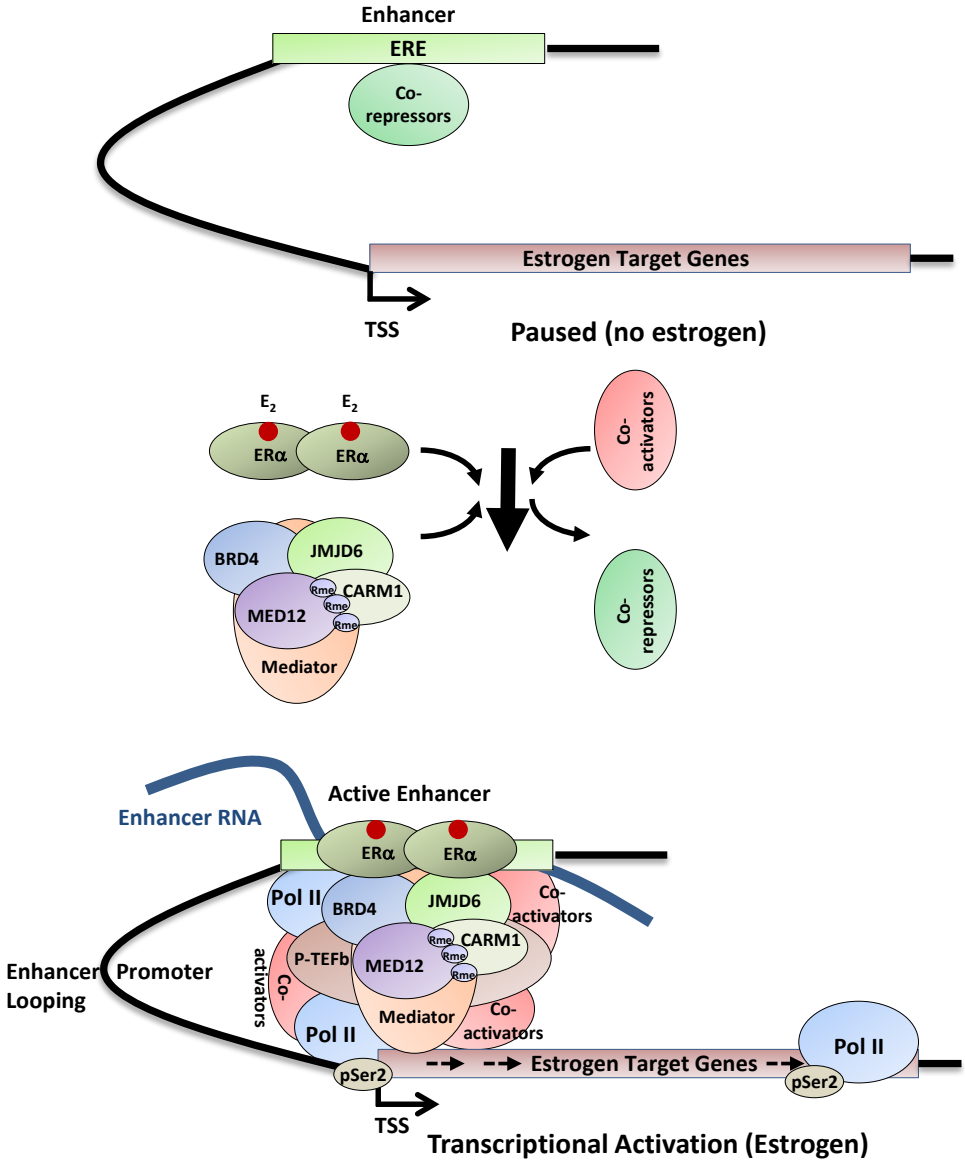


**Figure 14: A Proposed Model of JMJD6 Function in Estrogen/ERα-Regulated Enhancer and Coding Gene Activation**.

Upon estrogen stimulation, a coactivator complex constituting BRD4, JMJD6, MED12, CARM1 and others, accompanied by the exchange of co-repressors, was co-recruited with ERa onto active enhancers, leading to the transcriptional activation of these enhancers (Pol II recruitment and eRNA production) and cognate nearby coding genes (promoter-proximal Pol II pausing release and mRNA production). Mechanistically, BRD4/JMJD6 is required for MED12 to interact with CARM1, which methylates MED12 at multiple arginine residues at its c-terminus and mediates its chromatin binding.

**Figure S 8:JMJD6 is Recruited onto ERα-Bound Active Enhancers upon Estrogen Stimulation, Continued.**

(A) Kaplan Meier survival analyses for distal metastasis free survival (DMFS) of ERa-positive breast tumors using JMJD6 as input. The breast cancer outcome-linked gene expression data were accessed using the Gene Expression-Based Outcome for Breast Cancer Online (GOBO) tool.
(B) MCF7 cells treated with or without estrogen (E2, 10-7 M, 1 hr) were subjected to ChIP-seq with anti-JMJD6 specific antibody, and genomic distribution of JMJD6 sites without estrogen treatment was shown.
(C) ChIP-seq tag distribution, including ERa, H3K4me1, H3K4me2, H3K4me3, H3K27Ac, P300, H3K9me3 and H3K27me3, centered on all of its own sites (left panels) or estrogen-induced JMJD6 sites (right panels) (± 3,000 bp).
(D, E) Genome browser views of JMJD6, ERa, H3K4me1, H3K4me2, H3K4me3, H3K27Ac, P300, MED1, MED12, H3K9me3 and H3K27me3 ChIP-seq on selected active enhancer regions, such as the ones nearby estrogen-induced coding gene GREB1 (D) and SMAD7 (E), were shown. Boxed regions indicated active enhancers.

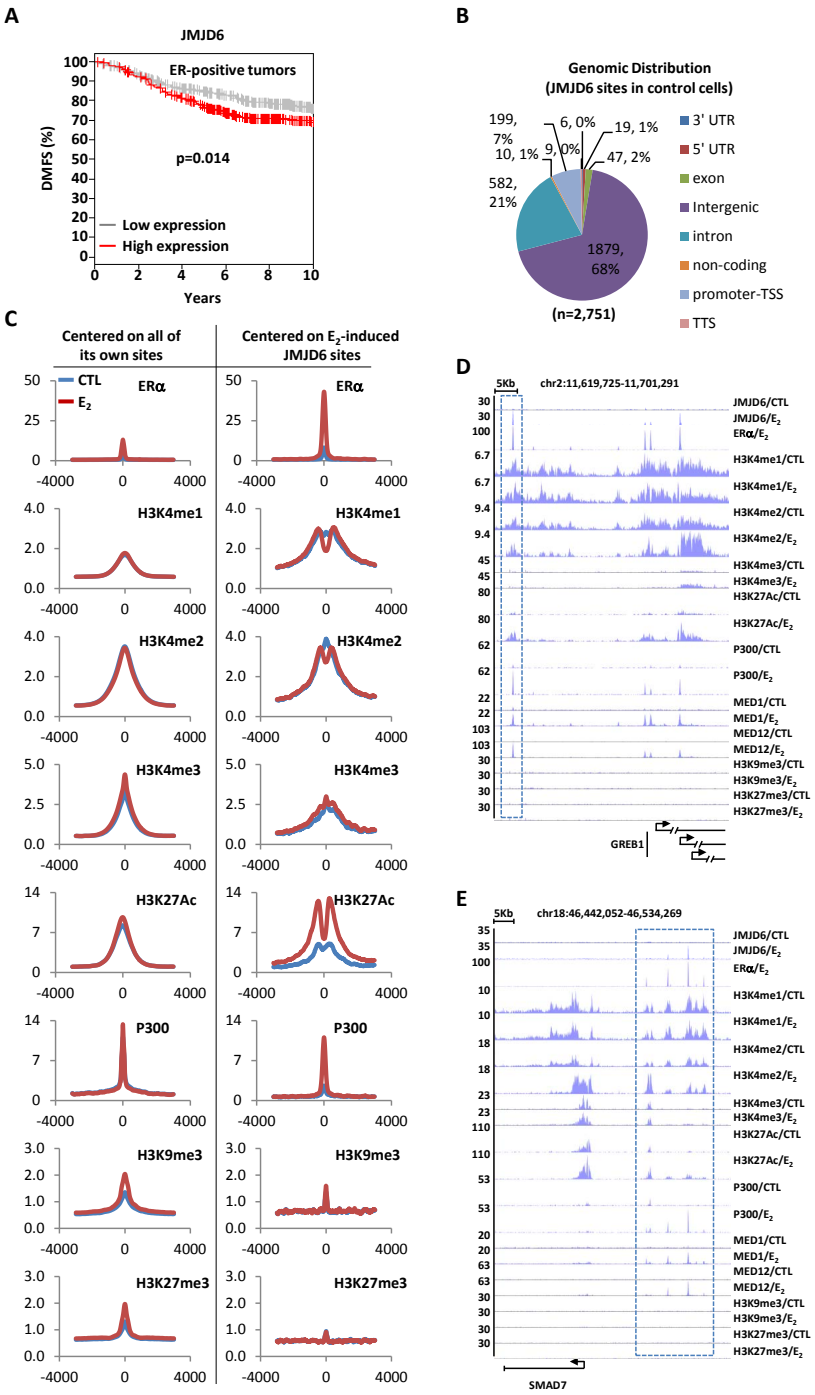
A
JMJD6
ER-positive tumors
p=0.014
Low expression
High expression
DMFS (%)
Years
B
Genomic Distribution
(JMJD6 sites in control cells)
199, 7%
6, 0%
19, 1%
10, 1%
9, 0%
47, 2%
582, 21%
1879, 68%
(n=2,751)
3' UTR
5' UTR
exon
Intergenic
intron
non-coding
promoter-TSS
TTS
C
Centered on all of its own sites
Centered on E2-induced JMJD6 sites
CTL
E2
ERα
H3K4me1
H3K4me2
H3K4me3
H3K27Ac
P300
H3K9me3
H3K27me3
D
5Kb
chr2:11,619,725-11,701,291
JMJD6/CTL
JMJD6/E2
ERα/E2
H3K4me1/CTL
H3K4me1/E2
H3K4me2/CTL
H3K4me2/E2
H3K4me3/CTL
H3K4me3/E2
H3K27Ac/CTL
H3K27Ac/E2
P300/CTL
P300/E2
MED1/CTL
MED1/E2
MED12/CTL
MED12/E2
H3K9me3/CTL
H3K9me3/E2
H3K27me3/CTL
H3K27me3/E2
GREB1
E
5Kb
chr18:46,442,052-46,534,269
SMAD7

**Figure S 9:JMJD6 Determines the Transcriptional Activation of ERα-Bound Enhancers, Continued.**

(A) Gro-seq tag distribution, as shown in Fig. 2A, both sense (+) and anti-sense (-), centered on ERa-bound enhancers without JMJD6 binding (± 5,000 bp).
(B) Heat map representation of Gro-seq tag density as shown in (A).
(C, D) Box plots displaying the change of Gro-seq tag density shown in Fig. 2A, both sense (C) and antisense (D).
(E) MCF7 cells as described in Fig. 2A were subjected to RNA extraction and RT-qPCR analysis to examine the expression of JMJD6.
(F) MCF7 cells as described in Fig. 2A were subjected to immunoblotting (IB) analysis to examine the protein level of JMJD6.
(G) Wild type (Xu et al.) and JMJD6 knockout (KO) MCF7 cells were subjected to immunoblotting (IB) using the antibodies as indicated.
(H) Genomic DNA was extracted from JMJD6 knock-out (KO) cells generated by CRISPR/Cas9 system, followed by PCR using specific primer sets surrounding gRNA targeting region (boxed in blue). The resultant PCR products were subjected to Sanger sequencing and one base pair, A, was inserted as shown in red.
(I) Pol II ChIP-seq tag distribution, as described in Fig. 2F, centered on ERa-bound enhancers without JMJD6 binding (± 6,000 bp) was shown.
(J) Heat map representation of Pol II ChIP-seq tag density as shown in (I).

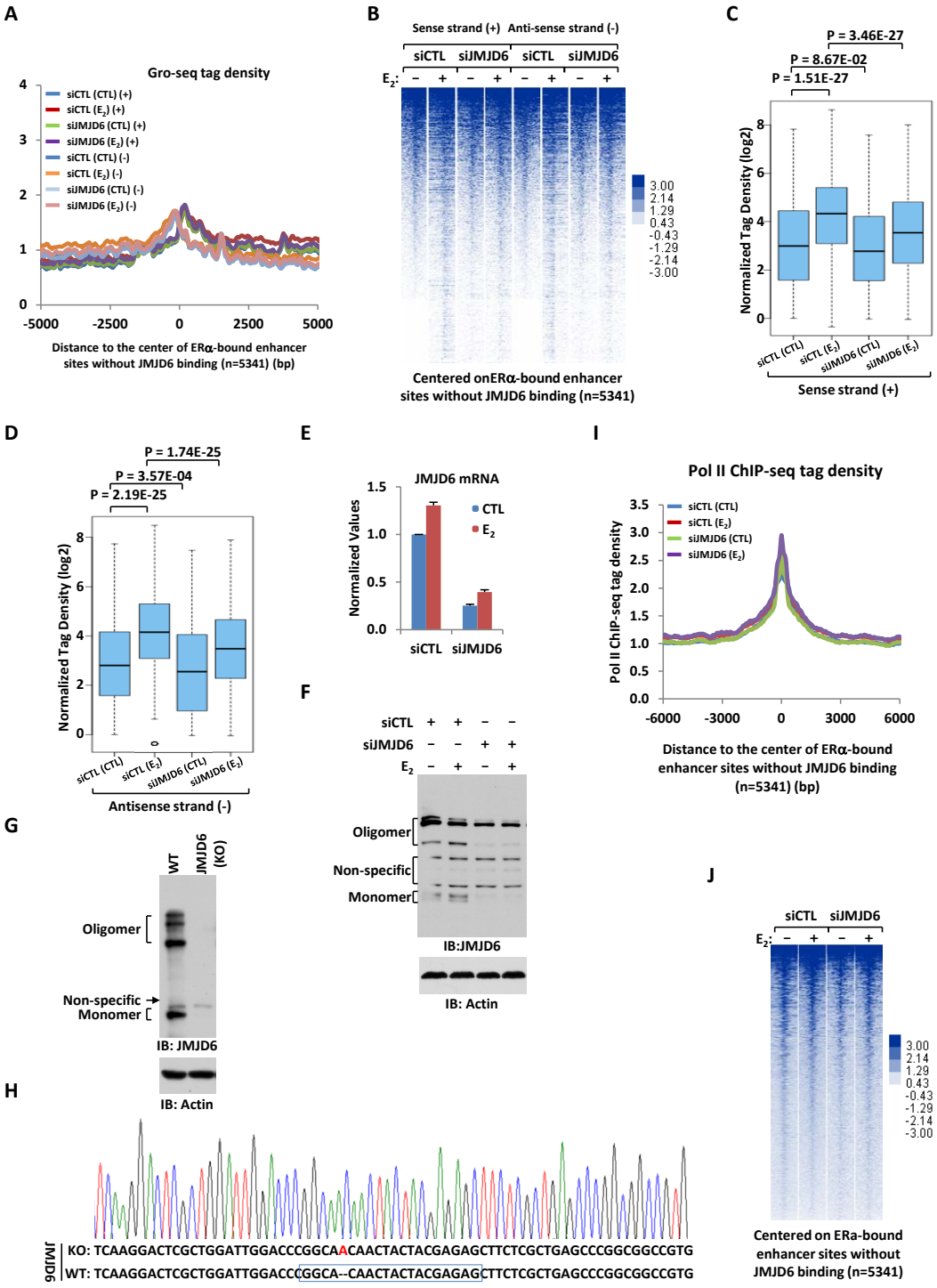
A
Gro-seq tag density
siCTL (CTL) (+)
siCTL (E2) (+)
siJMJD6 (CTL) (+)
siJMJD6 (E2) (+)
siCTL (CTL) (-)
siCTL (E2) (-)
siJMJD6 (CTL) (-)
siJMJD6 (E2) (-)
Distance to the center of ERα-bound enhancer sites without JMJD6 binding (n=5341) (bp)
B
Sense strand (+) Anti-sense strand (-)
siCTL siJMJD6 siCTL siJMJD6
E2:
Centered onERα-bound enhancer sites without JMJD6 binding (n=5341)
C
P = 3.46E-27
P = 8.67E-02
P = 1.51E-27
Normalized Tag Density (log2)
Sense strand (+)
D
P = 1.74E-25
P = 3.57E-04
P = 2.19E-25
Normalized Tag Density (log2)
Antisense strand (-)
E
JMJD6 mRNA
Normalized Values
CTL
E2
siCTL siJMJD6
F
siCTL
siJMJD6
E2
Oligomer
Non-specific
Monomer
IB:JMJD6
IB: Actin
G
WT
JMJD6 (KO)
Oligomer
Non-specific
Monomer
IB: JMJD6
IB: Actin
H
JMJD6
KO: TCAAGGACTCGCTGGATTGGACCCGGCAACAACTACTACGAGAGCTTCTCGCTGAGCCCGGCGGCCGTG
WT: TCAAGGACTCGCTGGATTGGACCCGGCA--CAACTACTACGAGAGCTTCTCGCTGAGCCCGGCGGCCGTG
I
Pol II ChIP-seq tag density
siCTL (CTL)
siCTL (E2)
siJMJD6 (CTL)
siJMJD6 (E2)
Pol II ChIP-seq tag density
Distance to the center of ERα-bound enhancer sites without JMJD6 binding (n=5341) (bp)
J
siCTL siJMJD6
E2:
Centered on ERa-bound enhancer sites without JMJD6 binding (n=5341)

**Figure S 10:JMJD6 Regulates MED12 Function in Estrogen-Induced Transcriptional Activation, Continued.**

(A) List of mediator subunits identified by mass spectrometry to be associated with JMJD6. Number of unique peptides identified for each subunit was shown as indicated.
(B) The binding of JMJD6 with MED12 was examined by SPR assay. The sensorgrams were obtained by injecting a series of concentration of MED12 over the immobilized JMJD6 chip. BIA evaluation software was used to determine the equilibrium dissociation constant (Kd).
(C) Correlation between fold change of expression levels for genes induced by estrogen before and after knocking down of JMJD6 or MED12 in the presence of estrogen.
(D, E) MCF7 cells as described in Fig. 4C were subjected to RT-qPCR (D) or immunoblotting (E) analysis to examine the expression of MED12.
(F) MED12 ChIP-seq tag distribution, as shown in Fig. 4H, centered on TTSs of genes induced by estrogen and dependent on both JMJD6 and MED12 (± 3,000 bp) was shown.
(G, H) Heat map (G) and box plot (H) representation of MED12 ChIP-seq tag density as described in (F).
(I, J) MCF7 cells as described in Fig. 4H were subjected to RT-qPCR (I) and immunoblotting (J) analysis to examine the expression of MED12.

A

| Official Gene Symbol | Gene Name | Number of Unique Peptides |
|---|---|---|
| MED1 | mediator complex subunit 1 | 15 |
| MED4 | mediator complex subunit 4 | 3 |
| MED6 | mediator complex subunit 6 | 2 |
| MED8 | mediator complex subunit 8 | 3 |
| MED9 | mediator complex subunit 9 | 3 |
| MED10 | mediator complex subunit 10 | 1 |
| MED11 | mediator complex subunit 11 | 2 |
| MED12 | mediator complex subunit 12 | 23 |
| MED13L | mediator complex subunit 13L | 3 |
| MED15 | mediator complex subunit 15 | 3 |
| MED16 | mediator complex subunit 16 | 2 |
| MED17 | mediator complex subunit 17 | 6 |
| MED18 | mediator complex subunit 18 | 2 |
| MED19 | mediator complex subunit 19 | 2 |
| MED20 | mediator complex subunit 20 | 2 |
| MED21 | mediator complex subunit 21 | 3 |
| MED22 | mediator complex subunit 22 | 2 |
| MED23 | mediator complex subunit 23 | 7 |
| MED24 | mediator complex subunit 24 | 6 |
| MED27 | mediator complex subunit 27 | 3 |
| MED28 | mediator complex subunit 28 | 2 |
| MED30 | mediator complex subunit 30 | 3 |
| MED31 | mediator complex subunit 31 | 2 |

B

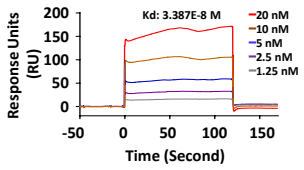


C

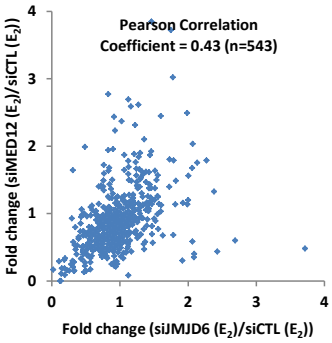


D

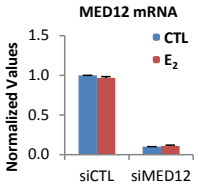


E

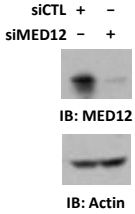


F

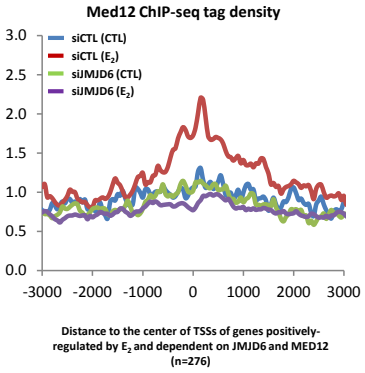


G

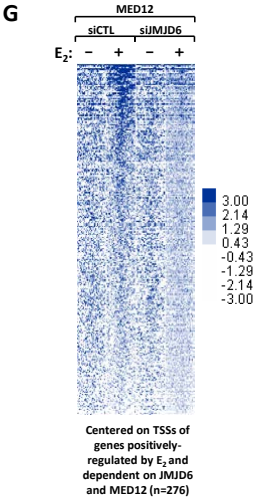


H

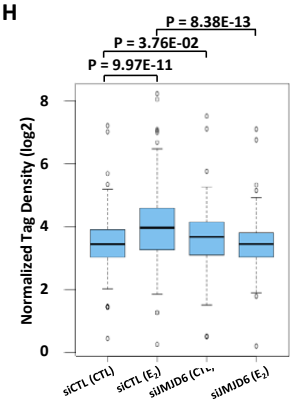


I

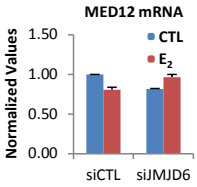


J

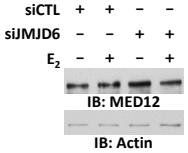

A

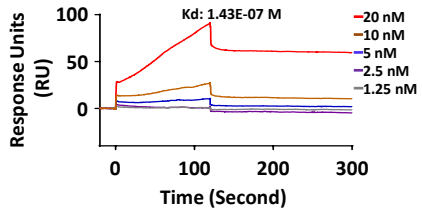


B

MED12 (NP_005111.2) aa1616-2177

LAKKLQKELGERQSDSLEKVRQLLPLPKQTRDVITCEP
QGSLIDTKGNKIAGFDSIFKKEGLQVSTKQKISPWDLF
EGLKPSAPLSWGWFGTVRVDRRVARGEEQQRLLLYHTH
LRPRPRAYYLEPLPLPPEDEEPPAPTLLEPEKKAPEPP
KTDKPGAAPPSTEERKKKSTKGKKRSQPATKTEDYGMG
PGRSGPYGVTVPPDLLHHPNPGSITHLNYRQGSIGLYT
QNQPLPAGGPRVDPYRPVRLPMQKLPTRPTYPGVLPTT
MTGVMGLEPSSYKTSVYRQQQPAVPQGQRLRQQLQQSQ
GMLGQSSVHQMTPSSSYGLQTSQGYTPYVSHVGLQQHT
GPAGTMVPPSYSSQPYQSTHPSTNPTLVDPTRHLQQRP
SGYVHQQAPTYGHGLTSTQRFSHQTLQQTPMISTMTPM
SAQGVQAGVRSTAILPEQQQQQQQQQQQQQQQQQQQQQ
QQQQQYHIRQQQQQQILRQQQQQQQQQQQQQQQQQQQQ
QQQQQQHQQQQQQQAAPPQPQPQSQPQFQRQGLQQTQQ
QQQTAALVRQLQQQLSNTQPQPSTNIFGRY

**Figure S 11:Arginine Methylation Sites Identified at the C-terminus of MED12.**

(A) The binding of JMJD6 with MED12 c-terminus (1616-2177) was examined by SPR assay. The sensorgrams were obtained by injecting a series of concentration of MED12 over the immobilized JMJD6 chip. BIA evaluation software was used to determine the equilibrium dissociation constant (Kd).
(B) Sequence of human MED12 c-terminus (amino acid (aa) 1616-2177). Arginine residues identified to be mono-methylated only were highlighted in red, and those with both mono- and di-methylation were highlighted in red and underlined.

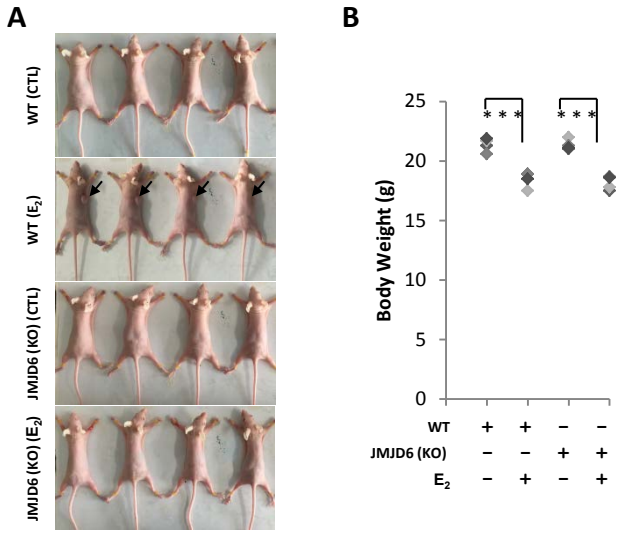


**Figure S 12:JMJD6 is Required for Estrogen-Induced Breast Cancer Cell Growth and Tumorigenesis.**

(A) Mice as described in Fig. 6K were euthanized, photographed and weighted.
(B) Significance test for body weight shown in (A) was performed (± s.e.m., ***P<0.001).

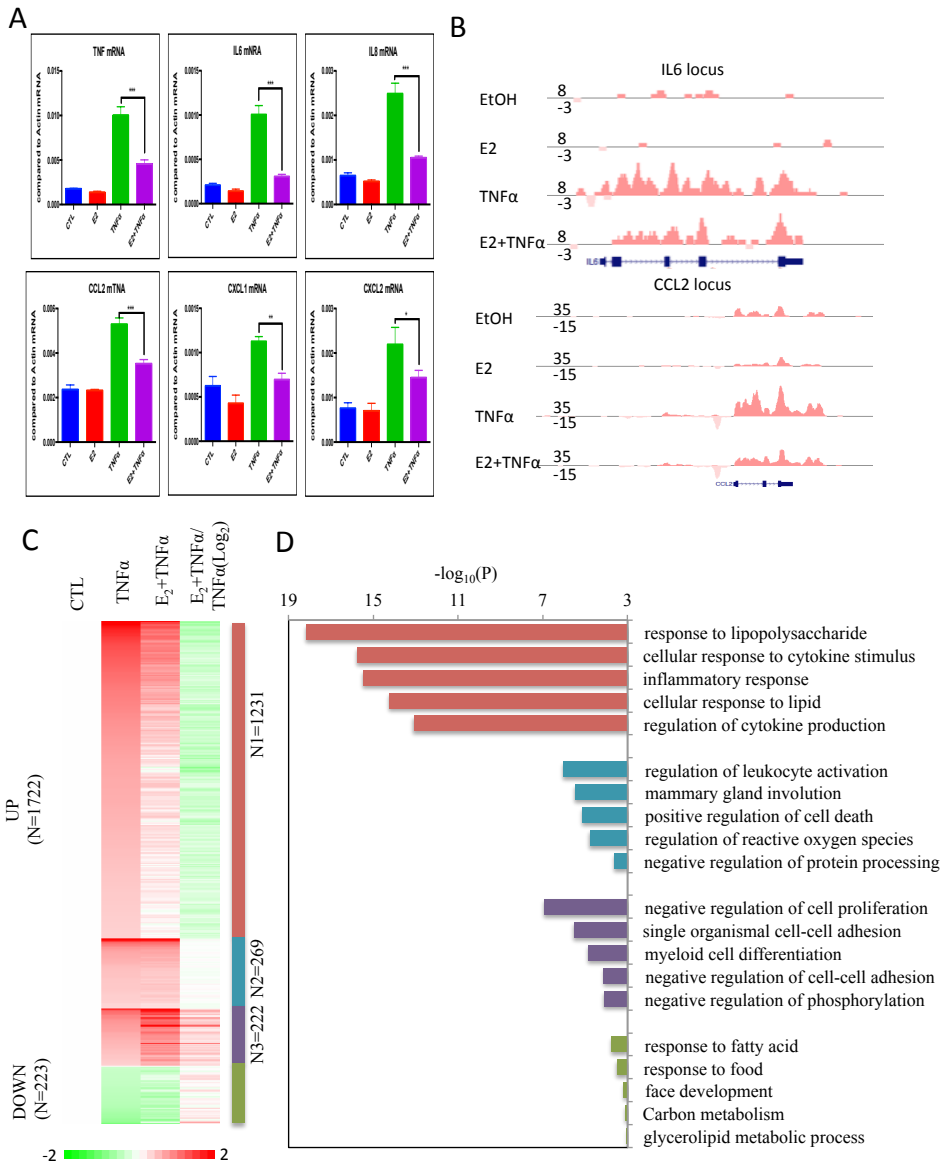


**Figure 15: E2 Downregulates TNFα Transcription Program**

(A) qPCR showing E2 could down regulate TNFα-induced genes.
(B) Representative genome browser snapshots for Gro-seq data at IL6 and CCL2 loci.
(C) Heatmap shows E2 effects on TNFα-induced genes.
(D) Gene ontology analysis by MetaScape of TNFα-induced genes.

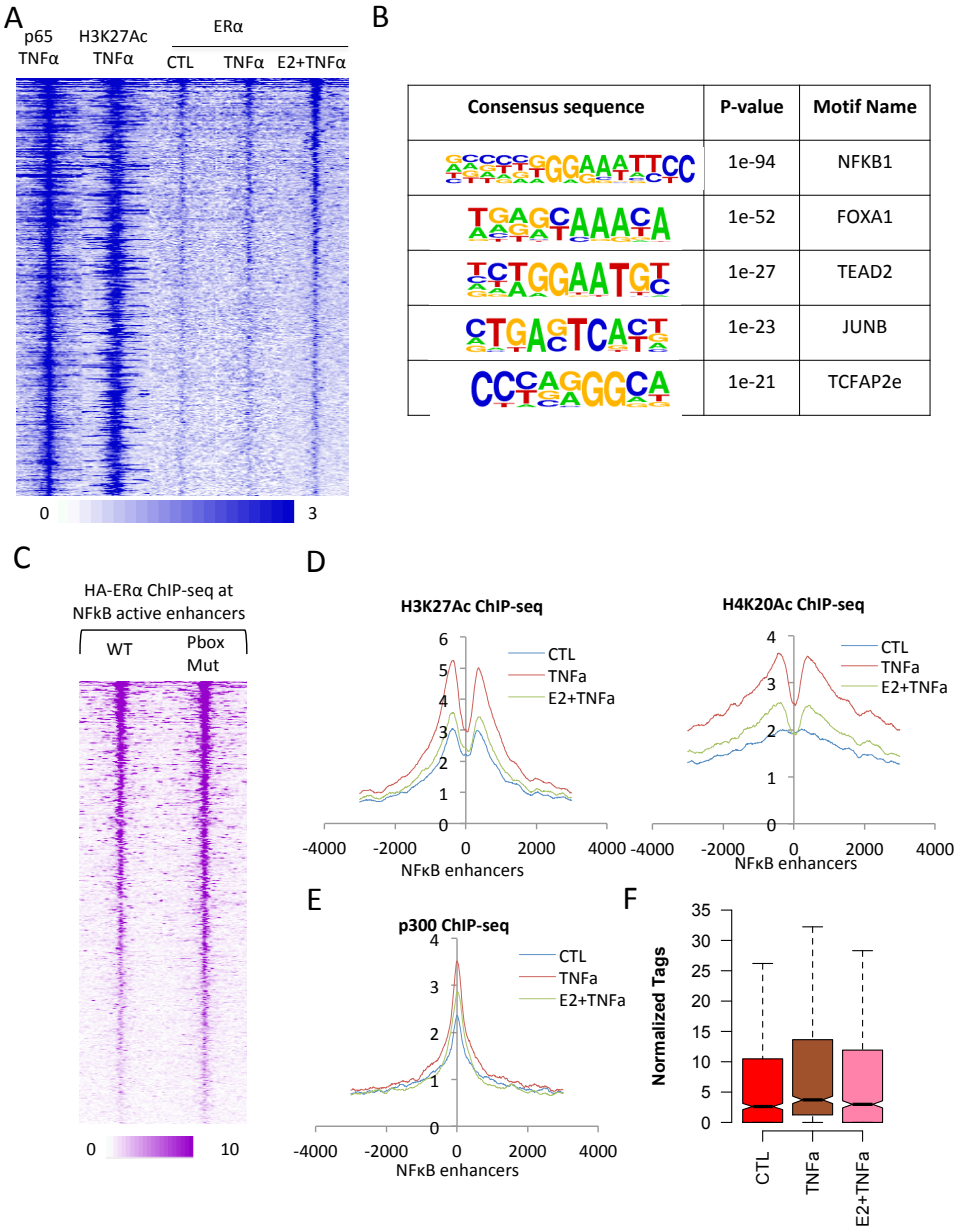


**Figure 16: ERα is Tethered to NFκB Enhancers to Repress Transcription**

(A) Heatmap analysis of ERα ChIP-seq enrichment on NFκB enhancers.
(B) Motif analysis of ERα-occupied NFkB enhancers.
(C) Heapmap showing wild type and DNA binding domain mutated (PBox Mut) ERα ChIP-seq enrichment on NFκB enhancers.
(D) Tag density map of histone H3K27Ac and H4K20Ac ChIP-seq enrichment at NFκB enhancers.
(E) Tag density map of co-activator p300 ChIP-seq enrichment at NFκB enhancers.
(F) Box plot showing tag counts of transcripts from NFκB enhancers.

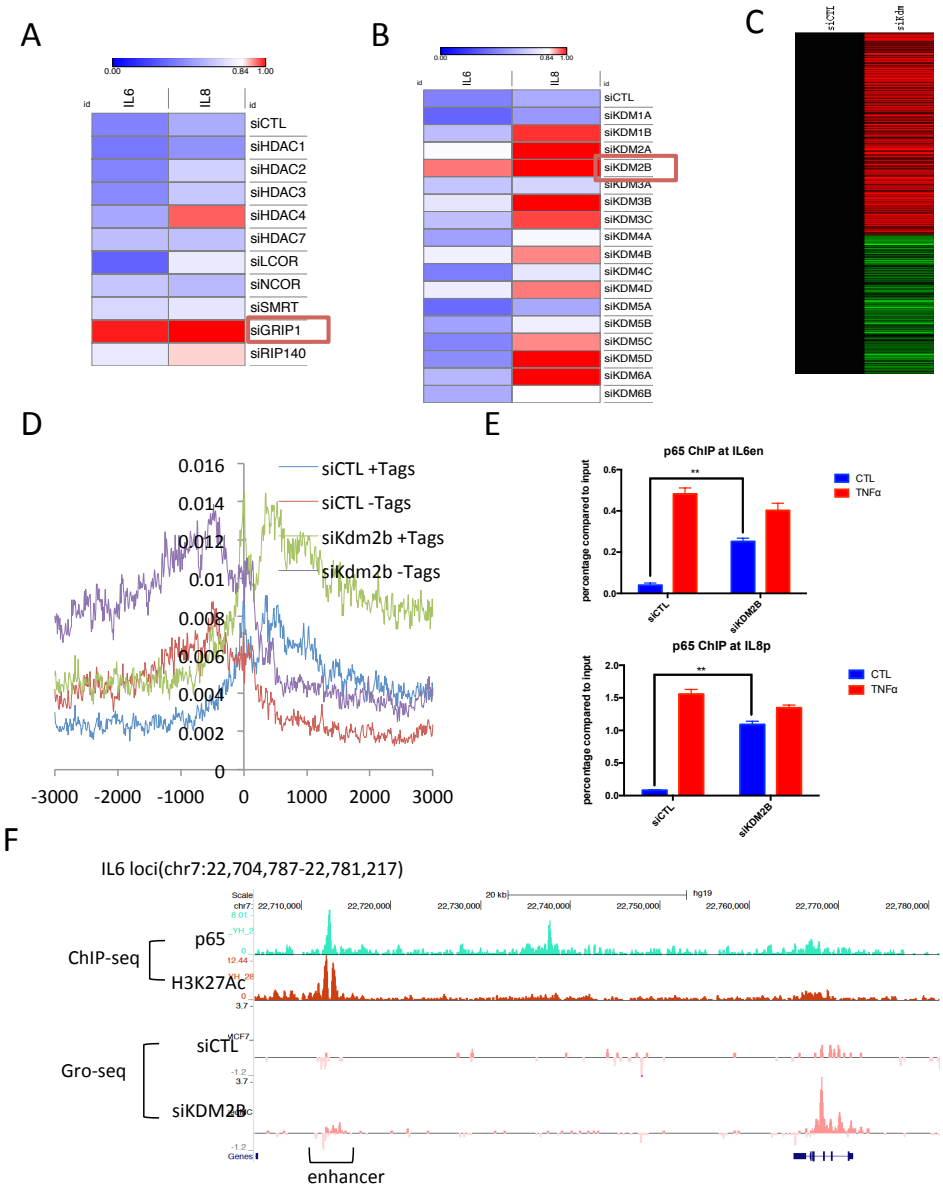


**Figure 17: KDM2B represses inflammation at basal condition**

(A) and (B) show siRNA screening results of repressors and histone demethylases on E2-dependent repression of pro-inflammatory genes IL6 and IL8.
(C) Heatmap showing GRO-seq analysis of KDM2B knockdown on TNFα-induced genes.
(D) Tag density map of KDM2B knockdown effect on transcripts from NFκB enhancers.
(E) Representative p65 ChIP-qPCR data on IL6 enhancer and IL8 promoter.
(F) Representative Gro-seq genome browser snapshot at IL6 locus.

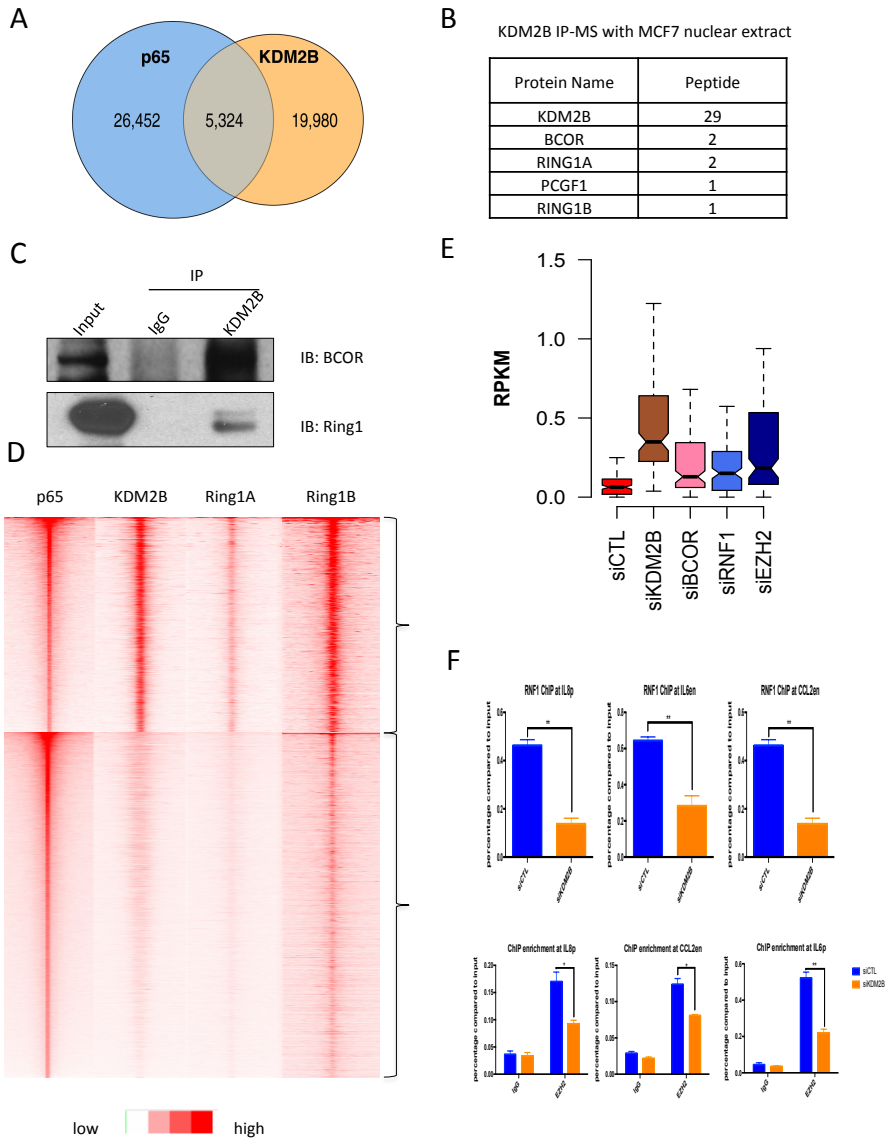


**Figure 18: KDM2B Nucleates PRC1 to Repress Inflammation**

(A) Venn diagram showing p65 binding sites identified by ChIP-seq at TNFα condition overlap with KDM2B binding sites at basal condition.
(B) Table showing HA-KDM2B IP-MS identified representative PRC1 complex proteins.
(C) IP-Western blots showing interaction between KDM2B and PRC1 components BCOR and Ring1A.
(D) Heatmap analysis of ChIP-seq data of p65, KDM2B and Ring1A, Ring1B.
(E) Boxplot analysis showing RNA-seq data focusing on knockdown of KDM2B, PRC1 components, and EZH2 impacts on TNFα-induced genes.
(F) ChIP-qPCR showing KDM2B knockdown reduced binding intensity of Ring1A and EZH2 on representative pro-inflammatory loci like IL6 enhancer, IL8 promoter and CCL2 enhancer.

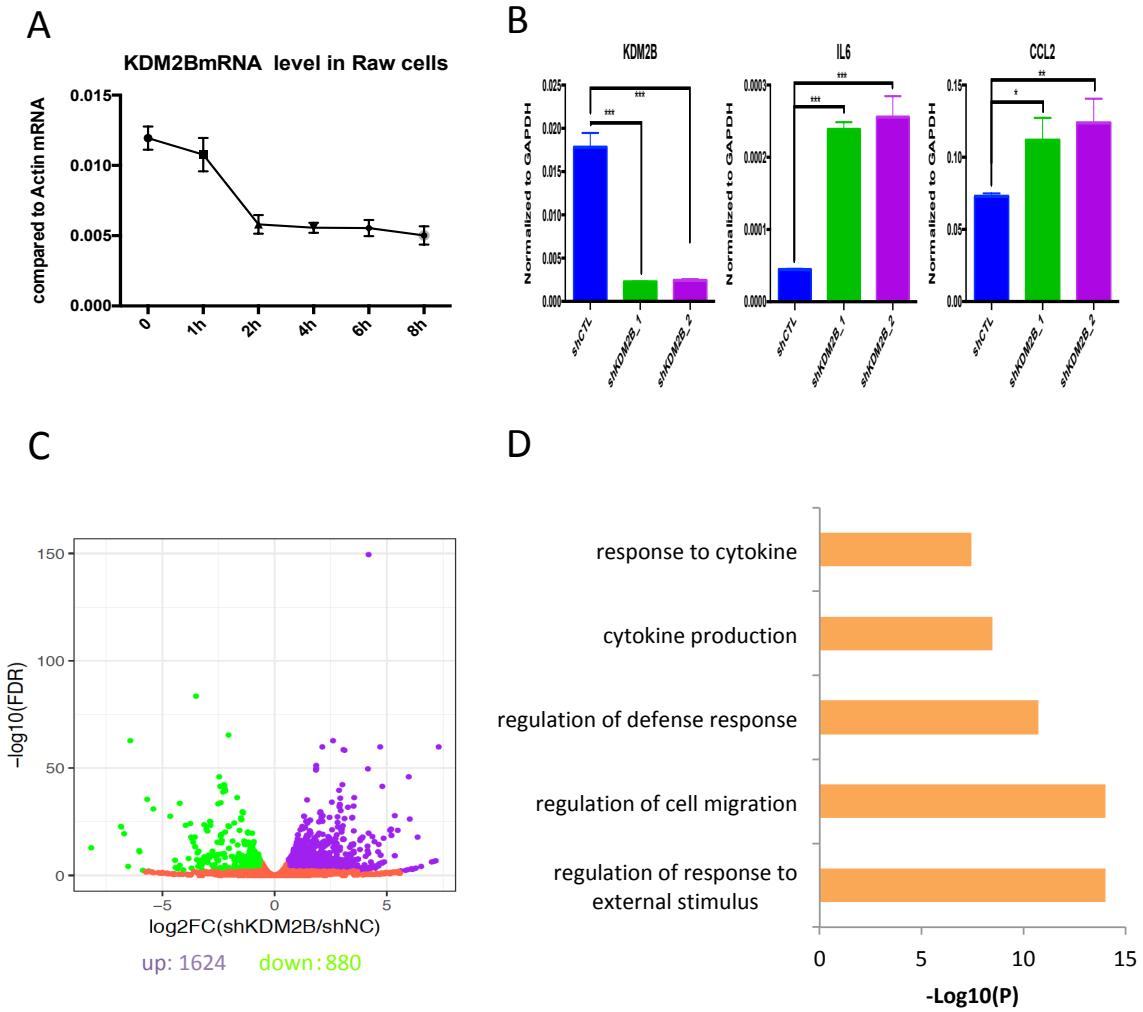


**Figure 19: KDM2B Represses Inflammation in Macrophage**

(A) RT-qPCR data showing KDM2B mRNA level decreases after LPS treatment in Raw 264.7 cells.
(B) RT-qPCR showing that two shRNAs efficiently targeting KDM2B lead to activation of pro-inflammatory genes like IL6 and CCL2 in Raw 264.7 cells.
(C) Scatter plot shows genes differentially regulated by KDM2B knockdown compared to shCTL.
(D) Gene Ontology analysis showing that KDM2B knockdown leads to upregulation of cytokine related genes in Raw 264.7 cells.

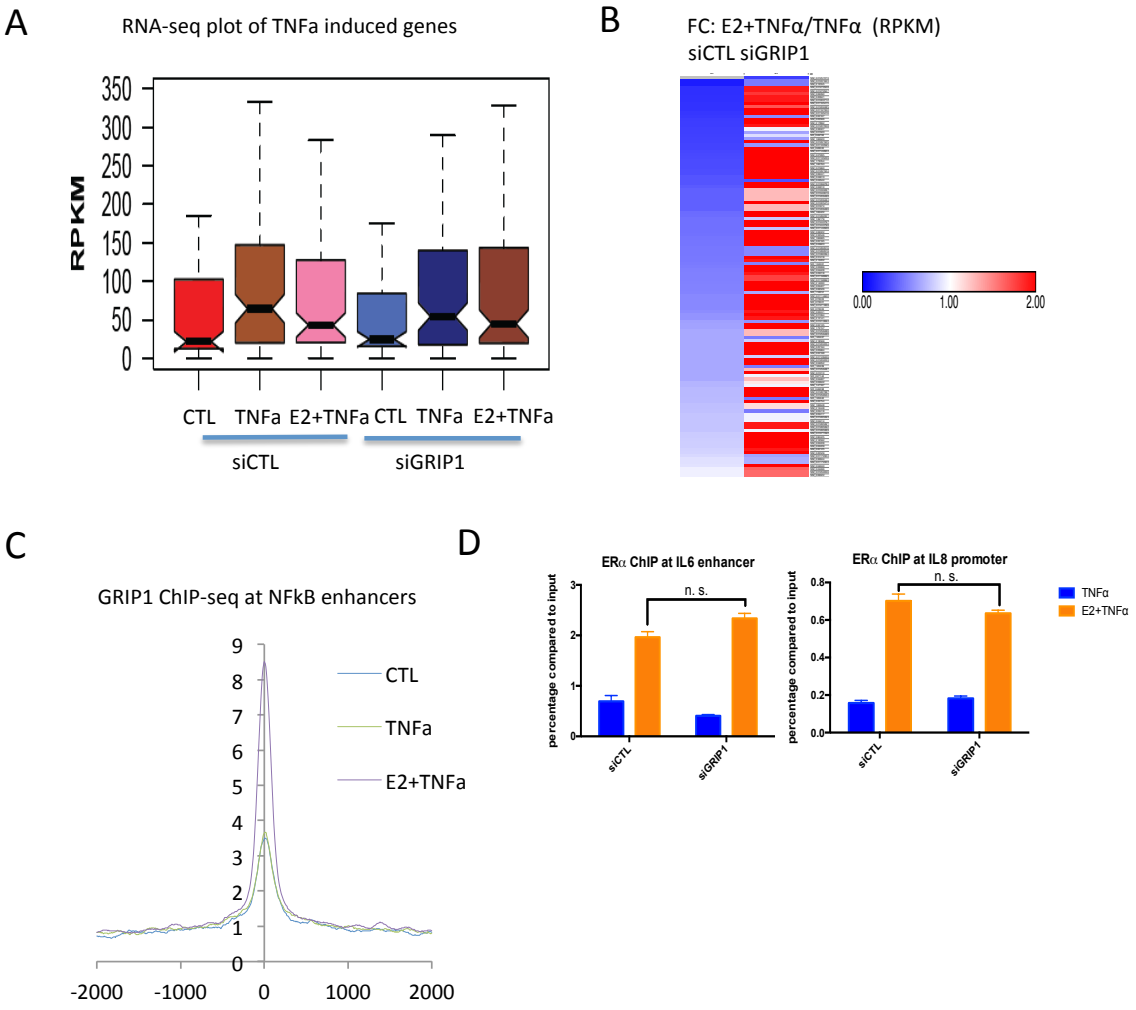


**Figure 20: GRIP1 mediates ERα repressive effects on NFκB genes**

(A) Boxplot showing effects of knockdown of GRIP1 on TNFα-induced genes under different conditions.
(B) Heatmap showing that knockdown of GRIP1 almost abolishes ERα transrepressive effects.
(C) Tag density plot showing ChIP-seq enrichment of GRIP1 on NFκB enhancers upon two signals treatment.
(D) Representative ERα ChIP-qPCR at siCTL or siGRIP1 condition.

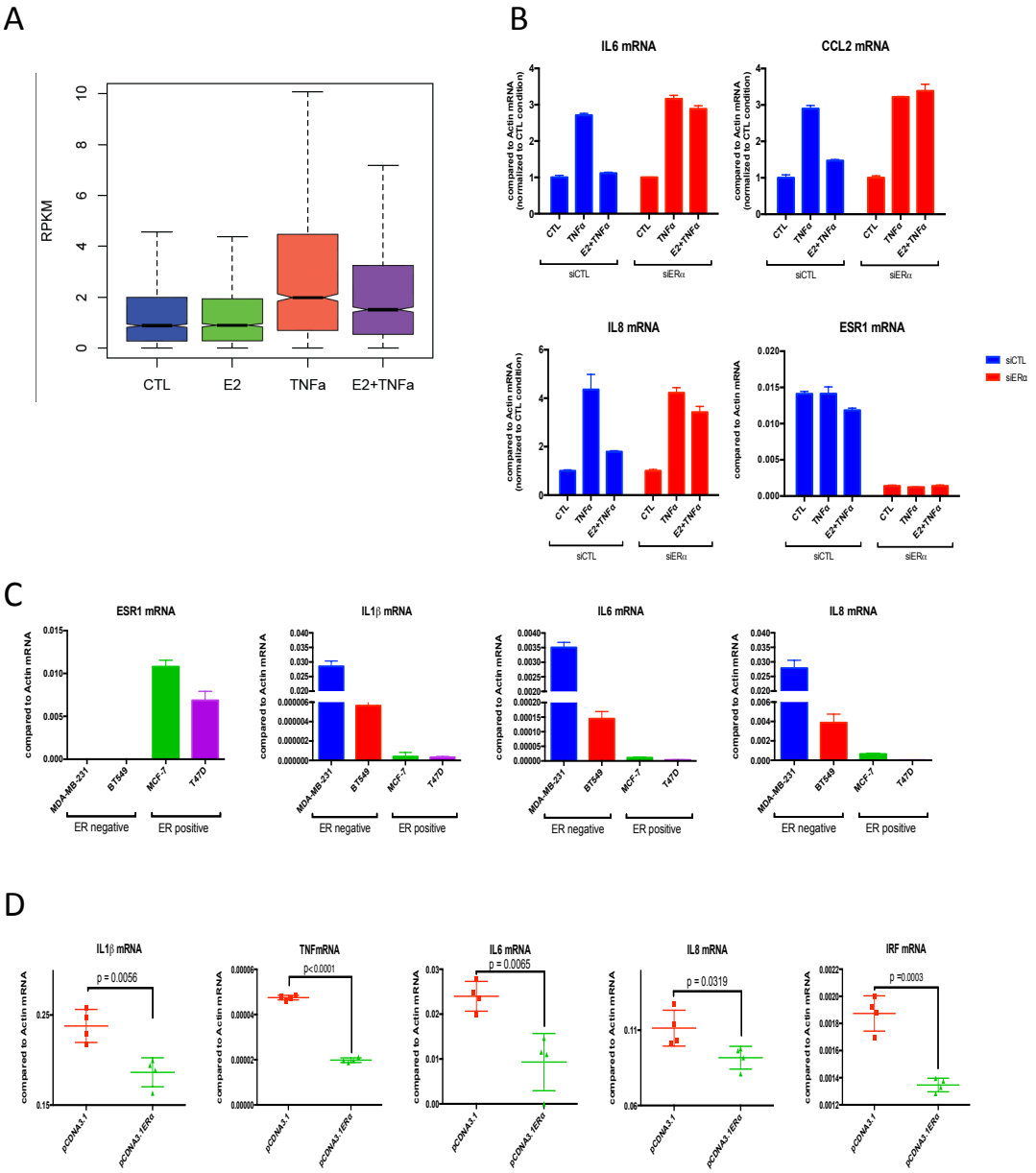


**Figure S 13:Additional Results for E2 Down-regulates TNFα Transcription Program**

(A) Boxplot showing that E2 plus TNFα dampens TNFα-induced gene activation.
(B) RT-qPCR showing that siRNA targeting ERα would abolish E2-mediated repression on TNFα-induced genes.
(C) RT-qPCR comparing pro-inflammatory genes expression difference between ERα positive and ERα negative breast cancer cell lines.
(D) RT-qPCR showing that transient expression of ERα in triple negative breast cancer cell line MDA-MB 231 cells leads to repression of pro-inflammatory genes expression.

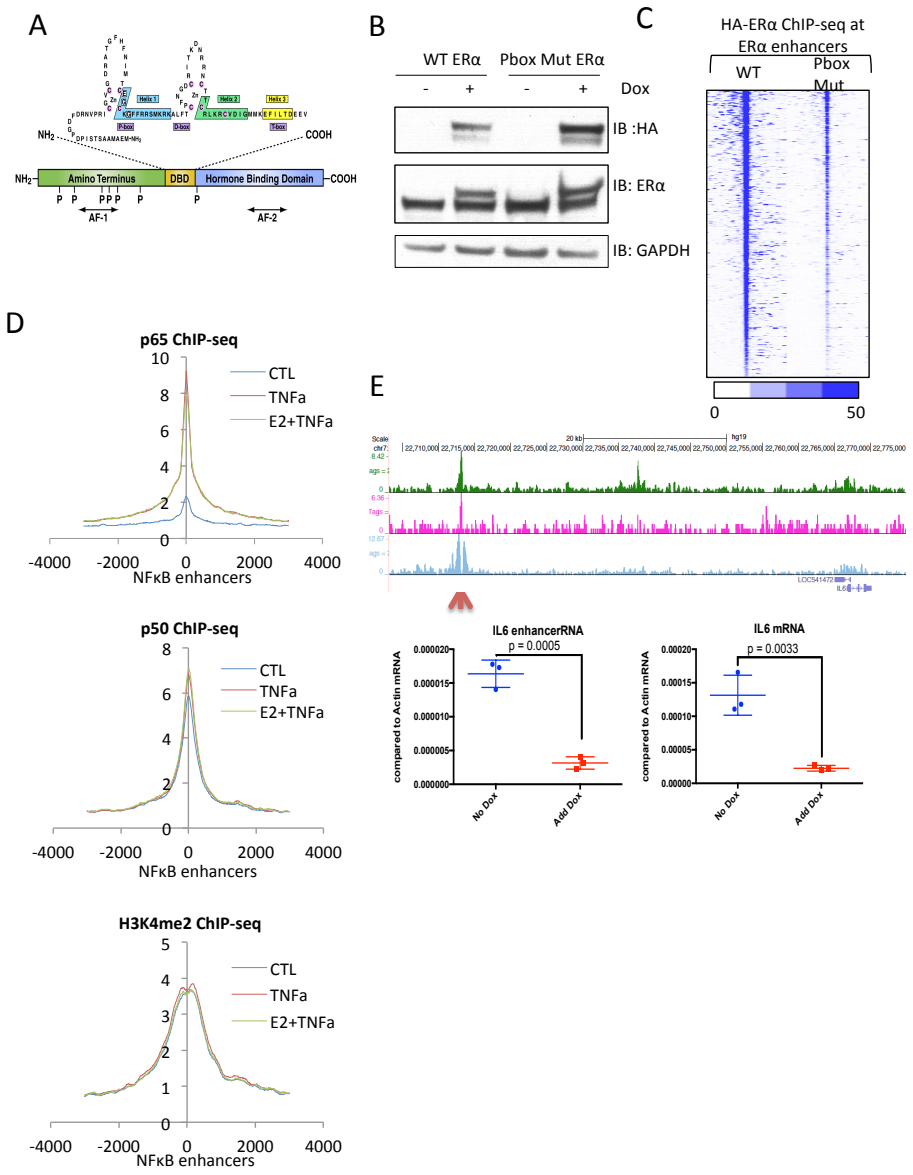


**Figure S 14: Additional Results for ERα is tethered to NFκB enhancers to repress transcription**

(A) Cartoon showing the P-Box mutation site on ERα DNA binding domain.
(B) Western Blots showing the inducible expression of HA-tagged wild type or P-Box mutated ERα.
(C) Heatmap of HA-tagged wild type or P-Box mutated ERα ChIP-seq enrichment at ERE-containing ERα enhancers.
(D) ChIP-seq tag density plots showing the enrichment of p65, p50 and histone mark H3K4me2 on NFκB enhancers.
(E) dCas9-KRAB with sgRNA specifically targeting to NFκB enhancer like IL6 enhancer leads to repression of both enhancer transcript and target gene IL6 expression.

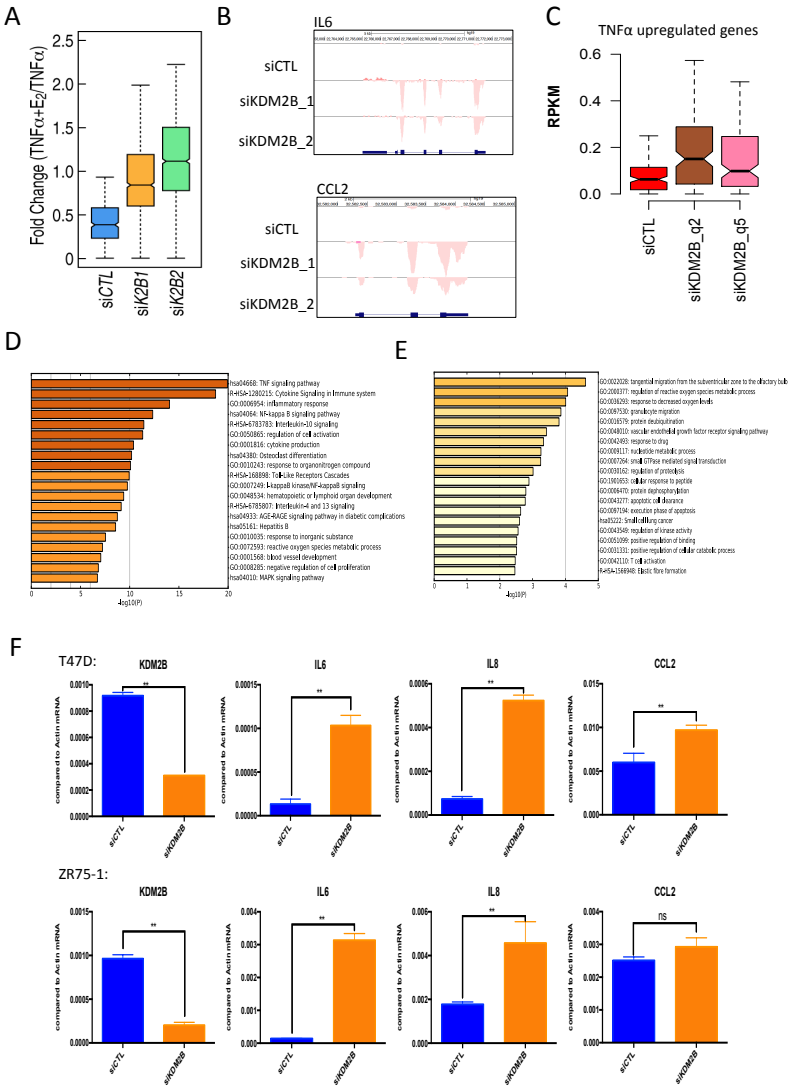


**Figure S 15: Additional Results for KDM2B represses inflammation at basal condition**

(A) Boxplot of RNA-seq data showing both siRNAs targeting KDM2B were able to derepress E2-repressed NFκB target genes.
(B) Representative RNA-seq genome browser image at IL6 and CCL2 gene showing knockdown of KDM2B induces pro-inflammatory gene expression.
(C) Boxplot of RNA-seq data showing that effects of KDM2B knockdown on TNFα-induced genes.
(D) and (E) Gene Ontology analysis by metascape of genes downregulated(D) or upregulated(E) by KDM2B knockdown.
(F) RT-qPCR of pro-inflammatory genes expression after KDM2B knockdown in ERα positive breast cancer cell lines T47D and ZR75-1.

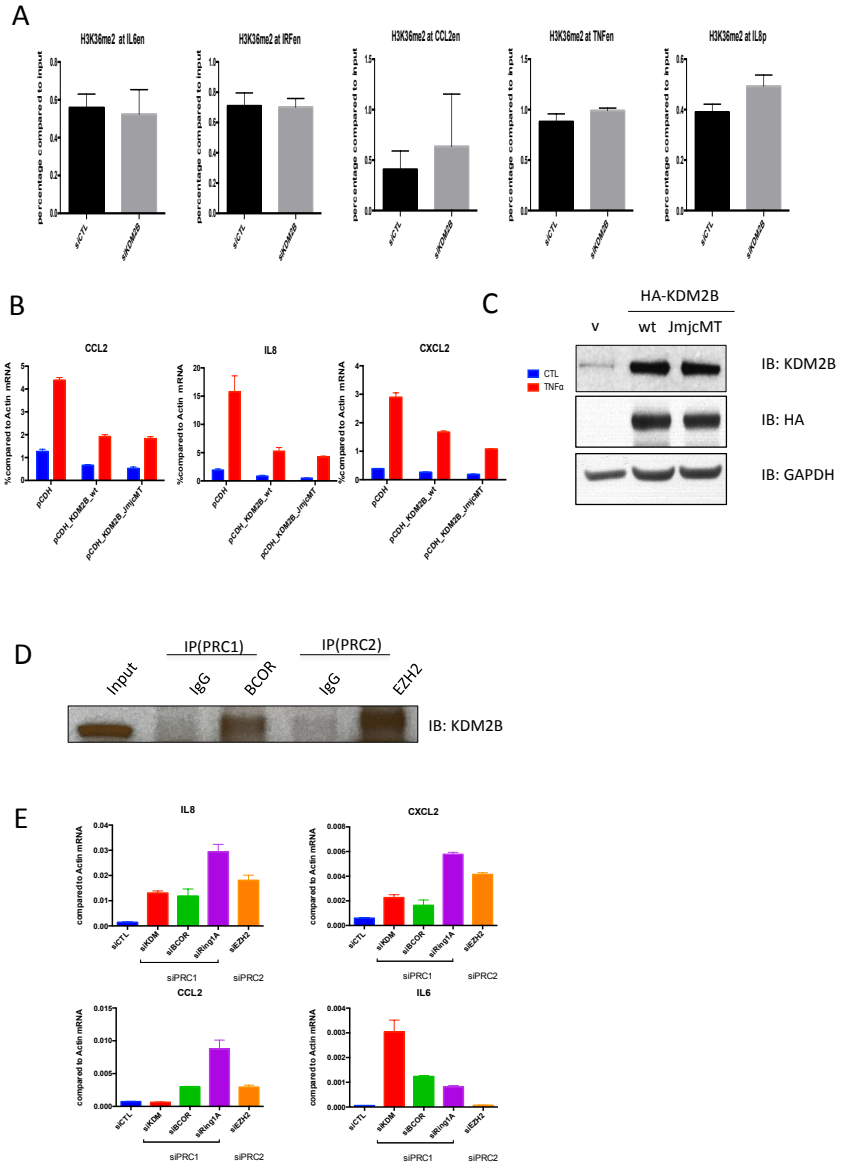


**Figure S 16: Additional Results for KDM2B Nucleates PRC1 to Repress Inflammation**

(A) H3K36me2 ChIP-qPCR showing that siKDM2B has almost no effect on H3K36me2 level on pro-inflammatory genes loci.
(B) and (C) RT-qPCR analysis showing that overexpression of wild type and jumonji domain mutated KDM2B can repress pro-inflammatory genes like IL8, CCL2, CXCL2.
(D) IP-Western Blot showing that both BCOR and EZH2 can interact with KDM2B.
(E) RT-qPCR of cytokine genes IL6, IL8, CCL2 and CXCL2 showing that knockdown of PRC1 components and PRC2 component EZH2 would derepress pro-inflammatory genes.

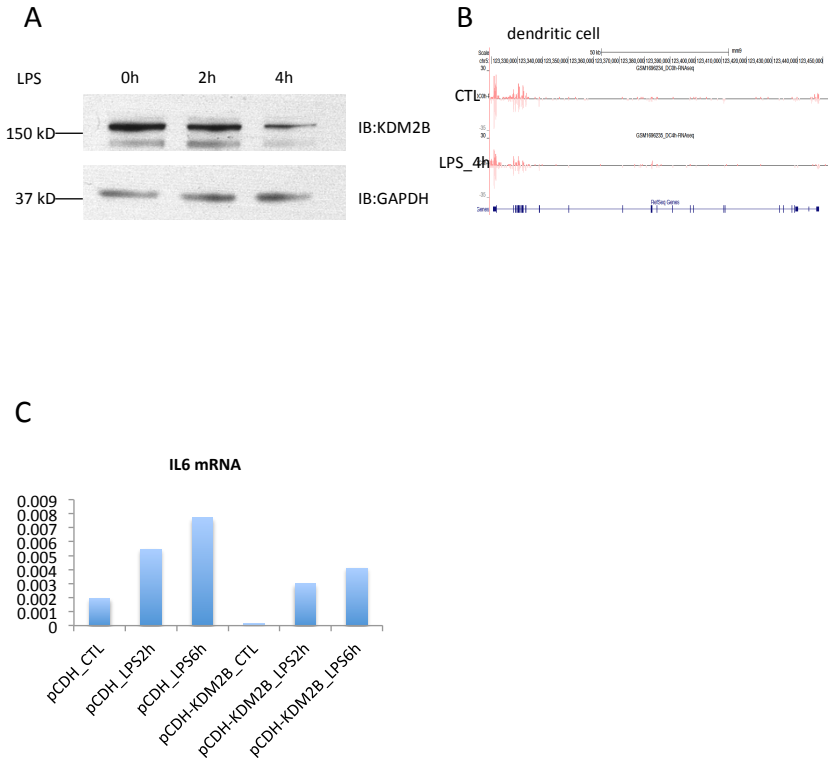


**Figure S 17: Additional Results for KDM2B Represses Inflammation in Macrophage.**

(A) Western Blot shows KDM2B protein level decreases after LPS treatment in Raw 264.7 cells.
(B) RNA-seq data of KDM2B locus with no treatment or 4 hours LPS treatment in bone marrow-derived dendritic cells.
(C) Overexpression of KDM2B represses IL6 expression before and after LPS treatment in Raw 264.7 cells.

References

A.J., W., A.F., S., and B.J., M. (2010). Condensin and cohesin complexity: the expanding repertoire of functions. Nature reviews Genetics *11*, 391-404.

Adelman, K., Marr, M.T., Werner, J., Saunders, A., Ni, Z., Andrulis, E.D., and Lis, J.T. (2005). Efficient release from promoter-proximal stall sites requires transcript cleavage factor TFIIS. Molecular cell *17*, 103-112.

Al-Dhaheri, M., Wu, J., Skliris, G.P., Li, J., Higashimato, K., Wang, Y., White, K.P., Lambert, P., Zhu, Y., Murphy, L.*, et al.* (2011). CARM1 is an important determinant of ERalpha-dependent breast cancer cell differentiation and proliferation in breast cancer cells. Cancer research *71*, 2118-2128.

An, J., Ribeiro, R.C., Webb, P., Gustafsson, J.A., Kushner, P.J., Baxter, J.D., and Leitman, D.C. (1999). Estradiol repression of tumor necrosis factor-alpha transcription requires estrogen receptor activation function-2 and is enhanced by coactivators. Proceedings of the National Academy of Sciences of the United States of America *96*, 15161-15166.

Andersson, R., Gebhard, C., Miguel-Escalada, I., Hoof, I., Bornholdt, J., Boyd, M., Chen, Y., Zhao, X., Schmidl, C., Suzuki, T.*, et al.* (2014a). An atlas of active enhancers across human cell types and tissues. Nature *507*, 455-461.

Andersson, R., Gebhard, C., Miguel-Escalada, I., Hoof, I., Bornholdt, J., Boyd, M., Chen, Y., Zhao, X., Schmidl, C., Suzuki, T.*, et al.* (2014b). An atlas of active enhancers across human cell types and tissues. Nature *507*, 455-461.

Aprelikova, O., Chen, K., El Touny, L.H., Brignatz-Guittard, C., Han, J., Qiu, T., Yang, H.H., Lee, M.P., Zhu, M., and Green, J.E. (2016). The epigenetic modifier JMJD6 is amplified in mammary tumors and cooperates with c-Myc to enhance cellular transformation, tumor progression, and metastasis. Clinical epigenetics *8*, 38.

Atianand, M.K., Hu, W., Satpathy, A.T., Shen, Y., Ricci, E.P., Alvarez-Dominguez, J.R., Bhatta, A., Schattgen, S.A., McGowan, J.D., Blin, J.*, et al.* (2016). A Long Noncoding RNA lincRNA-EPS Acts as a Transcriptional Brake to Restrain Inflammation. Cell *165*, 1672-1685.

Augereau, P., Badia, E., Balaguer, P., Carascossa, S., Castet, A., Jalaguier, S., and Cavailles, V. (2006). Negative regulation of hormone signaling by RIP140. The Journal of steroid biochemistry and molecular biology *102*, 51-59.

Banerji, J., Rusconi, S., and Schaffner, W. (1981). Expression of a beta-globin gene is enhanced by remote SV40 DNA sequences. Cell *27*, 299-308.

Baumgarten, S.C., and Frasor, J. (2012). Minireview: Inflammation: an instigator of more aggressive estrogen receptor (ER) positive breast cancers. Mol Endocrinol *26*, 360-371.

Berry, W.L., and Janknecht, R. (2013). KDM4/JMJD2 histone demethylases: epigenetic regulators in cancer cells. Cancer research *73*, 2936-2942.

Bhagwat, A.S., Roe, J.S., Mok, B.Y., Hohmann, A.F., Shi, J., and Vakoc, C.R. (2016). BET Bromodomain Inhibition Releases the Mediator Complex from Select cis-Regulatory Elements. Cell reports *15*, 519-530.

Bhatt, D.M., Pandya-Jones, A., Tong, A.J., Barozzi, I., Lissner, M.M., Natoli, G., Black, D.L., and Smale, S.T. (2012). Transcript dynamics of proinflammatory genes revealed by sequence analysis of subcellular RNA fractions. Cell *150*, 279-290.

Biswas, D.K., Cruz, A.P., Gansberger, E., and Pardee, A.B. (2000). Epidermal growth factor-induced nuclear factor kappa B activation: A major pathway of cell-cycle progression in estrogen-receptor negative breast cancer cells. Proceedings of the National Academy of Sciences of the United States of America *97*, 8542-8547.

Biswas, D.K., Shi, Q., Baily, S., Strickland, I., Ghosh, S., Pardee, A.B., and Iglehart, J.D. (2004). NF-kappa B activation in human breast cancer specimens and its role in cell proliferation and apoptosis. Proceedings of the National Academy of Sciences of the United States of America *101*, 10137-10142.

Blackledge, N.P., Farcas, A.M., Kondo, T., King, H.W., McGouran, J.F., Hanssen, L.L., Ito, S., Cooper, S., Kondo, K., Koseki, Y.*, et al.* (2014). Variant PRC1 complex-dependent H2A ubiquitylation drives PRC2 recruitment and polycomb domain formation. Cell *157*, 1445-1459.

Bose, J., Gruber, A.D., Helming, L., Schiebe, S., Wegener, I., Hafner, M., Beales, M., Kontgen, F., and Lengeling, A. (2004). The phosphatidylserine receptor has essential functions during embryogenesis but not in apoptotic cell removal. Journal of biology *3*, 15.

Bulger, M., and Groudine, M. (2011a). Functional and mechanistic diversity of distal transcription enhancers. Cell *144*, 327-339.

Bulger, M., and Groudine, M. (2011b). Functional and mechanistic diversity of distal transcription enhancers. Cell *144*, 327-339.

Cao, X., MacNaughton, P., Laurent, J.C., and Allen, J.G. (2017). Radon-induced lung cancer deaths may be overestimated due to failure to account for confounding by exposure to diesel engine exhaust in BEIR VI miner studies. PLoS One *12*, e0184298.

Carroll, J.S., Liu, X.S., Brodsky, A.S., Li, W., Meyer, C.A., Szary, A.J., Eeckhoute, J., Shao, W., Hestermann, E.V., Geistlinger, T.R*., et al.* (2005). Chromosome-wide mapping of estrogen receptor binding reveals long-range regulation requiring the forkhead protein FoxA1. Cell *122*, 33-43.

Carroll, J.S., Meyer, C.A., Song, J., Li, W., Geistlinger, T.R., Eeckhoute, J., Brodsky, A.S., Keeton, E.K., Fertuck, K.C., Hall, G.F*., et al.* (2006). Genome-wide analysis of estrogen receptor binding sites. Nature genetics *38*, 1289-1297.

Catic, A., Suh, C.Y., Hill, C.T., Daheron, L., Henkel, T., Orford, K.W., Dombkowski, D.M., Liu, T., Liu, X.S., and Scadden, D.T. (2013). Genome-wide map of nuclear protein degradation shows NCoR1 turnover as a key to mitochondrial gene regulation. Cell *155*, 1380-1395.

Chang, B., Chen, Y., Zhao, Y., and Bruick, R.K. (2007). JMJD6 is a histone arginine demethylase. Science *318*, 444-447.

Chen, C.F., Feng, X., Liao, H.Y., Jin, W.J., Zhang, J., Wang, Y., Gong, L.L., Liu, J.J., Yuan, X.H., Zhao, B.B*., et al.* (2014). Regulation of T cell proliferation by JMJD6 and PDGF-BB during chronic hepatitis B infection. Scientific reports *4*, 6359.

Chen, D., Ma, H., Hong, H., Koh, S.S., Huang, S.M., Schurter, B.T., Aswad, D.W., and Stallcup, M.R. (1999). Regulation of transcription by a protein methyltransferase. Science *284*, 2174-2177.

Chinenov, Y., Gupte, R., Dobrovolna, J., Flammer, J.R., Liu, B., Michelassi, F.E., and Rogatsky, I. (2012). Role of transcriptional coregulator GRIP1 in the anti-inflammatory actions of glucocorticoids. Proceedings of the National Academy of Sciences of the United States of America *109*, 11776-11781.

Cikala, M., Alexandrova, O., David, C.N., Proschel, M., Stiening, B., Cramer, P., and Bottger, A. (2004). The phosphatidylserine receptor from Hydra is a nuclear protein with potential Fe(II) dependent oxygenase activity. BMC Cell Biol *5*, 26.

Consortium, E.P. (2012). An integrated encyclopedia of DNA elements in the human genome. Nature *489*, 57-74.

Core, L.J., Waterfall, J.J., and Lis, J.T. (2008a). Nascent RNA sequencing reveals widespread pausing and divergent initiation at human promoters. Science (New York, NY) *322*, 1845-1848.

Core, L.J., Waterfall, J.J., and Lis, J.T. (2008b). Nascent RNA sequencing reveals widespread pausing and divergent initiation at human promoters. Science *322*, 1845-1848.

Couse, J.F., and Korach, K.S. (1999). Estrogen receptor null mice: what have we learned and where will they lead us? Endocrine reviews *20*, 358-417.

Cui, P., Qin, B., Liu, N., Pan, G., and Pei, D. (2004). Nuclear localization of the phosphatidylserine receptor protein via multiple nuclear localization signals. Experimental cell research *293*, 154-163.

Cuylen, S., Metz, J., Hruby, A., and Haering, C.H. (2013). Entrapment of chromosomes by condensin rings prevents their breakage during cytokinesis. Dev Cell *27*, 469-478.

Cvoro, A., Tzagarakis-Foster, C., Tatomer, D., Paruthiyil, S., Fox, M.S., and Leitman, D.C. (2006). Distinct roles of unliganded and liganded estrogen receptors in transcriptional repression. Molecular cell *21*, 555-564.

D'Ambrosio, C., Schmidt, C.K., Katou, Y., Kelly, G., Itoh, T., Shirahige, K., and Uhlmann, F. (2008). Identification of cis-acting sites for condensin loading onto budding yeast chromosomes. Genes Dev *22*, 2215-2227.

Das, A., Chai, J.C., Yang, C.S., Lee, Y.S., Das, N.D., Jung, K.H., and Chai, Y.G. (2015). Dual transcriptome sequencing reveals resistance of TLR4 ligand-activated bone marrow-derived macrophages to inflammation mediated by the BET inhibitor JQ1. Sci Rep *5*, 16932.

Dasgupta, S., Lonard, D.M., and O'Malley, B.W. (2014). Nuclear receptor coactivators: master regulators of human health and disease. Annu Rev Med *65*, 279-292.

De Santa, F., Barozzi, I., Mietton, F., Ghisletti, S., Polletti, S., Tusi, B.K., Muller, H., Ragoussis, J., Wei, C.L., and Natoli, G. (2010). A large fraction of extragenic RNA pol II transcription sites overlap enhancers. PLoS biology *8*, e1000384.

Di Ruscio, A., Ebralidze, A.K., Benoukraf, T., Amabile, G., Goff, L.A., Terragni, J., Figueroa, M.E., De Figueiredo Pontes, L.L., Alberich-Jorda, M., Zhang, P.*, et al.* (2013). DNMT1-interacting RNAs block gene-specific DNA methylation. Nature *503*, 371-376.

Ding, C., Li, Y., Kim, B.J., Malovannaya, A., Jung, S.Y., Wang, Y., and Qin, J. (2011). Quantitative analysis of cohesin complex stoichiometry and SMC3 modification-dependent protein interactions. Journal of proteome research *10*, 3652-3659.

Ding, N., Zhou, H., Esteve, P.O., Chin, H.G., Kim, S., Xu, X., Joseph, S.M., Friez, M.J., Schwartz, C.E., Pradhan, S.*, et al.* (2008). Mediator links epigenetic silencing of neuronal gene expression with x-linked mental retardation. Molecular cell *31*, 347-359.

Djebali, S., Davis, C.A., Merkel, A., Dobin, A., Lassmann, T., Mortazavi, A., Tanzer, A., Lagarde, J., Lin, W., Schlesinger, F.*, et al.* (2012). Landscape of transcription in human cells. Nature *489*, 101-108.

Dowen, J.M., Bilodeau, S., Orlando, D.A., Hubner, M.R., Abraham, B.J., Spector, D.L., and Young, R.A. (2013). Multiple structural maintenance of chromosome complexes at transcriptional regulatory elements. Stem cell reports *1*, 371-378.

Dunham, C.M., Cook, A.J., 2nd, Paparodis, A.M., and Huang, G.S. (2016). Practical one-dimensional measurements of age-related brain atrophy are validated by 3-dimensional values and clinical outcomes: a retrospective study. BMC Med Imaging *16*, 32.

Emmanuel, C., Gava, N., Kennedy, C., Balleine, R., Sharma, R., Wain, G., Brand, A., Hogg, R., Etemadmoghadam, D., George, J.*, et al.* (2011). Comparison of expression profiles in ovarian epithelium in vivo and ovarian cancer identifies novel candidate genes involved in disease pathogenesis. PloS one *6*.

Fadok, V.A., Bratton, D.L., Rose, D.M., Pearson, A., Ezekewitz, R.A., and Henson, P.M. (2000). A receptor for phosphatidylserine-specific clearance of apoptotic cells. Nature *405*, 85-90.

Farcas, A.M., Blackledge, N.P., Sudbery, I., Long, H.K., McGouran, J.F., Rose, N.R., Lee, S., Sims, D., Cerase, A., Sheahan, T.W.*, et al.* (2012). KDM2B links the Polycomb Repressive Complex 1 (PRC1) to recognition of CpG islands. Elife *1*, e00205.

Feng, Q., Zhang, Z., Shea, M.J., Creighton, C.J., Coarfa, C., Hilsenbeck, S.G., Lanz, R., He, B., Wang, L., Fu, X.*, et al.* (2014). An epigenomic approach to therapy for tamoxifen-resistant breast cancer. Cell research *24*, 809-819.

Foulds, C.E., Feng, Q., Ding, C., Bailey, S., Hunsaker, T.L., Malovannaya, A., Hamilton, R.A., Gates, L.A., Zhang, Z., Li, C.*, et al.* (2013). Proteomic analysis of coregulators bound to ERalpha on DNA and nucleosomes reveals coregulator dynamics. Molecular cell *51*, 185-199.

Franco, H.L., Nagari, A., and Kraus, W.L. (2015). TNFalpha signaling exposes latent estrogen receptor binding sites to alter the breast cancer cell transcriptome. Molecular cell *58*, 21-34.

Frasor, J., El-Shennawy, L., Stender, J.D., and Kastrati, I. (2015). NFkappaB affects estrogen receptor expression and activity in breast cancer through multiple mechanisms. Mol Cell Endocrinol *418 Pt 3*, 235-239.

Frasor, J., Weaver, A., Pradhan, M., Dai, Y., Miller, L.D., Lin, C.Y., and Stanculescu, A. (2009). Positive Cross-Talk between Estrogen Receptor and NF-kB in Breast Cancer. Cancer research *69*, 8918-8925.

Fullwood, M., Liu, M., Pan, Y., Liu, J., Xu, H., Mohamed, Y., Orlov, Y., Velkov, S., Ho, A., Mei, P.*, et al.* (2009). An oestrogen-receptor-alpha-bound human chromatin interactome. Nature *462*, 58-64.

Galien, R., and Garcia, T. (1997). Estrogen receptor impairs interleukin-6 expression by preventing protein binding on the NF-kappaB site. Nucleic acids research *25*, 2424-2429.

Gao, W.W., Xiao, R.Q., Peng, B.L., Xu, H.T., Shen, H.F., Huang, M.F., Shi, T.T., Yi, J., Zhang, W.J., Wu, X.N.*, et al.* (2015). Arginine methylation of HSP70 regulates retinoid acid-mediated RARbeta2 gene activation. Proceedings of the National Academy of Sciences of the United States of America *112*, E3327-3336.

Ghisletti, S., Meda, C., Maggi, A., and Vegeto, E. (2005). 17beta-estradiol inhibits inflammatory gene expression by controlling NF-kappaB intracellular localization. Molecular and cellular biology *25*, 2957-2968.

Glass, C.K., and Saijo, K. (2010). Nuclear receptor transrepression pathways that regulate inflammation in macrophages and T cells. Nature Reviews Immunology *10*, 365-376.

Graham, J.M., Jr., and Schwartz, C.E. (2013). MED12 related disorders. American journal of medical genetics Part A *161A*, 2734-2740.

Green, L., Kalitsis, P., Chang, T., Cipetic, M., Kim, J., Marshall, O., Turnbull, L., Whitchurch, C., Vagnarelli, P., Samejima, K.*, et al.* (2012). Contrasting roles of condensin I and condensin II in mitotic chromosome formation. Journal of cell science *125*, 1591-1604.

Grivennikov, S.I., Greten, F.R., and Karin, M. (2010). Immunity, inflammation, and cancer. Cell *140*, 883-899.

Guttman, M., Betts, G.N., Barnes, H., Ghassemian, M., van der Geer, P., and Komives, E.A. (2009). Interactions of the NPXY microdomains of the low density lipoprotein receptor-related protein 1. Proteomics *9*, 5016-5028.

Hah, N., Danko, C.G., Core, L., Waterfall, J.J., Siepel, A., Lis, J.T., and Kraus, W.L. (2011). A rapid, extensive, and transient transcriptional response to estrogen signaling in breast cancer cells. Cell *145*, 622-634.

Hah, N., Murakami, S., Nagari, A., Danko, C., and Kraus, W. (2013a). Enhancer transcripts mark active estrogen receptor binding sites. Genome research *23*, 1210-1223.

Hah, N., Murakami, S., Nagari, A., Danko, C.G., and Kraus, W.L. (2013b). Enhancer transcripts mark active estrogen receptor binding sites. Genome research *23*, 1210-1223.

Hahn, P., Bose, J., Edler, S., and Lengeling, A. (2008). Genomic structure and expression of Jmjd6 and evolutionary analysis in the context of related JmjC domain containing proteins. BMC genomics *9*, 293.

Hahn, P., Wegener, I., Burrells, A., Bose, J., Wolf, A., Erck, C., Butler, D., Schofield, C.J., Bottger, A., and Lengeling, A. (2010). Analysis of Jmjd6 cellular localization and testing for its involvement in histone demethylation. PLoS One *5*, e13769.

Hanahan, D., and Weinberg, R.A. (2011). Hallmarks of cancer: the next generation. Cell *144*, 646-674.

Hannedouche, S., Zhang, J., Yi, T., Shen, W., Nguyen, D., Pereira, J.P., Guerini, D., Baumgarten, B.U., Roggo, S., Wen, B.*, et al.* (2011). Oxysterols direct immune cell migration via EBI2. Nature *475*, 524-527.

He, J., Kallin, E.M., Tsukada, Y., and Zhang, Y. (2008). The H3K36 demethylase Jhdm1b/Kdm2b regulates cell proliferation and senescence through p15(Ink4b). Nature structural & molecular biology *15*, 1169-1175.

He, J., Shen, L., Wan, M., Taranova, O., Wu, H., and Zhang, Y. (2013). Kdm2b maintains murine embryonic stem cell status by recruiting PRC1 complex to CpG islands of developmental genes. Nature cell biology *15*, 373-384.

Heale, J.T., Ball, A.R., Jr., Schmiesing, J.A., Kim, J.S., Kong, X., Zhou, S., Hudson, D.F., Earnshaw, W.C., and Yokomori, K. (2006). Condensin I interacts with the PARP-1-XRCC1 complex and functions in DNA single-strand break repair. Mol Cell *21*, 837-848.

Heim, A., Grimm, C., Muller, U., Haussler, S., Mackeen, M.M., Merl, J., Hauck, S.M., Kessler, B.M., Schofield, C.J., Wolf, A.*, et al.* (2014). Jumonji domain containing protein 6 (Jmjd6) modulates splicing and specifically interacts with arginine-serine-rich (RS) domains of SR- and SR-like proteins. Nucleic acids research *42*, 7833-7850.

Heintzman, N.D., Hon, G.C., Hawkins, R.D., Kheradpour, P., Stark, A., Harp, L.F., Ye, Z., Lee, L.K., Stuart, R.K., Ching, C.W.*, et al.* (2009). Histone modifications at human enhancers reflect global cell-type-specific gene expression. Nature *459*, 108-112.

Heinz, S., Benner, C., Spann, N., Bertolino, E., Lin, Y., Laslo, P., Cheng, J., Murre, C., Singh, H., and Glass, C. (2010a). Simple combinations of lineage-determining transcription factors prime cis-regulatory elements required for macrophage and B cell identities. Molecular cell *38*, 576-589.

Heinz, S., Benner, C., Spann, N., Bertolino, E., Lin, Y.C., Laslo, P., Cheng, J.X., Murre, C., Singh, H., and Glass, C.K. (2010b). Simple combinations of lineage-determining transcription factors prime cis-regulatory elements required for macrophage and B cell identities. Molecular cell *38*, 576-589.

Heinz, S., Romanoski, C.E., Benner, C., Allison, K.A., Kaikkonen, M.U., Orozco, L.D., and Glass, C.K. (2013). Effect of natural genetic variation on enhancer selection and function. Nature *503*, 487-492.

Hervouet, E., Cartron, P.F., Jouvenot, M., and Delage-Mourroux, R. (2013). Epigenetic regulation of estrogen signaling in breast cancer. Epigenetics *8*, 237-245.

Hirano, T. (2012). Condensins: universal organizers of chromosomes with diverse functions. Genes Dev *26*, 1659-1678.

Ho, P.C., Tsui, Y.C., Feng, X., Greaves, D.R., and Wei, L.N. (2012). NF-kappaB-mediated degradation of the coactivator RIP140 regulates inflammatory responses and contributes to endotoxin tolerance. Nat Immunol *13*, 379-386.

Hsieh, C.-L., Fei, T., Chen, Y., Li, T., Gao, Y., Wang, X., Sun, T., Sweeney, C., Lee, G.-S.M., Chen, S.*, et al.* (2014a). Enhancer RNAs participate in androgen receptor-driven looping that selectively enhances gene activation. Proceedings of the National Academy of Sciences of the United States of America.

Hsieh, C.L., Fei, T., Chen, Y., Li, T., Gao, Y., Wang, X., Sun, T., Sweeney, C.J., Lee, G.S., Chen, S.*, et al.* (2014b). Enhancer RNAs participate in androgen receptor-driven looping that selectively enhances gene activation. Proceedings of the National Academy of Sciences of the United States of America *111*, 7319-7324.

Hsu, S.M., Chen, Y.C., and Jiang, M.C. (2000). 17 beta-estradiol inhibits tumor necrosis factor-alpha-induced nuclear factor-kappa B activation by increasing nuclear factor-kappa B p105 level in MCF-7 breast cancer cells. Biochem Biophys Res Commun *279*, 47-52.

Hu, Y.J., Belaghzal, H., Hsiao, W.Y., Qi, J., Bradner, J.E., Guertin, D.A., Sif, S., and Imbalzano, A.N. (2015). Transcriptional and post-transcriptional control of adipocyte differentiation by Jumonji domain-containing protein 6. Nucleic acids research.

Huang, S., Holzel, M., Knijnenburg, T., Schlicker, A., Roepman, P., McDermott, U., Garnett, M., Grernrum, W., Sun, C., Prahallad, A.*, et al.* (2012). MED12 controls the response to multiple cancer drugs through regulation of TGF-beta receptor signaling. Cell *151*, 937-950.

Hudson, D., Ohta, S., Freisinger, T., Macisaac, F., Sennels, L., Alves, F., Lai, F., Kerr, A., Rappsilber, J., and Earnshaw, W. (2008). Molecular and genetic analysis of condensin function in vertebrate cells. Molecular biology of the cell *19*, 3070-3079.

Ignatiadis, M., and Sotiriou, C. (2013). Luminal breast cancer: from biology to treatment. Nat Rev Clin Oncol *10*, 494-506.

Jans, J., Gladden, J., Ralston, E., Pickle, C., Michel, A., Pferdehirt, R., Eisen, M., and Meyer, B. (2009). A condensin-like dosage compensation complex acts at a distance to control expression throughout the genome. Genes & development *23*, 602-618.

Jeppsson, K., Kanno, T., Shirahige, K., and Sjogren, C. (2014). The maintenance of chromosome structure: positioning and functioning of SMC complexes. Nature reviews Molecular cell biology *15*, 601-614.

Kagey, M.H., Newman, J.J., Bilodeau, S., Zhan, Y., Orlando, D.A., van Berkum, N.L., Ebmeier, C.C., Goossens, J., Rahl, P.B., Levine, S.S.*, et al.* (2010). Mediator and cohesin connect gene expression and chromatin architecture. Nature *467*, 430-435.

Kaikkonen, M., Spann, N., Heinz, S., Romanoski, C., Allison, K., Stender, J., Chun, H., Tough, D., Prinjha, R., Benner, C.*, et al.* (2013a). Remodeling of the enhancer landscape during macrophage activation is coupled to enhancer transcription. Molecular cell *51*, 310-325.

Kaikkonen, M.U., Spann, N.J., Heinz, S., Romanoski, C.E., Allison, K.A., Stender, J.D., Chun, H.B., Tough, D.F., Prinjha, R.K., Benner, C.*, et al.* (2013b). Remodeling of the enhancer landscape during macrophage activation is coupled to enhancer transcription. Molecular cell *51*, 310-325.

Kim, J.H., Zhang, T., Wong, N.C., Davidson, N., Maksimovic, J., Oshlack, A., Earnshaw, W.C., Kalitsis, P., and Hudson, D.F. (2013). Condensin I associates with structural and gene regulatory regions in vertebrate chromosomes. Nat Commun *4*, 2537.

Kim, S., Xu, X., Hecht, A., and Boyer, T.G. (2006). Mediator is a transducer of Wnt/beta-catenin signaling. The Journal of biological chemistry *281*, 14066-14075.

Kim, T.-K., Hemberg, M., Gray, J., Costa, A., Bear, D., Wu, J., Harmin, D., Laptewicz, M., Barbara-Haley, K., Kuersten, S.*, et al.* (2010a). Widespread transcription at neuronal activity-regulated enhancers. Nature *465*, 182-187.

Kim, T.K., Hemberg, M., Gray, J.M., Costa, A.M., Bear, D.M., Wu, J., Harmin, D.A., Laptewicz, M., Barbara-Haley, K., Kuersten, S.*, et al.* (2010b). Widespread transcription at neuronal activity-regulated enhancers. Nature *465*, 182-187.

Kranz, A.L., Jiao, C.Y., Winterkorn, L.H., Albritton, S.E., Kramer, M., and Ercan, S. (2013). Genome-wide analysis of condensin binding in Caenorhabditis elegans. Genome Biol *14*, R112.

Kunisaki, Y., Masuko, S., Noda, M., Inayoshi, A., Sanui, T., Harada, M., Sasazuki, T., and Fukui, Y. (2004). Defective fetal liver erythropoiesis and T lymphopoiesis in mice lacking the phosphatidylserine receptor. Blood *103*, 3362-3364.

Kwok, J., O'Shea, M., Hume, D.A., and Lengeling, A. (2017). Jmjd6, a JmjC Dioxygenase with Many Interaction Partners and Pleiotropic Functions. Frontiers in genetics *8*, 32.

Lagarou, A., Mohd-Sarip, A., Moshkin, Y.M., Chalkley, G.E., Bezstarosti, K., Demmers, J.A., and Verrijzer, C.P. (2008). dKDM2 couples histone H2A ubiquitylation to histone H3 demethylation during Polycomb group silencing. Genes & development *22*, 2799-2810.

Lai, F., Orom, U., Cesaroni, M., Beringer, M., Taatjes, D., Blobel, G., and Shiekhattar, R. (2013a). Activating RNAs associate with Mediator to enhance chromatin architecture and transcription. Nature *494*, 497-501.

Lai, F., Orom, U.A., Cesaroni, M., Beringer, M., Taatjes, D.J., Blobel, G.A., and Shiekhattar, R. (2013b). Activating RNAs associate with Mediator to enhance chromatin architecture and transcription. Nature *494*, 497-501.

Lam, M., Cho, H., Lesch, H., Gosselin, D., Heinz, S., Tanaka-Oishi, Y., Benner, C., Kaikkonen, M., Kim, A., Kosaka, M.*, et al.* (2013a). Rev-Erbs repress macrophage gene expression by inhibiting enhancer-directed transcription. Nature *498*, 511-515.

Lam, M.T., Cho, H., Lesch, H.P., Gosselin, D., Heinz, S., Tanaka-Oishi, Y., Benner, C., Kaikkonen, M.U., Kim, A.S., Kosaka, M.*, et al.* (2013b). Rev-Erbs repress macrophage gene expression by inhibiting enhancer-directed transcription. Nature *498*, 511-515.

Lam, M.T., Li, W., Rosenfeld, M.G., and Glass, C.K. (2014a). Enhancer RNAs and regulated transcriptional programs. Trends in biochemical sciences *39*, 170-182.

Lam, M.T., Li, W., Rosenfeld, M.G., and Glass, C.K. (2014b). Enhancer RNAs and regulated transcriptional programs. Trends in biochemical sciences *39*, 170-182.

Lawrence, P., Conderino, J.S., and Rieder, E. (2014). Redistribution of demethylated RNA helicase A during foot-and-mouth disease virus infection: role of Jumonji C-domain containing protein 6 in RHA demethylation. Virology *452-453*, 1-11.

Lee, Y.F., Miller, L.D., Chan, X.B., Black, M.A., Pang, B., Ong, C.W., Salto-Tellez, M., Liu, E.T., and Desai, K.V. (2012). JMJD6 is a driver of cellular proliferation and motility and a marker of poor prognosis in breast cancer. Breast cancer research : BCR *14*, R85.

Leiserson, M.D., Vandin, F., Wu, H., Dobson, J.R., Eldridge, J.V., Thomas, J.L., Papoutsaki, A., Kim, Y., Niu, B., McLellan, M.*, et al.* (2014). Pan-cancer network analysis identifies combinations of rare somatic mutations across pathways and protein complexes. Nat Genet.

Lengronne, A., Katou, Y., Mori, S., Yokobayashi, S., Kelly, G.P., Itoh, T., Watanabe, Y., Shirahige, K., and Uhlmann, F. (2004). Cohesin relocation from sites of chromosomal loading to places of convergent transcription. Nature *430*, 573-578.

Li, M.O., Sarkisian, M.R., Mehal, W.Z., Rakic, P., and Flavell, R.A. (2003). Phosphatidylserine receptor is required for clearance of apoptotic cells. Science *302*, 1560-1563.

Li, W., Hu, Y., Oh, S., Ma, Q., Merkurjev, D., Song, X., Zhou, X., Liu, Z., Tanasa, B., He, X.*, et al.* (2015). Condensin I and II Complexes License Full Estrogen Receptor alpha-Dependent Enhancer Activation. Molecular cell *59*, 188-202.

Li, W., Notani, D., Ma, Q., Tanasa, B., Nunez, E., Chen, A., Merkurjev, D., Zhang, J., Ohgi, K., Song, X.*, et al.* (2013a). Functional roles of enhancer RNAs for oestrogen-dependent transcriptional activation. Nature *498*, 516-520.

Li, W., Notani, D., Ma, Q., Tanasa, B., Nunez, E., Chen, A.Y., Merkurjev, D., Zhang, J., Ohgi, K., Song, X.*, et al.* (2013b). Functional roles of enhancer RNAs for oestrogen-dependent transcriptional activation. Nature *498*, 516-520.

Li, W., Notani, D., and Rosenfeld, M.G. (2016). Enhancers as non-coding RNA transcription units: recent insights and future perspectives. Nature reviews Genetics *17*, 207-223.

Li, X., Zhou, Q., Sunkara, M., Kutys, M.L., Wu, Z., Rychahou, P., Morris, A.J., Zhu, H., Evers, B.M., and Huang, C. (2013c). Ubiquitylation of phosphatidylinositol 4-phosphate 5-kinase type I γ by HECTD1 regulates focal adhesion dynamics and cell migration. Journal of cell science *126*, 2617-2628.

Liu, W., Ma, Q., Wong, K., Li, W., Ohgi, K., Zhang, J., Aggarwal, A.K., and Rosenfeld, M.G. (2013). Brd4 and JMJD6-associated anti-pause enhancers in regulation of transcriptional pause release. Cell *155*, 1581-1595.

Liu, W., Tanasa, B., Tyurina, O.V., Zhou, T.Y., Gassmann, R., Liu, W.T., Ohgi, K.A., Benner, C., Garcia-Bassets, I., Aggarwal, A.K.*, et al.* (2010). PHF8 mediates histone H4 lysine 20 demethylation events involved in cell cycle progression. Nature *466*, 508-512.

Liu, Z., Auboeuf, D., Wong, J., Chen, J.D., Tsai, S.Y., Tsai, M.J., and O'Malley, B.W. (2002). Coactivator/corepressor ratios modulate PR-mediated transcription by the selective receptor modulator RU486. Proc Natl Acad Sci U S A *99*, 7940-7944.

Liu, Z., Merkurjev, D., Yang, F., Li, W., Oh, S., Friedman, M.J., Song, X., Zhang, F., Ma, Q., Ohgi, K.A.*, et al.* (2014). Enhancer activation requires trans-recruitment of a mega transcription factor complex. Cell *159*, 358-373.

Lonard, D.M., Nawaz, Z., Smith, C.L., and O'Malley, B.W. (2000). The 26S proteasome is required for estrogen receptor-alpha and coactivator turnover and for efficient estrogen receptor-alpha transactivation. Molecular cell *5*, 939-948.

Lupien, M., Eeckhoute, J., Meyer, C.A., Krum, S.A., Rhodes, D.R., Liu, X.S., and Brown, M. (2009). Coactivator function defines the active estrogen receptor alpha cistrome. Molecular and cellular biology *29*, 3413-3423.

Mader, S., Kumar, V., de Verneuil, H., and Chambon, P. (1989). Three amino acids of the oestrogen receptor are essential to its ability to distinguish an oestrogen from a glucocorticoid-responsive element. Nature *338*, 271-274.

Malik, S., and Roeder, R.G. (2010). The metazoan Mediator co-activator complex as an integrative hub for transcriptional regulation. Nature reviews Genetics *11*, 761-772.

Mantri, M., Loik, N.D., Hamed, R.B., Claridge, T.D., McCullagh, J.S., and Schofield, C.J. (2011). The 2-oxoglutarate-dependent oxygenase JMJD6 catalyses oxidation of lysine residues to give 5S-hydroxylysine residues. Chembiochem : a European journal of chemical biology *12*, 531-534.

Melgar, M., Collins, F., and Sethupathy, P. (2011a). Discovery of active enhancers through bidirectional expression of short transcripts. Genome biology *12*.

Melgar, M.F., Collins, F.S., and Sethupathy, P. (2011b). Discovery of active enhancers through bidirectional expression of short transcripts. Genome biology *12*, R113.

Melo, C., Drost, J., Wijchers, P., van de Werken, H., de Wit, E., Oude Vrielink, J., Elkon, R., Melo, S., Léveillé, N., Kalluri, R*., et al.* (2013a). eRNAs are required for p53-dependent enhancer activity and gene transcription. Molecular cell *49*, 524-535.

Melo, C.A., Drost, J., Wijchers, P.J., van de Werken, H., de Wit, E., Oude Vrielink, J.A., Elkon, R., Melo, S.A., Leveille, N., Kalluri, R*., et al.* (2013b). eRNAs are required for p53-dependent enhancer activity and gene transcription. Molecular cell *49*, 524-535.

Metivier, R., Penot, G., Hubner, M.R., Reid, G., Brand, H., Kos, M., and Gannon, F. (2003). Estrogen receptor-alpha directs ordered, cyclical, and combinatorial recruitment of cofactors on a natural target promoter. Cell *115*, 751-763.

Mousavi, K., Zare, H., Dell'orso, S., Grontved, L., Gutierrez-Cruz, G., Derfoul, A., Hager, G., and Sartorelli, V. (2013a). eRNAs promote transcription by establishing chromatin accessibility at defined genomic loci. Molecular cell *51*, 606-617.

Mousavi, K., Zare, H., Dell'orso, S., Grontved, L., Gutierrez-Cruz, G., Derfoul, A., Hager, G.L., and Sartorelli, V. (2013b). eRNAs promote transcription by establishing chromatin accessibility at defined genomic loci. Molecular cell *51*, 606-617.

Murakami-Tonami, Y., Kishida, S., Takeuchi, I., Katou, Y., Maris, J., Ichikawa, H., Kondo, Y., Sekido, Y., Shirahige, K., Murakami, H*., et al.* (2014). Inactivation of SMC2

shows a synergistic lethal response in MYCN-amplified neuroblastoma cells. Cell cycle (Georgetown, Tex) *13*.

Nagarajan, S., Benito, E., Fischer, A., and Johnsen, S.A. (2015). H4K12ac is regulated by estrogen receptor-alpha and is associated with BRD4 function and inducible transcription. Oncotarget *6*, 7305-7317.

Nagarajan, S., Hossan, T., Alawi, M., Najafova, Z., Indenbirken, D., Bedi, U., Taipaleenmaki, H., Ben-Batalla, I., Scheller, M., Loges, S.*, et al.* (2014). Bromodomain protein BRD4 is required for estrogen receptor-dependent enhancer activation and gene transcription. Cell reports *8*, 460-469.

Natoli, G., and Andrau, J.-C. (2012a). Noncoding transcription at enhancers: general principles and functional models. Annual review of genetics *46*, 1-19.

Natoli, G., and Andrau, J.C. (2012b). Noncoding transcription at enhancers: general principles and functional models. Annual review of genetics *46*, 1-19.

Nawaz, Z., Lonard, D., Smith, C., Lev-Lehman, E., Tsai, S., Tsai, M., and O'Malley, B. (1999). The Angelman syndrome-associated protein, E6-AP, is a coactivator for the nuclear hormone receptor superfamily. Molecular and cellular biology *19*, 1182-1189.

Nettles, K.W., Gil, G., Nowak, J., Metivier, R., Sharma, V.B., and Greene, G.L. (2008). CBP Is a dosage-dependent regulator of nuclear factor-kappaB suppression by the estrogen receptor. Mol Endocrinol *22*, 263-272.

Ong, C.T., and Corces, V.G. (2011). Enhancer function: new insights into the regulation of tissue-specific gene expression. Nature reviews Genetics *12*, 283-293.

Ono, T., Losada, A., Hirano, M., Myers, M., Neuwald, A., and Hirano, T. (2003). Differential contributions of condensin I and condensin II to mitotic chromosome architecture in vertebrate cells. Cell *115*, 109-121.

Osmanbeyoglu, H.U., Lu, K.N., Oesterreich, S., Day, R.S., Benos, P.V., Coronnello, C., and Lu, X. (2013). Estrogen represses gene expression through reconfiguring chromatin structures. Nucleic acids research *41*, 8061-8071.

Paimela, T., Ryhanen, T., Mannermaa, E., Ojala, J., Kalesnykas, G., Salminen, A., and Kaarniranta, K. (2007). The effect of 17beta-estradiol on IL-6 secretion and NF-kappaB DNA-binding activity in human retinal pigment epithelial cells. Immunol Lett *110*, 139-144.

Philibert, R.A., and Madan, A. (2007). Role of MED12 in transcription and human behavior. Pharmacogenomics *8*, 909-916.

Piazza, I., Rutkowska, A., Ori, A., Walczak, M., Metz, J., Pelechano, V., Beck, M., and Haering, C.H. (2014). Association of condensin with chromosomes depends on DNA binding by its HEAT-repeat subunits. Nat Struct Mol Biol *21*, 560-568.

Plank, J.L., and Dean, A. (2014a). Enhancer function: mechanistic and genome-wide insights come together. Molecular cell *55*, 5-14.

Plank, J.L., and Dean, A. (2014b). Enhancer Function: Mechanistic and Genome-Wide Insights Come Together. Molecular cell *55*, 5-14.

Pnueli, L., Rudnizky, S., Yosefzon, Y., and Melamed, P. (2015). RNA transcribed from a distal enhancer is required for activating the chromatin at the promoter of the gonadotropin alpha-subunit gene. Proceedings of the National Academy of Sciences of the United States of America *112*, 4369-4374.

Poulard, C., Rambaud, J., Hussein, N., Corbo, L., and Le Romancer, M. (2014). JMJD6 regulates ERalpha methylation on arginine. PloS one *9*, e87982.

Poulard, C., Rambaud, J., Lavergne, E., Jacquemetton, J., Renoir, J.M., Tredan, O., Chabaud, S., Treilleux, I., Corbo, L., and Le Romancer, M. (2015). Role of JMJD6 in Breast Tumourigenesis. PloS one *10*, e0126181.

Pradhan, M., Bembinster, L.A., Baumgarten, S.C., and Frasor, J. (2010). Proinflammatory cytokines enhance estrogen-dependent expression of the multidrug transporter gene ABCG2 through estrogen receptor and NF{kappa}B cooperativity at adjacent response elements. J Biol Chem *285*, 31100-31106.

Rahman, S., Sowa, M.E., Ottinger, M., Smith, J.A., Shi, Y., Harper, J.W., and Howley, P.M. (2011). The Brd4 extraterminal domain confers transcription activation independent of pTEFb by recruiting multiple proteins, including NSD3. Molecular and cellular biology *31*, 2641-2652.

Ramadoss, S., Guo, G., and Wang, C.Y. (2017). Lysine demethylase KDM3A regulates breast cancer cell invasion and apoptosis by targeting histone and the non-histone protein p53. Oncogene *36*, 47-59.

Reppas, N.B., Wade, J.T., Church, G.M., and Struhl, K. (2006). The transition between transcriptional initiation and elongation in E. coli is highly variable and often rate limiting. Molecular cell *24*, 747-757.

Risheg, H., Graham, J.M., Jr., Clark, R.D., Rogers, R.C., Opitz, J.M., Moeschler, J.B., Peiffer, A.P., May, M., Joseph, S.M., Jones, J.R.*, et al.* (2007). A recurrent mutation in MED12 leading to R961W causes Opitz-Kaveggia syndrome. Nature genetics *39*, 451-453.

Rocha, P.P., Scholze, M., Bleiss, W., and Schrewe, H. (2010). Med12 is essential for early mouse development and for canonical Wnt and Wnt/PCP signaling. Development *137*, 2723-2731.

Rogatsky, I., Luecke, H.F., Leitman, D.C., and Yamamoto, K.R. (2002). Alternate surfaces of transcriptional coregulator GRIP1 function in different glucocorticoid receptor activation and repression contexts. Proceedings of the National Academy of Sciences of the United States of America *99*, 16701-16706.

Rogatsky, I., Zarember, K.A., and Yamamoto, K.R. (2001). Factor recruitment and TIF2/GRIP1 corepressor activity at a collagenase-3 response element that mediates regulation by phorbol esters and hormones. Embo Journal *20*, 6071-6083.

Rollins, D.A., Coppo, M., and Rogatsky, I. (2015). Minireview: nuclear receptor coregulators of the p160 family: insights into inflammation and metabolism. Mol Endocrinol *29*, 502-517.

Rollins, D.A., Kharlyngdoh, J.B., Coppo, M., Tharmalingam, B., Mimouna, S., Guo, Z., Sacta, M.A., Pufall, M.A., Fisher, R.P., Hu, X.*, et al.* (2017). Glucocorticoid-induced phosphorylation by CDK9 modulates the coactivator functions of transcriptional cofactor GRIP1 in macrophages. Nat Commun *8*, 1739.

Ross-Innes, C., Stark, R., Holmes, K., Schmidt, D., Spyrou, C., Russell, R., Massie, C., Vowler, S., Eldridge, M., and Carroll, J. (2010). Cooperative interaction between retinoic acid receptor-alpha and estrogen receptor in breast cancer. Genes & development *24*, 171-182.

Rotin, D., and Kumar, S. (2009). Physiological functions of the HECT family of ubiquitin ligases. Nature reviews Molecular cell biology *10*, 398-409.

Ryu, B., Kim, D., Deluca, A., and Alani, R. (2007). Comprehensive expression profiling of tumor cell lines identifies molecular signatures of melanoma progression. PloS one *2*.

Sandhu, H.K., Sarkar, M., Turner, B.M., Wassink, T.H., and Philibert, R.A. (2003). Polymorphism analysis of HOPA: a candidate gene for schizophrenia. American journal of medical genetics Part B, Neuropsychiatric genetics : the official publication of the International Society of Psychiatric Genetics *123B*, 33-38.

Sarkar, A., and Zohn, I. (2012). Hectd1 regulates intracellular localization and secretion of Hsp90 to control cellular behavior of the cranial mesenchyme. The Journal of cell biology *196*, 789-800.

Schaukowitch, K., Joo, J.Y., Liu, X., Watts, J.K., Martinez, C., and Kim, T.K. (2014). Enhancer RNA facilitates NELF release from immediate early genes. Molecular cell *56*, 29-42.

Schiano, C., Casamassimi, A., Rienzo, M., de Nigris, F., Sommese, L., and Napoli, C. (2014). Involvement of Mediator complex in malignancy. Biochimica et biophysica acta *1845*, 66-83.

Schmidt, D., Schwalie, P., Ross-Innes, C., Hurtado, A., Brown, G., Carroll, J., Flicek, P., and Odom, D. (2010). A CTCF-independent role for cohesin in tissue-specific transcription. Genome research *20*, 578-588.

Schwartz, C.E., Tarpey, P.S., Lubs, H.A., Verloes, A., May, M.M., Risheg, H., Friez, M.J., Futreal, P.A., Edkins, S., Teague, J.*, et al.* (2007). The original Lujan syndrome family has a novel missense mutation (p.N1007S) in the MED12 gene. Journal of medical genetics *44*, 472-477.

Shalem, O., Sanjana, N.E., Hartenian, E., Shi, X., Scott, D.A., Mikkelsen, T.S., Heckl, D., Ebert, B.L., Root, D.E., Doench, J.G.*, et al.* (2014). Genome-scale CRISPR-Cas9 knockout screening in human cells. Science *343*, 84-87.

Shang, Y., Hu, X., DiRenzo, J., Lazar, M.A., and Brown, M. (2000). Cofactor dynamics and sufficiency in estrogen receptor-regulated transcription. Cell *103*, 843-852.

Skowronska-Krawczyk, D., Ma, Q., Schwartz, M., Scully, K., Li, W., Liu, Z., Taylor, H., Tollkuhn, J., Ohgi, K.A., Notani, D.*, et al.* (2014). Required enhancer-matrin-3 network interactions for a homeodomain transcription program. Nature.

Smale, S.T., and Natoli, G. (2014). Transcriptional control of inflammatory responses. Cold Spring Harb Perspect Biol *6*, a016261.

St-Pierre, J., Douziech, M., Bazile, F., Pascariu, M., Bonneil, E., Sauvé, V., Ratsima, H., and D'Amours, D. (2009). Polo kinase regulates mitotic chromosome condensation by hyperactivation of condensin DNA supercoiling activity. Molecular cell *34*, 416-426.

Stender, J.D., Kim, K., Charn, T.H., Komm, B., Chang, K.C., Kraus, W.L., Benner, C., Glass, C.K., and Katzenellenbogen, B.S. (2010). Genome-wide analysis of estrogen receptor alpha DNA binding and tethering mechanisms identifies Runx1 as a novel tethering factor in receptor-mediated transcriptional activation. Molecular and cellular biology *30*, 3943-3955.

Taatjes, D.J. (2010). The human Mediator complex: a versatile, genome-wide regulator of transcription. Trends in biochemical sciences *35*, 315-322.

Tada, K., Susumu, H., Sakuno, T., and Watanabe, Y. (2011). Condensin association with histone H2A shapes mitotic chromosomes. Nature *474*, 477-483.

Taylor-Papadimitriou, J., and Burchell, J. (2017). JARID1/KDM5 demethylases as cancer targets? Expert opinion on therapeutic targets *21*, 5-7.

Tibrewal, N., Liu, T., Li, H., and Birge, R.B. (2007). Characterization of the biochemical and biophysical properties of the phosphatidylserine receptor (PS-R) gene product. Mol Cell Biochem *304*, 119-125.

Tikhanovich, I., Kuravi, S., Artigues, A., Villar, M.T., Dorko, K., Nawabi, A., Roberts, B., and Weinman, S.A. (2015). Dynamic arginine methylation of TNF receptor associated factor 6 regulates Toll-like receptor signaling. The Journal of biological chemistry.

Turunen, M., Spaeth, J.M., Keskitalo, S., Park, M.J., Kivioja, T., Clark, A.D., Makinen, N., Gao, F., Palin, K., Nurkkala, H.*, et al.* (2014). Uterine leiomyoma-linked MED12 mutations disrupt mediator-associated CDK activity. Cell reports *7*, 654-660.

Unoki, M., Masuda, A., Dohmae, N., Arita, K., Yoshimatsu, M., Iwai, Y., Fukui, Y., Ueda, K., Hamamoto, R., Shirakawa, M.*, et al.* (2013). Lysyl 5-hydroxylation, a novel histone modification, by Jumonji domain containing 6 (JMJD6). The Journal of biological chemistry *288*, 6053-6062.

Van Bortle, K., Nichols, M.H., Li, L., Ong, C.-T.T., Takenaka, N., Qin, Z.S., and Corces, V.G. (2014). Insulator function and topological domain border strength scale with architectural protein occupancy. Genome biology *15*.

Van Laere, S.J., Van der Auwera, I., Van den Eynden, G.G., van Dam, P., Van Marck, E.A., Vermeulen, P.B., and Dirix, L.Y. (2007). NF-kappaB activation in inflammatory breast cancer is associated with oestrogen receptor downregulation, secondary to EGFR and/or ErbB2 overexpression and MAPK hyperactivation. Br J Cancer *97*, 659-669.

Villalobos, M., Olea, N., Brotons, J.A., Olea-Serrano, M.F., Almodovar, J.M.R.d., and Pedraza, V. (1995). The E-screen assay: a comparison of different MCF7 cell stocks. Environmental Health Perspectives *103*.

Wakeling, A., Dukes, M., and Bowler, J. (1991). A potent specific pure antiestrogen with clinical potential. Cancer research *51*, 3867-3873.

Wang, D., Garcia-Bassets, I., Benner, C., Li, W., Su, X., Zhou, Y., Qiu, J., Liu, W., Kaikkonen, M.U., Ohgi, K.A.*, et al.* (2011). Reprogramming transcription by distinct classes of enhancers functionally defined by eRNA. Nature *474*, 390-394.

Wang, F., He, L., Huangyang, P., Liang, J., Si, W., Yan, R., Han, X., Liu, S., Gui, B., Li, W.*, et al.* (2014a). JMJD6 promotes colon carcinogenesis through negative regulation of p53 by hydroxylation. PLoS biology *12*, e1001819.

Wang, L., Zeng, H., Wang, Q., Zhao, Z., Boyer, T.G., Bian, X., and Xu, W. (2015). MED12 methylation by CARM1 sensitizes human breast cancer cells to chemotherapy drugs. Science advances *1*, e1500463.

Wang, L., Zhao, Z., Meyer, M.B., Saha, S., Yu, M., Guo, A., Wisinski, K.B., Huang, W., Cai, W., Pike, J.W., *et al.* (2014b). CARM1 methylates chromatin remodeling factor BAF155 to enhance tumor progression and metastasis. Cancer cell *25*, 21-36.

Wang, X., Wu, Y.C., Fadok, V.A., Lee, M.C., Gengyo-Ando, K., Cheng, L.C., Ledwich, D., Hsu, P.K., Chen, J.Y., Chou, B.K., *et al.* (2003). Cell corpse engulfment mediated by C. elegans phosphatidylserine receptor through CED-5 and CED-12. Science *302*, 1563-1566.

Wang, Y., Zhang, H., Chen, Y., Sun, Y., Yang, F., Yu, W., Liang, J., Sun, L., Yang, X., Shi, L., *et al.* (2009). LSD1 is a subunit of the NuRD complex and targets the metastasis programs in breast cancer. Cell *138*, 660-672.

Watson, P.J., Fairall, L., and Schwabe, J.W. (2012). Nuclear hormone receptor co-repressors: structure and function. Molecular and cellular endocrinology *348*, 440-449.

Webby, C.J., Wolf, A., Gromak, N., Dreger, M., Kramer, H., Kessler, B., Nielsen, M.L., Schmitz, C., Butler, D.S., Yates, J.R., 3rd, *et al.* (2009). Jmjd6 catalyses lysyl-hydroxylation of U2AF65, a protein associated with RNA splicing. Science *325*, 90-93.

White, K.A., Yore, M.M., Deng, D., and Spinella, M.J. (2005). Limiting effects of RIP140 in estrogen signaling: potential mediation of anti-estrogenic effects of retinoic acid. The Journal of biological chemistry *280*, 7829-7835.

Wu, H., Nord, A.S., Akiyama, J.A., Shoukry, M., Afzal, V., Rubin, E.M., Pennacchio, L.A., and Visel, A. (2014a). Tissue-specific RNA expression marks distant-acting developmental enhancers. PLoS genetics *10*.

Wu, H., Nord, A.S., Akiyama, J.A., Shoukry, M., Afzal, V., Rubin, E.M., Pennacchio, L.A., and Visel, A. (2014b). Tissue-specific RNA expression marks distant-acting developmental enhancers. PLoS genetics *10*, e1004610.

Wu, T.F., Yao, Y.L., Lai, I.L., Lai, C.C., Lin, P.L., and Yang, W.M. (2015). Loading of PAX3 to Mitotic Chromosomes Is Mediated by Arginine Methylation and Associated with Waardenburg Syndrome. The Journal of biological chemistry *290*, 20556-20564.

Xu, B., Gerin, I., Miao, H., Vu-Phan, D., Johnson, C.N., Xu, R., Chen, X.W., Cawthorn, W.P., MacDougald, O.A., and Koenig, R.J. (2010). Multiple roles for the non-coding RNA SRA in regulation of adipogenesis and insulin sensitivity. PLoS One *5*, e14199.

Xu, X., Zhou, H., and Boyer, T.G. (2011). Mediator is a transducer of amyloid-precursor-protein-dependent nuclear signalling. EMBO reports *12*, 216-222.

Zeitlinger, J., Stark, A., Kellis, M., Hong, J.W., Nechaev, S., Adelman, K., Levine, M., and Young, R.A. (2007). RNA polymerase stalling at developmental control genes in the Drosophila melanogaster embryo. Nature genetics *39*, 1512-1516.

Zhang, J., Ni, S.S., Zhao, W.L., Dong, X.C., and Wang, J.L. (2013). High expression of JMJD6 predicts unfavorable survival in lung adenocarcinoma. Tumour biology : the journal of the International Society for Oncodevelopmental Biology and Medicine *34*, 2397-2401.

Zhang, Q., Zhao, K., Shen, Q., Han, Y., Gu, Y., Li, X., Zhao, D., Liu, Y., Wang, C., Zhang, X*., et al.* (2015). Tet2 is required to resolve inflammation by recruiting Hdac2 to specifically repress IL-6. Nature *525*, 389-393.

Zhang, W.J., Wu, X.N., Shi, T.T., Xu, H.T., Yi, J., Shen, H.F., Huang, M.F., Shu, X.Y., Wang, F.F., Peng, B.L*., et al.* (2016). Regulation of Transcription Factor Yin Yang 1 by SET7/9-mediated Lysine Methylation. Scientific reports *6*, 21718.

Zhao, Y., Wang, L., Ren, S., Wang, L., Blackburn, P.R., McNulty, M.S., Gao, X., Qiao, M., Vessella, R.L., Kohli, M*., et al.* (2016). Activation of P-TEFb by Androgen Receptor-Regulated Enhancer RNAs in Castration-Resistant Prostate Cancer. Cell reports *15*, 599-610.

Zhou, J., Bi, D., Lin, Y., Chen, P., Wang, X., and Liang, S. (2012). Shotgun proteomics and network analysis of ubiquitin-related proteins from human breast carcinoma epithelial cells. Molecular and cellular biochemistry *359*, 375-384.

Zhou, Y., Eppenberger-Castori, S., Eppenberger, U., and Benz, C.C. (2005). The NFkappaB pathway and endocrine-resistant breast cancer. Endocr Relat Cancer *12 Suppl 1*, S37-46.